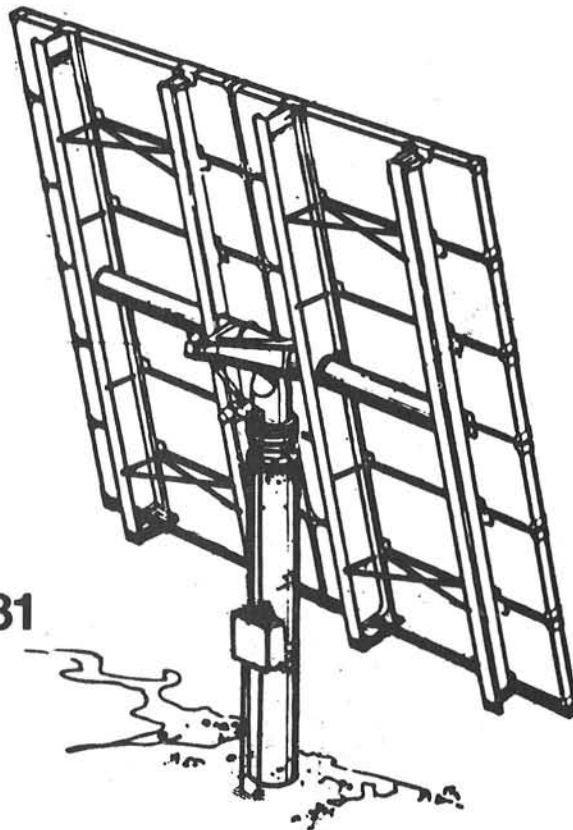


*When printing a copy of any digitized SAND Report, you are required to update the markings to current standards.*

Final Report

# **Second Generation Heliostat Development**

for SOLAR CENTRAL RECEIVERS



March 31, 1981

**Detail Design Report  
Volume I**

**SAND 81-8175**

**FINAL REPORT  
SECOND GENERATION HELIOSTAT DEVELOPMENT  
FOR SOLAR CENTRAL RECEIVERS**

**VOLUME I  
DETAIL DESIGN REPORT**

**MARCH 31, 1981**

**BOEING ENGINEERING & CONSTRUCTION  
(A Division of The Boeing Company)  
P.O. Box 3707  
SEATTLE, WASHINGTON 98124**

**PREPARED FOR  
SANDIA NATIONAL LABORATORIES  
LIVERMORE, CALIFORNIA  
UNDER CONTRACT 83-2729C**

## ABSTRACT

A production heliostat for a 50 MW<sub>e</sub> solar-electric power plant is described. The detail design, along with trades, analyses and testing in support of the design are presented. The collector subsystem's performance is assessed. Fabrication, check-out and installation of two prototypes at the Department of Energy Central Receiver Test Facility is described. Appendices are provided which describe details of design, analysis and test.

## FOREWORD

This report was prepared to satisfy the requirements of Task 2.E of Sandia Laboratories contract 83-2729C. It describes the trade studies, detail design, testing, analyses and assessment of a Second Generation Heliostat for solar central receiver plants. Production plans and cost estimates ( results of subtasks 2.E.2 and 2.E.4) are reported in Volume 2. The engineering drawings and specifications required by subtask 2.E.5 have been submitted separately.

The development project for the Second Generation Heliostat was performed by the Boeing Engineering & Construction Co. (BEC), under the direction of Mr. Roger Gillette, Program Manager. The Sandia Technical Manager was Mr. Charles Pignolet. Mr. Marcus Berry prepared the Detail Design Report. BEC personnel contributing to the program included: Don Bartlett (Engineering Manager), Rich Clark (Operations Manager), Earl Umbinetti, Ken Hernley, Don Weyer, Mike LaSalle, Al Quynn, Ferg Mahony, William Yeckel, Harry Dursch, Cheryl Warner, Dave Kirkbride, Ron Miller, Lloyd Tomlinson, Dave Plummer, and Mark Rubeck.

BEC was assisted in this project by two major subcontractors: Ford Aerospace and Communications Corporation (Western Development Laboratories Division), (FACC) and Pittsburgh Corning Corporation. Ford designed and fabricated the prototype gimbal-drive assemblies and planned the production capability for the gimbal and frame. Mr. Howard Sund was program manager at FACC. Principal technical contributors at Ford included Mr. Earl Lewis and Punkaj Nanavati. Pittsburgh Corning fabricated the prototype facet assemblies, and performed the production planning for the facet. Key contributors at Pittsburgh Corning were Mr. Rick Greene and Mr. Jack Binder.

BEC was also assisted by two electric utilities; Public Service Company of New Mexico, and Arizona Public Service Company. Abbas Akhil (Public Service Co. of New Mexico) and Darryl Barnes (Arizona Public Service Co.) provided helpful technical advice during the design phase.

## TABLE OF CONTENTS

PARAGRAPH		PAGE
1.0	Introduction and Summary	1
1.1	Design Overview	1
1.2	Prototype Development and Fabrication	10
2.0	Heliostat Design	12
2.1	Reflector Assembly	12
2.1.1	Facet	12
2.1.2	Attachment Bracket	23
2.2	Frame Assembly	26
2.3	Gimbal Actuator	31
2.3.1	Gimbal Actuator Drive Assembly	31
2.3.2	Drive Motors	44
2.3.3	Sensors	46
2.4	Pedestal/Foundation	52
2.5	Control System	58
3.0	Collector Subsystem	93
3.1	Subsystem Description	93
3.2	Performance Analysis	93
3.2.1	Reflected Energy From Single Heliostat	96
3.2.2	Collector Subsystem Efficiency and Power Output	96
3.2.3	Availability	100
3.2.4	Safety	107
4.0	Prototype Fabrication, Checkout and Installation	110
4.1	Fabrication	110
4.2	Assembly and Checkout	117
4.2.1	Life Cycle Wear Testing of Elevation Actuator Screw and Nut	117
4.2.2	Gimbal Tests	120
4.2.3	Form/Fit/Functional Checkout	131

PARAGRAPH		PAGE
4.3	Installation at CRTF	140
4.3.1	Pedestal	140
4.3.2	Gimbal Drive	142
4.3.3	Structural Frame	145
4.3.4	Reflectors	145
4.3.5	Controls	152
4.3.6	Canting	153
4.3.7	Alignment	155
5.0	References	165

## APPENDICES

### VOLUME I

- A. Requirements
- B. Azimuth Drive/Bearing Assembly Test Data
- C. Assembled Gimbal/Actuator Drive Assembly Test Data
- D. Actuator Screw and Nut Test
- E. Reflector Materials/Assembly Tests
- F. Drive Motor Specification
- G. Mode Operation and Software Organization
- H. Control System Data Base

### VOLUME II

Contains References 2-5; Gimbal Trade Studies, Design Analyses, Test Reports and Procedures.

## 1.0 INTRODUCTION AND SUMMARY

Boeing Engineering and Construction Company (BEC), under contract with Sandia National Laboratories, Livermore, submits herein the detail design report of a Second Generation Heliostat for a 50 MWe central receiver solar thermal electric power plant. This work was performed under Contract 83-2729C, and the heliostat is in compliance with Sandia Specification A10772D. The primary objective of the effort was to develop a mass producible, low cost, Second Generation Heliostat design. Pursuant to this objective, major tasks completed include: preliminary and detail designs, cost analyses, production planning, and fabrication and installation of two heliostat prototypes at the Central Receiver Test Facility (CRTF) near Albuquerque, New Mexico.

### 1.1 DESIGN OVERVIEW

The collector subsystem field layout for a 50 MWe plant, using BEC Second Generation Heliostats is shown in Figure 1.1-1. Approximately 6914 heliostats would be laid out in circular, staggered rows around the receiver tower. This results in an overall field area of 1.268 Km<sup>2</sup> contained within maximum dimensions of 1600m x 1200m in east/west and north/south directions, respectively. The field is controlled by a computerized digital electronic system, which in turn, is an integral part of the overall plant control system.

Figure 1.1-2 shows the major elements of the heliostat and Figures 1.1-3 and 1.1-4 show front and back photographs of the heliostat installed at the CRTF.

The heliostats' twelve, 1.24m x 3.07m (4 ft. x 10 ft.) reflector facets are made by laminating fusion glass skins on a cellular glass core. The reflector assembly is 7.62m x 6.15m (25 ft. x 20.2 ft.) , has a nominal reflective area of 44m<sup>2</sup> (474 ft<sup>2</sup>) and has a reflectivity of 0.94. The facets are supported with adjustable brackets on deep section steel beams. The beams are connected together and to the gimbal actuator via a 3 section steel torque tube. The Az/EI gimbal actuator is supported on a prestressed concrete piling (pedestal/foundation).

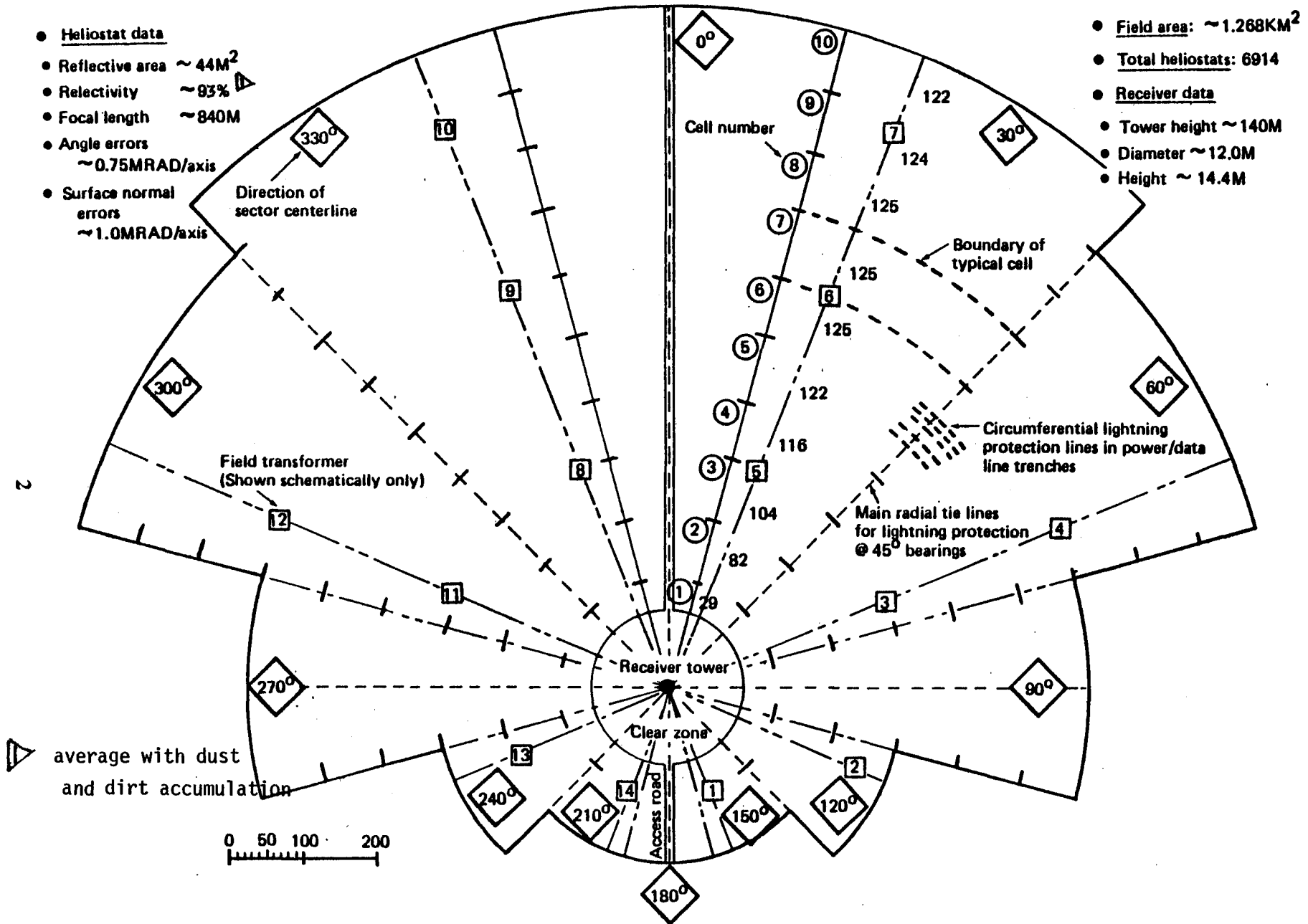


Figure 1.1-1. Collector Subsystem, General Field Layout, 50 MW Solar-Electric Plant



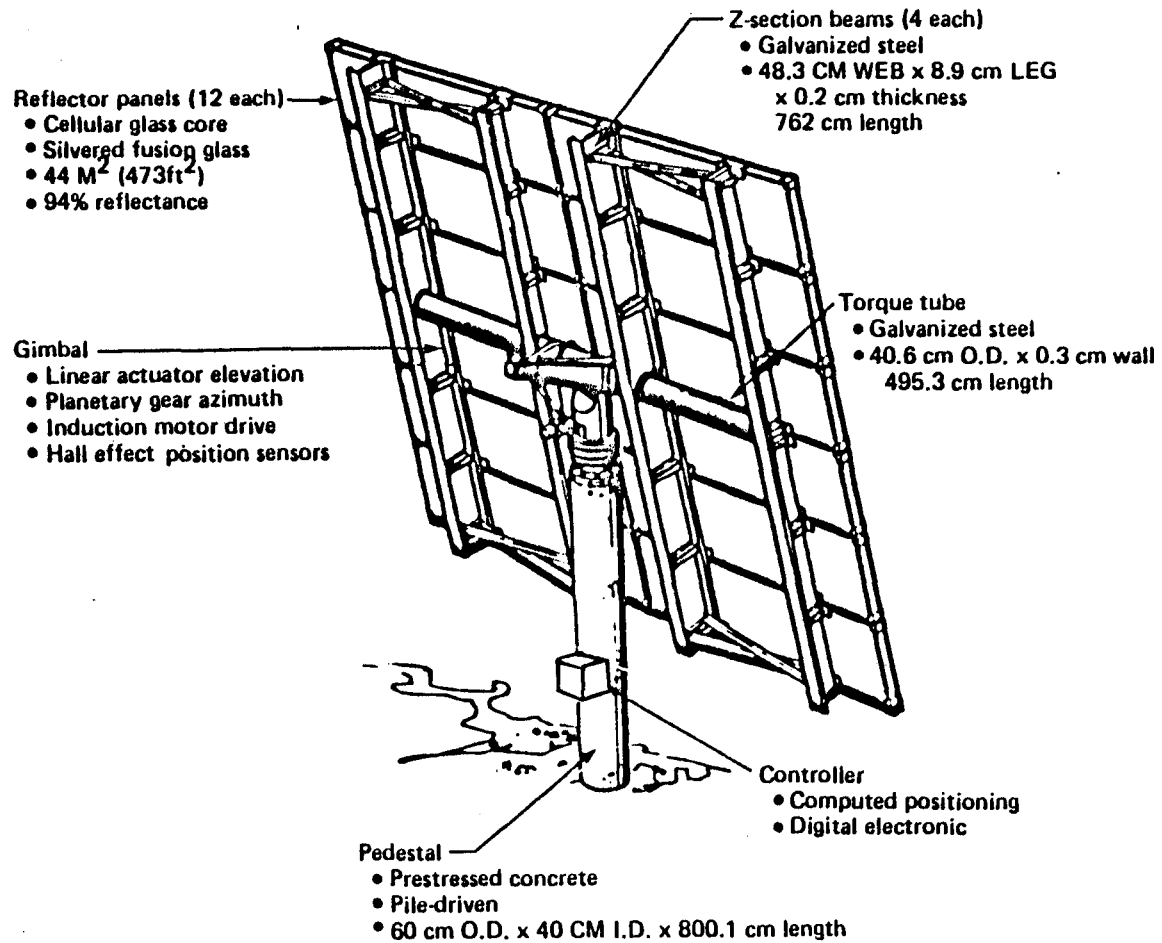


Figure 1.1-2. Collector Subsystem Heliostat

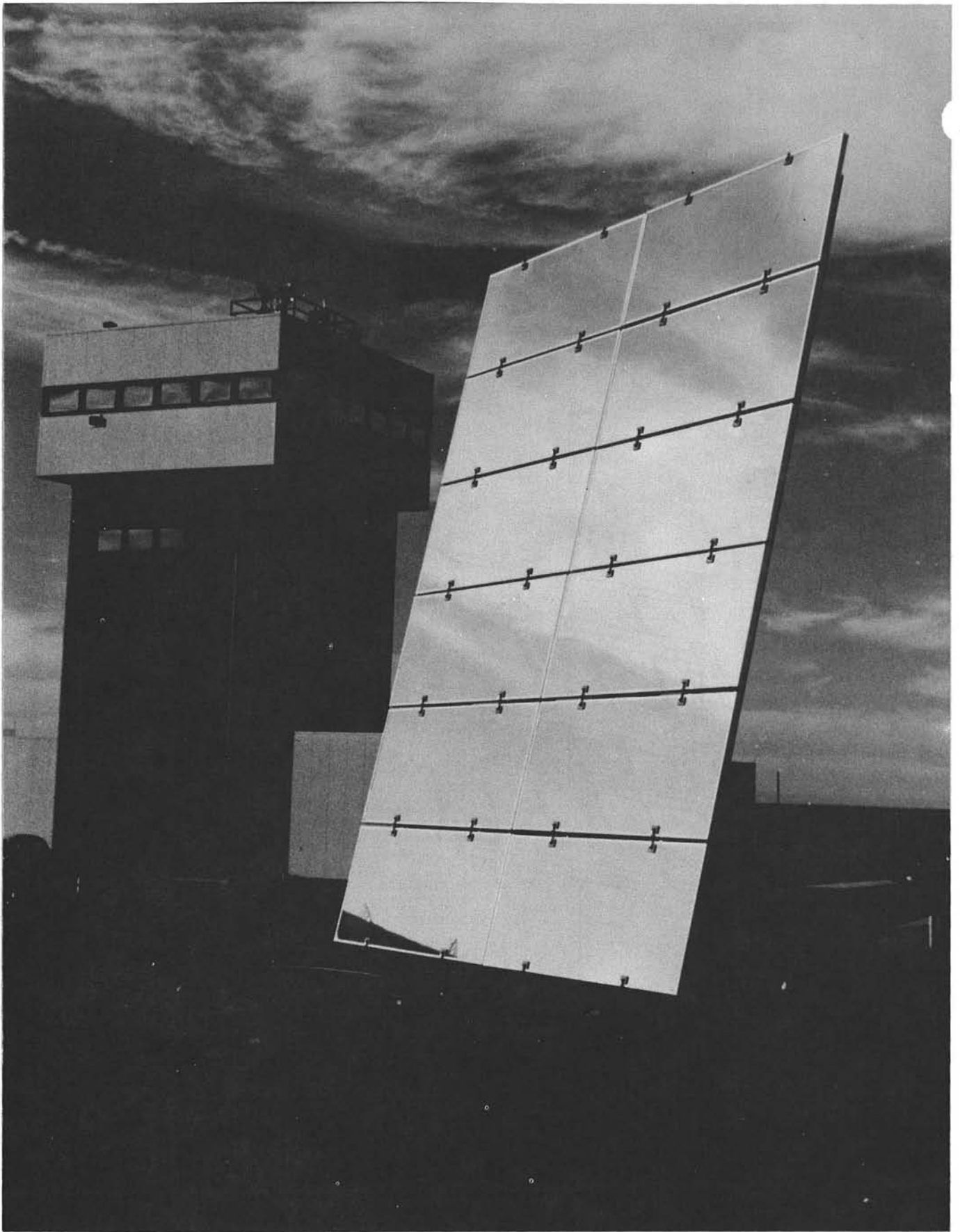


Figure 1.1-3. Prototype Heliostat, Front View

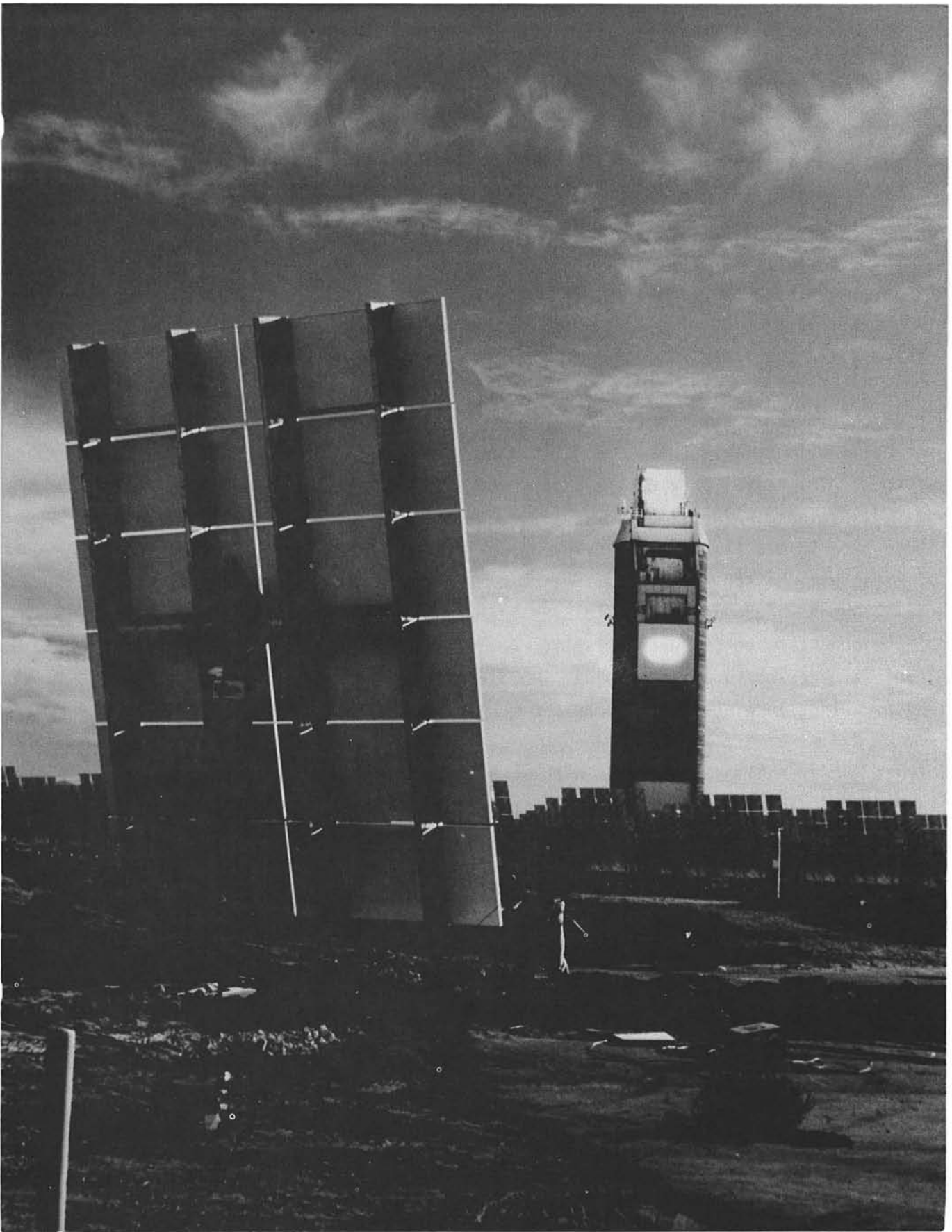


Figure 1.1-4. Prototype Heliostat, Rear View

A digital electronic control system operates the gimbal, utilizing computed azimuth/elevation pointing angles and feedback from motor rotation counters and reference position sensors on each axis. The heliostat detail design presented herein describes a control system and software capable of operating the two prototypes and demonstrating algorithms and control principles of a production system. Development of designs for a production control system, and for field power and wiring were beyond the scope of this contract.

Elevation travel is confined to  $-3^{\circ}$  through  $93^{\circ}$ , where  $0^{\circ}$  is reflector surface vertical. Azimuth axis travel is constrained only by the locations of limit switches. The travel rate of the azimuth axis is  $12^{\circ}/\text{minute}$  and the elevation axis,  $6.2^{\circ}/\text{minute}$ . The gimbal drives are capable of moving at the rates in winds up to  $16 \text{ m/s}$  ( $35 \text{ mph}$ ). During normal non-operational periods the heliostat will be stowed with the reflector surface vertical. This stow orientation has been determined to result in comparable dust-dirt accumulation to face-down stowage (reference 1-1), reduces gimbal/torque tube costs and minimizes power consumed in stowing. Horizontal, mirror up, stowage will be used for winds in excess of  $22.3 \text{ m/s}$  ( $50 \text{ mph}$ ).

Weights for assemblies are given in the table below. The heliostat weight (excluding pedestal, power and signal wiring and controls) is  $1808 \text{ Kg}$  ( $3986 \text{ lbs}$ ), or  $41 \text{ kg/m}^2$ .

Component/Assembly	Weight Kg (Lb)
Reflector Facets	887 (1956)
Frame (Including beams, 3 torque tube sections, brackets, fasteners)	606 (1335)
Gimbal	315 (695)
Pedestal	3293 (7261)

The reflector facets on prototype heliostats were constructed by laminating sheets of 0.15 cm (0.058) inch Corning 0317 aluminosilicate fusion glass\*, to a core of 5.08 cm (2.0 inch) thick aluminoborosilicate cellular glass (Pittsburgh Corning Foamsil75). The front sheet is second-surface silvered, while the back sheet is coated with white paint. The edges of the facet are capped with painted 24-gage steel strips for protection from moisture intrusion and physical damage. This facet design offers the following features:

- o High reflectivity silvered glass - 0.94 measured\*\*
- o Matched thermal coefficients - stable with temperature
- o Facet encapsulation - resistance to moisture damage
- o Hailstone resistant - cap strip and material thicknesses - tested
- o Maximized use of glass - chemically stable, low cost/lb
- o Contour variable - manufacture flat or curved
- o White coating on backside - minimizes thermal distortions from backlighting
- o Closed cell core material - minimizes pumping pressure gradient across seals.

Each facet interfaces with the H-frame by means of four support brackets. The bracket design uses only mechanical connections, avoiding bonded joints, provides adjustment capability for canting, and allows for individual facet replacement.

The structural frame assembly selected for Second Generation Heliostats utilizes lightweight sheet-steel Z-beams and a horizontal torque tube, in a double H-frame configuration. This concept was selected based on its

---

\*Corning 7809 fusion glass will be substituted for 0317 in finalized production design, pending success of trial production run and cost effectiveness.

\*\*0.96 to 0.97 is the expected reflectance based on the measured transmittance of Corning 0317 and 7809 and optical properties of silver. Modification of silvering process may be required to achieve higher reflectance.

structural and manufacturing simplicity, which equate to low cost. Beams of this design can be roll-formed at high production rates and low tooling costs. The torque tube is split into three sections; two identical outboard sections which support Z-beams, and a center section which interfaces with the gimbal. The split torque-tube design permits a modular transportation and field installation approach, wherein a 6-facet reflector array (assembled in a site building), can be installed in the field with a simple bolted-flange joint. Other key features of the structural frame assembly include:

- o 14 gage, 48 cm (19 in) deep Z-beams and 40.6cm (16 in) O.D. by 0.27cm (0.105 in) wall torque tube - adequate stiffness to meet Specification A10772D deflection requirements in a 12m/s (27 mph) wind.
- o Unique Z-section design which, when coupled with web-loading, provides lateral stability under loading.
- o Alignment pins in mating torque-tube flanges to provide proper alignment of reflector panel subassemblies during field assembly.
- o Galvanized finish for low maintenance 30 yr. life.

The gimbal actuator design selected for the Second Generation Heliostat utilizes a unique planetary gear drive for azimuth motion, and a jack-screw for elevation motion. The azimuth planetary gear drive was selected on the basis of its compactness, high stiffness, adaptability to the cylindrical pedestal O.D., and low cost. The elevation jack-screw uses a conventional gear reduction unit, but incorporates a new polymeric-nut stainless-steel screw actuator which eliminates the cost of lubrication and protective enclosures for lubricated surfaces. Additional features of the gimbal design include:

- o A.C. 3-phase induction drive motors (1/6 hp azimuth and 1/3 hp elevation).
- o Azimuth ball bearing on 53.8cm (21.2 in) diameter circle resulting in:
  - low friction
  - high strength and reliability
  - cost savings through machining of bearing-races in existing parts

- o Cost savings by specifying loose tolerances on orthogonality ( $\pm 0.25^\circ$ ) and azimuth axis perpendicularity to the base mounting surface ( $\pm 0.2^\circ$ ). Compensation for mechanical tolerances is accomplished in software.
- o Low-cost Hall-effect sensors for counting motor revolutions and reference position sensing on each axis.
- o Automatic compensation for elevation drive mechanism wear using sensors and control system.
- o Painted surfaces for corrosion protection.
- o No planned maintenance.
- o  $93^\circ$  of elevation motion and  $180^\circ$  of azimuth motion in 15 minutes.
- o Limit switches on both elevation and azimuth axes to prevent mechanical damage in the event of controls failure.

The pedestal and foundation selected for Second Generation Heliostats is a single-piece piling. It is a commercially available prestressed concrete pile, 7.92m (26 feet) long, and 60cm (23.6in) O.D. and 40cm (15.8 in) I.D. The pile has a relatively high stiffness/weight ratio, resulting from a unique spin casting fabrication process and its hollow section. Galvanized steel bands at top and bottom, and the gimbal interface flange are integral parts of the pedestal. Installation is accomplished by a standard pile driver, to a depth of approximately 4.51m (14.8 ft). The single-piece pile foundation approach was selected because it minimizes field operations, requiring no excavation, form work, re-bar installation, or concrete pouring and curing. The pile design requires no surface finish, is maintenance free and has an indefinite life. It is recognized that the driven-pile design will not be applicable to power plant sites where highly solidified soil and rock strata are present. For those applications, alternate foundation/pedestal designs will have to be used.

The control system designed and built to operate prototype heliostats is a two-tier system composed of; a Digital Equipment Corporation (DEC) LSI 11/2 processor and memory, an ADAC Corporation 1000 M computer chassis, a Data Systems floppy disk unit; an ADM 3A CRT, and a heliostat electronics package. A DEC LA-120 keyboard printer and a DELTEC Model DLC 1260 line voltage regulator were also provided as optional peripheral equipment. The prototype controls provide in a two-tier arrangement, demonstration of the operational

mode capabilities and algorithms required for a more complex "full-field" control system. Production system functions of the heliostat array controller (HAC), heliostat field controller (HFC), and selected functions of the heliostat controller (HC) were consolidated in one microcomputer. Communications between the computer and heliostat are direct signal lines.

Technical and cost saving features demonstrated in the design are:

- o correction for non-vertical azimuth axis and non-orthogonality of gimbal axes
- o compensation of elevation axis wear and mechanical deflection
- o no encoders required - low cost position and motor rotation sensors
- o simplicity of operation with a CRT/terminal
- o weatherproof heliostat electronics

## 1.2 PROTOTYPE DEVELOPMENT AND FABRICATION

Engineering component development testing was conducted primarily on the reflector facets and gimbal. Tests on facets were performed to aid in the selection of materials, provide design data, verify design margins, and substantiate analytical models. In addition, load tests on full-scale facets were conducted to verify structural integrity.

The prototype hardware was fabricated by BEC and various subcontractors. Pittsburgh Corning Co. manufactured the reflector facets at their plant in Port Allegany, Pennsylvania. Ford Aerospace and Communications Corporation of Palo Alto, California, fabricated the gimbal with the support of several subcontractors (Winsmith, et. al.). Centrecon, Inc. of Everett, Washington, manufactured the pedestals. The control system, structural frame and other small components were fabricated by BEC. The components were shipped to Tukwila, WA, where they were assembled and checked out in BEC shops.



After form/fit/function tests, the prototypes were shipped to the Central Receiver Test Facility near Albuquerque, New Mexico. There, pedestals were driven at 314 m (1030 ft.) and 237 m (777 ft.) ranges from the test tower. The heliostats were assembled, aligned, and checked out in preparation for the Sandia test program. Testing was in progress at the time of preparation of this report.

## 2.0 HELIOSTAT DESIGN

### 2.1 Reflector Assembly

The reflector assembly consists of two subassemblies of 6 facets each. Each facet is installed on an H-frame assembly with four adjustable attachment brackets. A complete reflector assembly along with H-frames is shown in Figure 2.1-1.

Figure 2.1-2 is a drawing of the reflector installation.

#### 2.1.1 Facet

##### 2.1.1.1 Detail Design Description

The facet design (Figure 2.1-3) is a composite structure consisting of front and back skins of .015 cm ( 0.058 inch) thick fusion glass sheets, and a cellular glass core. Corning Glass Code 0317 fusion glass was used on production prototype facets, however, Code 7809 is planned for production facets . These sheets are bonded to the core with a two part epoxy polyamide adhesive. The core is fabricated by bonding together blocks of Pittsburgh Corning Foamsil 75 closed-cell cellular glass. The glass skins and core have closely matched thermal coefficients of expansion. This feature minimizes thermal stress and distortions caused by ambient temperature changes. Thermal stability of the facet should produce constant reflected image quality on the receiver over the expected operational temperature range. Materials for the facet are listed in Table 2.1-1.

The facet is designed for quarter point edge mounting using four attachment brackets. These load transfer points plus the magnitude of the loads were used to determine the composite modulus of rigidity required for the facet to meet the deflection requirement and minimize the component stress.

The facet is designed to prevent moisture penetration into the core and glass/core interfaces. Design features incorporated to prevent moisture penetration include: (1) application of a commercial glazing grade hot-melt Butyl sealant to glass-skin-to-core edges;(2) use of a closed-cell glass core

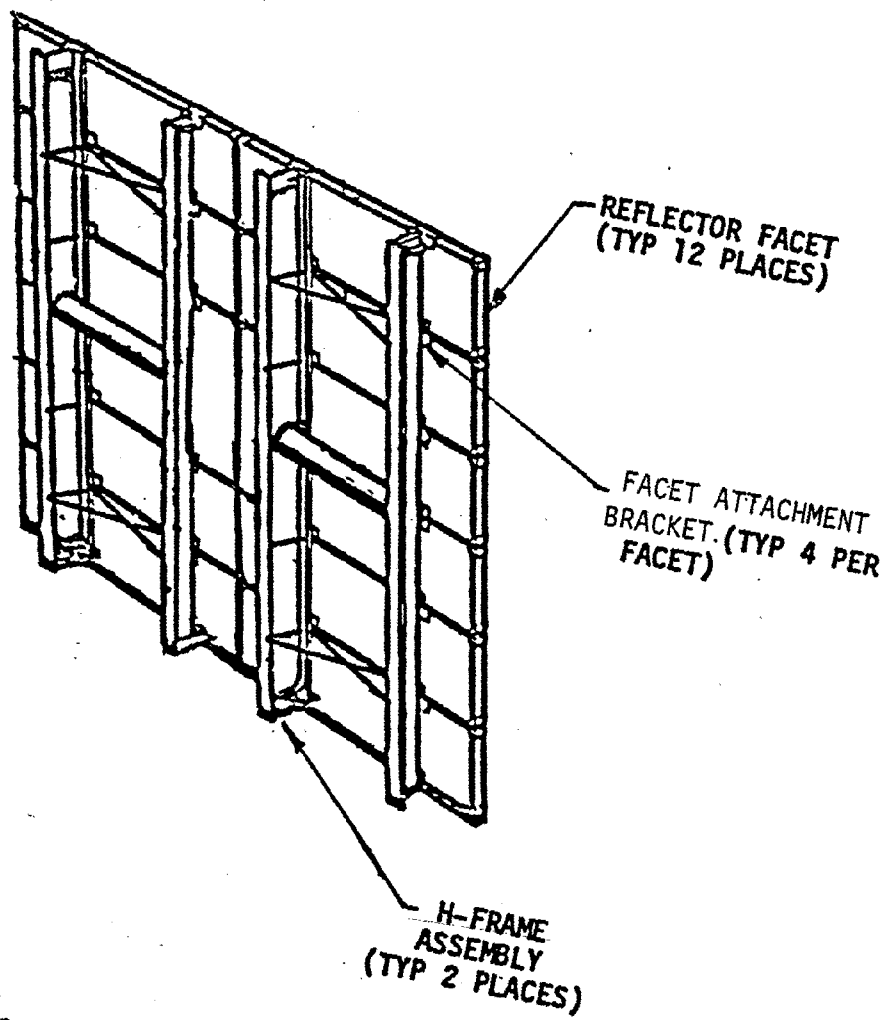
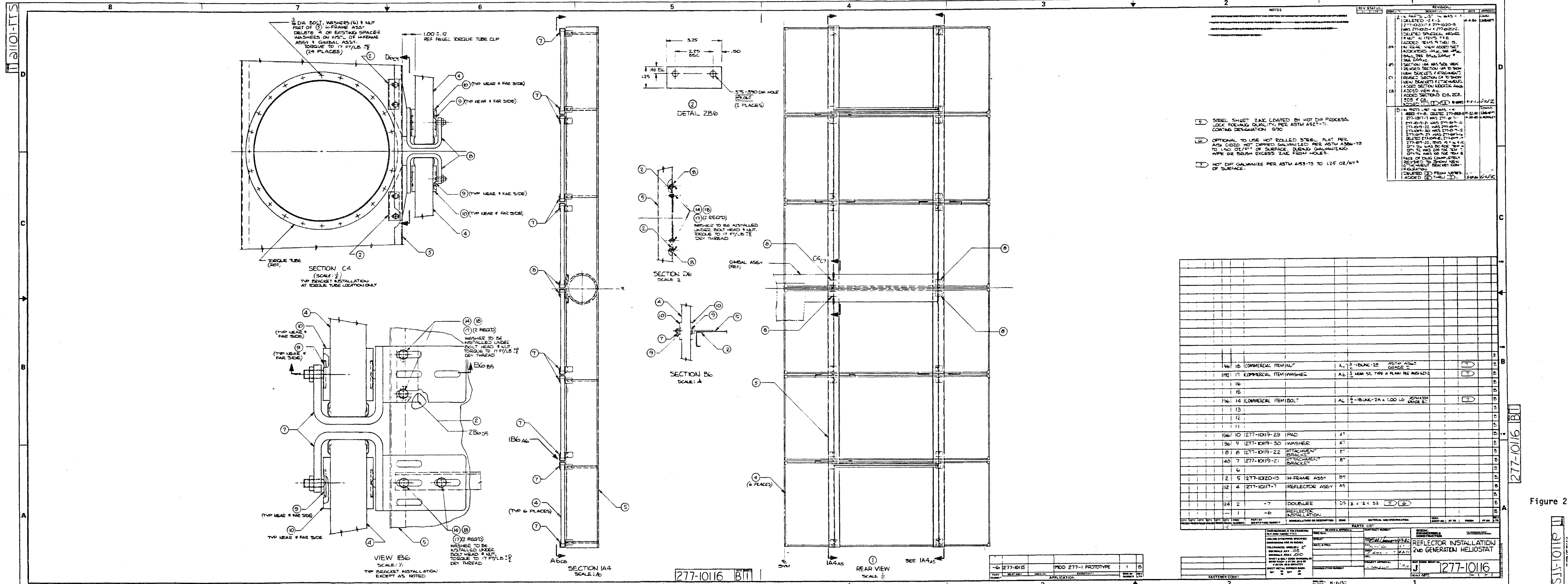


Figure 2.1-1. Reflector Assembly



- NOTES
- 1 STEEL SHEET ZINC COATED BY HOT DIP PROCESS. LOCK FORMING QUALITY PER ASTM A521-71. COATING DESIGNATION G90
  - 2 OPTIONAL TO USE HOT ROLLED STEEL FLAT PER A513-75. HOT ROLLED GALVANIZED PER ASTM A513-75 TO 150 OZ/FT<sup>2</sup> OF SURFACE. BRUSH GALVANIZING W/FE OR BRUSH EXCESS ZINC FROM HOLES.
  - 3 HOT DIP GALVANIZE PER ASTM A513-75 TO 125 OZ/FT<sup>2</sup> OF SURFACE.

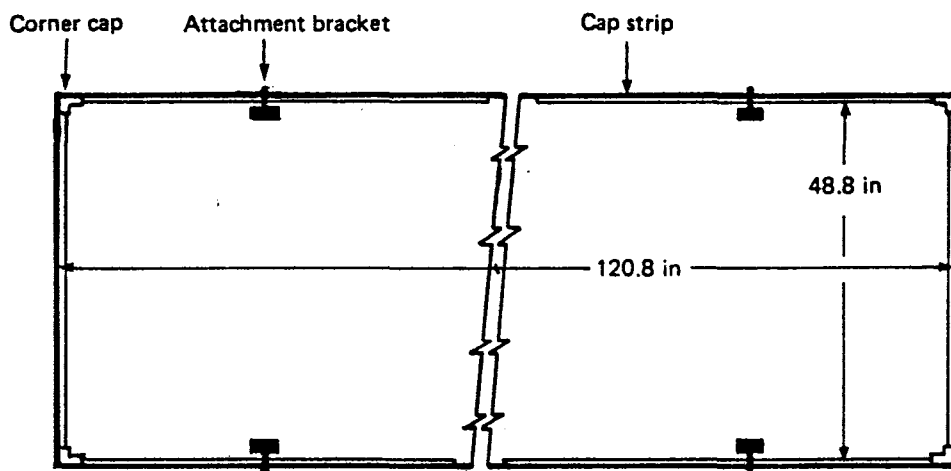
REV.	DESCRIPTION	DATE	BY	CHKD.
1	ISSUED FOR CONSTRUCTION	11-22-80	LM/MTT	
2	REVISED SECTION IA4 TO SHOW NEW BRACKETS & EQUIPMENT	11-22-80	LM/MTT	
3	REVISED SECTION CA TO SHOW NEW BRACKETS & EQUIPMENT	11-22-80	LM/MTT	
4	ADDED SECTION B6 & B7	11-22-80	LM/MTT	
5	ADDED SECTION D6	11-22-80	LM/MTT	
6	ADDED SECTION IB6	11-22-80	LM/MTT	
7	ADDED SECTION IA4	11-22-80	LM/MTT	
8	ADDED SECTION IB6	11-22-80	LM/MTT	
9	ADDED SECTION IB6	11-22-80	LM/MTT	
10	ADDED SECTION IB6	11-22-80	LM/MTT	
11	ADDED SECTION IB6	11-22-80	LM/MTT	
12	ADDED SECTION IB6	11-22-80	LM/MTT	
13	ADDED SECTION IB6	11-22-80	LM/MTT	
14	ADDED SECTION IB6	11-22-80	LM/MTT	
15	ADDED SECTION IB6	11-22-80	LM/MTT	
16	ADDED SECTION IB6	11-22-80	LM/MTT	
17	ADDED SECTION IB6	11-22-80	LM/MTT	
18	ADDED SECTION IB6	11-22-80	LM/MTT	

NO.	DESCRIPTION	QTY	UNIT	MATERIAL	REMARKS
196	18 COMMERCIAL ITEM/WASHER	A6	3	1-BUNK-28 ASTM A562 GRADE C	
192	17 COMMERCIAL ITEM/WASHER	A6	2	NOM SL TYPE A PLAN PER AWS D12	
16					
15					
196	14 COMMERCIAL ITEM/BOLT	A6	2	1-BUNK-2A x 1.00 LG ASTM A325 GRADE B	
13					
12					
11					
196	10 1277-1019-29	IPAD	A7		
196	9 1277-1019-30	WASHER	A7		
18	8 1277-1019-22	ATTACHMENT BRACKET	B		
40	7 1277-1019-21	ATTACHMENT BRACKET	B		
6					
2	5 1277-1019-15	H-FRAME ASSY	B5		
12	4 1277-1017-7	REFLECTOR ASSY	A5		
24	2	-7	DOUBLEE	DS 8 x 12 x 3/4	
1	-6	REFLECTOR INSTALLATION			

REV.	DESCRIPTION	DATE	BY	CHKD.
1	ISSUED FOR CONSTRUCTION	11-22-80	LM/MTT	
2	REVISED SECTION IA4 TO SHOW NEW BRACKETS & EQUIPMENT	11-22-80	LM/MTT	
3	REVISED SECTION CA TO SHOW NEW BRACKETS & EQUIPMENT	11-22-80	LM/MTT	
4	ADDED SECTION B6 & B7	11-22-80	LM/MTT	
5	ADDED SECTION D6	11-22-80	LM/MTT	
6	ADDED SECTION IB6	11-22-80	LM/MTT	
7	ADDED SECTION IA4	11-22-80	LM/MTT	
8	ADDED SECTION IB6	11-22-80	LM/MTT	
9	ADDED SECTION IB6	11-22-80	LM/MTT	
10	ADDED SECTION IB6	11-22-80	LM/MTT	
11	ADDED SECTION IB6	11-22-80	LM/MTT	
12	ADDED SECTION IB6	11-22-80	LM/MTT	
13	ADDED SECTION IB6	11-22-80	LM/MTT	
14	ADDED SECTION IB6	11-22-80	LM/MTT	
15	ADDED SECTION IB6	11-22-80	LM/MTT	
16	ADDED SECTION IB6	11-22-80	LM/MTT	
17	ADDED SECTION IB6	11-22-80	LM/MTT	
18	ADDED SECTION IB6	11-22-80	LM/MTT	

Figure 2.1-2


277-10116



<b>Material usage/weight</b>	<b>~ lbs</b>	<b>Reflector panel</b>
• Fusion glass	55	<b>Dimensions</b>
• Cellular glass	85.0	120.8 in x 48.8 in x 2.2 in
• Steel	9.5	<b>Reflective area</b>
• Adhesive	4.5	3.66 M <sup>2</sup>
<b>Predicted weight</b>	<b>154 lbs</b>	<b>Specular reflectance</b>
		94%
<b>Actual average weight</b>	<b>164 lbs</b>	

Figure 2.1-3. Facet

**Table 2.1-1. Facet Assembly Materials**

Item	Properties		
	Density lbs/cu in	Coef-ther Exp 10 <sup>-6</sup> 	Elast ~ Mod 10 <sup>6</sup> psi
Reflector panel Core: Foamsil 75	0.007	3.5 @ 70°F	0.24
Reflective lite: Prototype — Fusion glass (0317) Production — Fusion glass (7809)	0.08 0.08	4.6 @ 70°F 4.2 @ 70°F	10 10
Adhesive Epoxy-polyamide	—	10 12	—
Sealant Butyl	—	—	—
Cap strip Formed stl. sht ASTM A 366		8.0 8.3	30

 in/in-F°

to minimize air pocket pumping within the sandwich; (3) encapsulation of the entire facet edge with an asphalt/urethane adhesive/sealant; and (4) a painted steel cap strip at all edges. The formed 24-gage steel cap-strip protects the asphalt/urethane and Butyl sealants from ultraviolet radiation, and provides hailstone and handling protection. Figure 2.1-4 shows facet edge configuration details.

The facet's reflective surface, is silvered by a wet silvering process with a minimum silver deposition of 85 mg/ft<sup>2</sup> followed by a deposited copper layer, and finished with a short-oil acrylic primer coat. The high specular transmission of the thin fusion glass sheet (92%), coupled with the reflectivity of the silver, results in a facet specular reflectivity of 0.94. No effort was made to obtain higher reflectance, however, it is expected that a reflectance of 96-97% could be achieved by proper selection of the silvering process (Reference 2-1 and 2-2).

Detailed facet dimensions are shown on the drawing Figure 2.1-5.

#### 2.1.1.2 Trade Studies

A number of trade studies were performed to select the optimal design configuration. Configuration options were resolved on the basis of structural and functional requirements.

Total reflective area was one of the first considerations to be studied. The scope of the study was purposely restrained to include only sizes representing present and near-term glass availability. The study was further limited to heliostat configurations which minimized the number of facets required for a given reflector area. Thus, multiple small-facet configurations were not considered. The reason for this limitation was based on the increased complexity in support framing, mounting and aligning for large numbers of small facets. Three configurations were then selected for evaluation:

1. A 44 m<sup>2</sup> (474 ft.<sup>2</sup>) nominal reflective area using 12 fusion glass facets, each measuring 1.24 m (4 ft.) by 3.07 m (10 ft.).

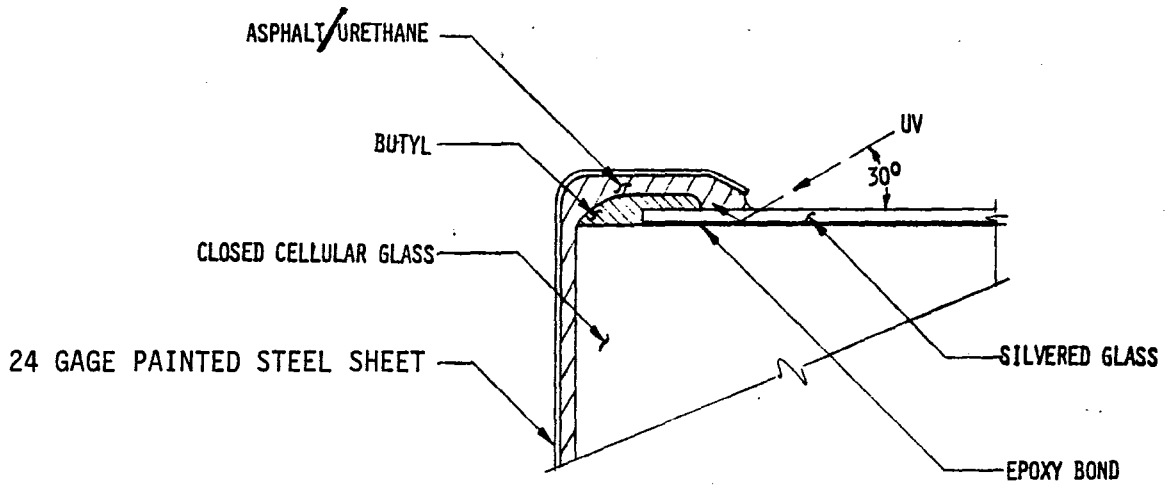
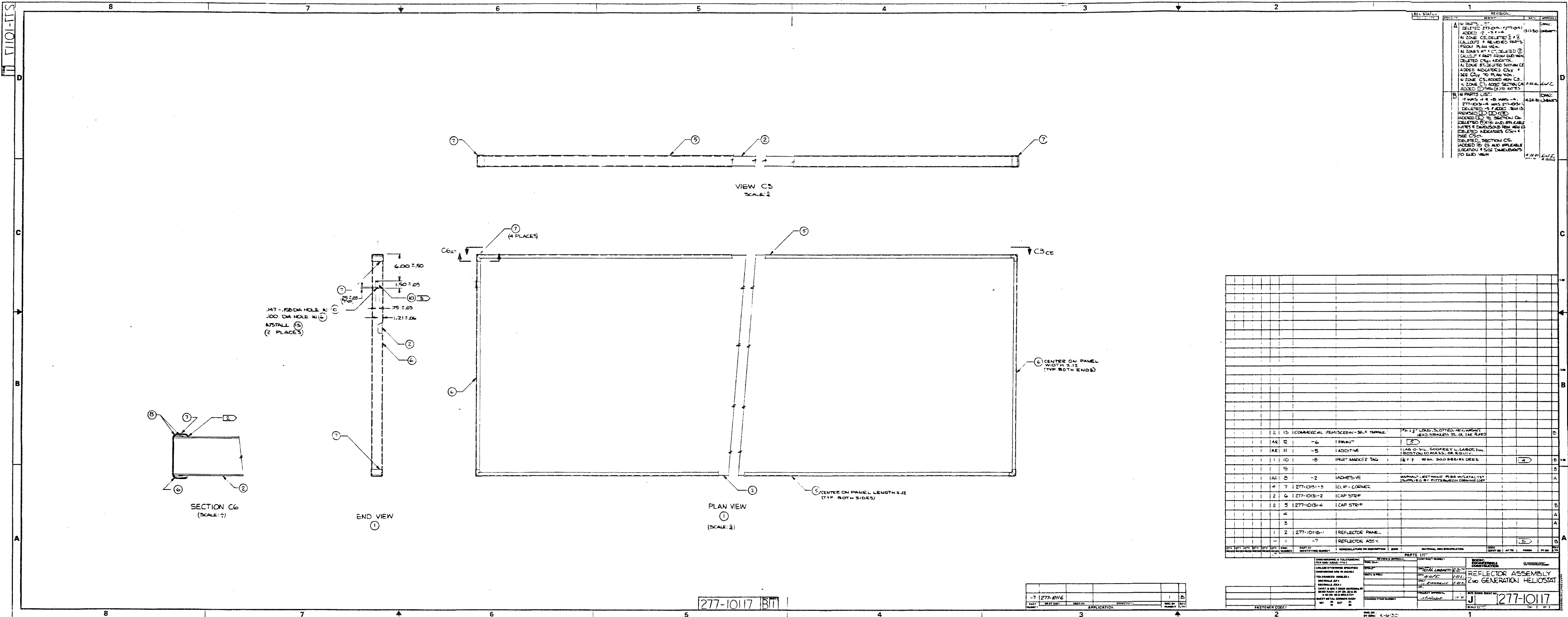


Figure 2.1-4. Facet Assembly Edge Detail





REV	STATUS	REVISION	DATE	APPROVED
A	REVISED	1. IN PARTS LIST 2. DELETED 277-1011-1277-0117 3. ADDED 277-1011-1277-0117 4. IN ZONE CS, DELETED 5 & 6 5. CALLOUTS & RELATED PARTS FROM PLAN VIEW. 6. IN ZONES AT 4, 5, DELETED ② 7. CALLOUT ① & ② FROM END VIEW. 8. DELETED CS ①, ADGATOR. 9. IN ZONE CS, DELETED SECTION C6 10. ADDED INDICATORS C5 ① & 11. SEE C5 ① TO PLAN VIEW. 12. IN ZONE CS, ADDED VIEW C5. 13. IN ZONE C1, ADDED SECTION C4 14. ADDED ① FROM ② TO NOTES.	15-11-80	LIBRARY
B	REVISED	1. IN PARTS LIST: 2. 7 WAS 4 & 8 WAS 5. 3. 277-1011-4 WAS 277-1011-1 4. DELETED 5 & 6 FROM TEAM 15 5. REVISED ① ② ③ ④ ⑤ ⑥ ⑦ ⑧ 6. ADDED ① TO SECTION C6 7. DELETED ② AND APPLICABLE NOTES & DIMENSIONS FROM NEW C6 8. DELETED INDICATORS C5 ① & 9. SEE C5 ①. 10. DELETED SECTION C5. 11. ADDED ② ③ ALSO APPLICABLE LOCATION & SIZE DIMENSIONS TO END VIEW.	4-24-80	LIBRARY

QTY	PART NO.	DESCRIPTION	MATERIAL AND SPECIFICATION	UNIT	REMARKS
12	15	COMMERCIAL ITEM SCREW - SELF TAPPING	1/4" x 2" LK60, SLOTTED, HEAT TREATING HEAD, STRIPPED ST. OR LK60 PLATED		
1	12	FRANK			
1	11	ADHESIVE	1 LB. 0-511, GODFREY L. LABOR, INC. 1 BOTTLE TO MASS. OR EQUIV.		
1	10	PART MARKER TAG	1/2" x 2" NEGA. 300 SERIES CREES		
1	9	ADHESIVE	1/2" x 2" NEGA. 300 SERIES CREES		
1	8	ADHESIVE	1/2" x 2" NEGA. 300 SERIES CREES		
4	7	277-1011-3	CLIP - CORNER		
2	6	277-1011-2	CAP STRIP		
2	5	277-1011-4	CAP STRIP		
1	2	277-1011-1	REFLECTOR PANEL		
1	1	277-1011-1	REFLECTOR ASSY.		

Figure 2.1-5

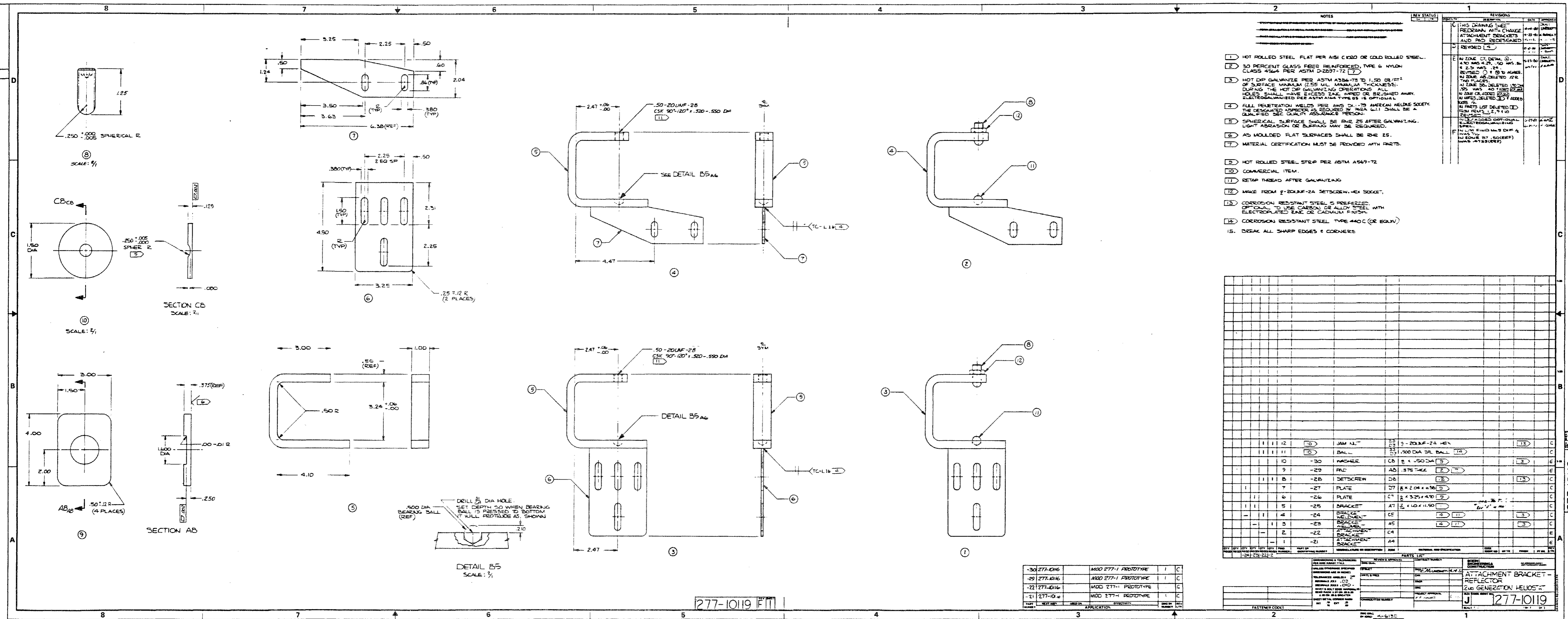
277-10117 BIT

277-10116	1	B
-----------	---	---

**FASTENER CODES:**

**REFLECTOR ASSEMBLY**  
C60 GENERATION HELIOSTAT

277-10117



REV STATUS

NO.	DATE	BY	APP'D	REVISIONS
1	10-18-68	J. J. B. /	W. B. B. /	THIS DRAWING SHEET REDRAWN WITH CHANGE ATTACHMENT BRACKETS AND HOLE DELETED
2	11-21-68	J. J. B. /	W. B. B. /	REMOVED (15)
3	11-21-68	J. J. B. /	W. B. B. /	IN ZONE C7, DETAIL ⑩, 4.90 WAS CHANGED TO 4.90 W/AS 4.24, .50 W/AS .24, .50 W/AS .24, HOLE DELETED (12) IN ZONE A8, DELETED (12) TWO PLACES, IN ZONE B6, DELETED (10) W/AS 4.00 W/AS (12) IN ZONE C8, DELETED (12) IN ZONE C7, DELETED (12) W/AS 4.00 W/AS (12)
4	11-21-68	J. J. B. /	W. B. B. /	IN ZONE C7, DETAIL ⑩, .50 W/AS .24, .50 W/AS .24, HOLE DELETED (12) IN ZONE C7, DELETED (12) W/AS 4.00 W/AS (12)
5	11-21-68	J. J. B. /	W. B. B. /	IN ZONE C7, DETAIL ⑩, .50 W/AS .24, .50 W/AS .24, HOLE DELETED (12) IN ZONE C7, DELETED (12) W/AS 4.00 W/AS (12)
6	11-21-68	J. J. B. /	W. B. B. /	IN ZONE C7, DETAIL ⑩, .50 W/AS .24, .50 W/AS .24, HOLE DELETED (12) IN ZONE C7, DELETED (12) W/AS 4.00 W/AS (12)
7	11-21-68	J. J. B. /	W. B. B. /	IN ZONE C7, DETAIL ⑩, .50 W/AS .24, .50 W/AS .24, HOLE DELETED (12) IN ZONE C7, DELETED (12) W/AS 4.00 W/AS (12)

- NOTES:
- HOT ROLLED STEEL FLAT PER AISI C1020 OR COLD ROLLED STEEL.
  - 30 PERCENT GLASS FIBER REINFORCED, TYPE 6 NYLON CLASS 4564 PER ASTM D-2897-72
  - HOT DIP GALVANIZE PER ASTM A564-75 TO 1.50 OZ./FT<sup>2</sup> OF SURFACE MINIMUM (2.55 MIL. MINIMUM THICKNESS). DURING THE HOT DIP GALVANIZING OPERATIONS, ALL HOLES SHALL HAVE EXCESS ZINC WIPED OR BRUSHED AWAY. ELECTROGALVANIZED PER ASTM A1184 TYPE G5 IS OPTIONAL.
  - FULL PENETRATION WELDS PER AWS D1.1 TO AMERICAN WELDER SOCIETY. THE DESIGNATED WELDER AS REQUIRED BY AWS D1.1 SHALL BE A QUALIFIED WELDER QUALITY ASSURANCE PERSONNEL.
  - SPHERICAL SURFACE SHALL BE RMR 25 AFTER GALVANIZING. LIGHT ABRASION OR BUFFING MAY BE REQUIRED.
  - AS MOULDED FLAT SURFACES SHALL BE RMR 25.
  - MATERIAL CERTIFICATION MUST BE PROVIDED WITH PARTS.
  - HOT ROLLED STEEL STRIP PER ASTM A569-72
  - COMMERCIAL ITEM.
  - RETap THREAD AFTER GALVANIZING.
  - MAKE FROM 2-Z0UNF-2A SETSCREW-4E4 SOCKET.
  - CORROSION RESISTANT STEEL IS PREFERRED. OPTIONAL TO USE CARBON OR ALLOY STEEL WITH ELECTROPLATED ZINC OR CADMIUM FINISH.
  - CORROSION RESISTANT STEEL TYPE 440 C (OR EQUIV.)
  - BREAK ALL SHARP EDGES & CORNERS.

QTY	REV	QTY	REV	QTY	REV	QTY	REV	QTY	REV	PART DESCRIPTION	UNIT	REVISIONS	REVISIONS	
										2-Z0UNF-2A HEX		(13)	C	
										1.500 DIA DR BALL		(14)	C	
										WASHER	CB	1.500 DIA	(15)	E
										PLATE	AD	.375 THK	(16)	E
										SETSCREW	DB		(17)	C
										PLATE	D7	6 x 2.06 x .36	(18)	C
										PLATE	C7	4 x 3.25 x .41	(19)	C
										BRACKET	A7	1/2 x 1.0 x 1.50	(20)	C
										BRACKET	CE		(21)	C
										BRACKET	A5		(22)	C
										BRACKET	C4		(23)	E
										BRACKET	A4		(24)	E

REV	QTY	REV	QTY	REV	QTY	REV	QTY	REV	QTY	PART DESCRIPTION	UNIT	REVISIONS	REVISIONS	
										2-Z0UNF-2A HEX		(13)	C	
										1.500 DIA DR BALL		(14)	C	
										WASHER	CB	1.500 DIA	(15)	E
										PLATE	AD	.375 THK	(16)	E
										SETSCREW	DB		(17)	C
										PLATE	D7	6 x 2.06 x .36	(18)	C
										PLATE	C7	4 x 3.25 x .41	(19)	C
										BRACKET	A7	1/2 x 1.0 x 1.50	(20)	C
										BRACKET	CE		(21)	C
										BRACKET	A5		(22)	C
										BRACKET	C4		(23)	E
										BRACKET	A4		(24)	E

REV	QTY	REV	QTY	REV	QTY	REV	QTY	REV	QTY	PART DESCRIPTION	UNIT	REVISIONS	REVISIONS	
										2-Z0UNF-2A HEX		(13)	C	
										1.500 DIA DR BALL		(14)	C	
										WASHER	CB	1.500 DIA	(15)	E
										PLATE	AD	.375 THK	(16)	E
										SETSCREW	DB		(17)	C
										PLATE	D7	6 x 2.06 x .36	(18)	C
										PLATE	C7	4 x 3.25 x .41	(19)	C
										BRACKET	A7	1/2 x 1.0 x 1.50	(20)	C
										BRACKET	CE		(21)	C
										BRACKET	A5		(22)	C
										BRACKET	C4		(23)	E
										BRACKET	A4		(24)	E

277-1019

2. A 48.36 m<sup>2</sup> (520 ft<sup>2</sup>) net reflective area using 12 low iron float glass facets, each measuring 1.24 m (4 ft.) by 3.35 m (11 ft.).
3. A 51.42 m<sup>2</sup> (553 ft<sup>2</sup>) net reflective area using 14 fusion glass facets, each measuring 1.24 m (4 ft.) by 3.07 m (10 ft.).

The support structures for these configurations consisted of 2 H-frames and a gimbal torque tube. The structural sizing of the support members was derived based on maintaining the same deflection allowables. Other heliostat components were also adjusted to maintain the same performance level for the three configurations. Cost estimates were then developed for the three configurations.

The DELSOL computer program provided by Sandia was then used to predict busbar energy costs for each configuration. No significant difference between the three configurations was found, based on this analysis. Therefore, the smaller of the three configurations using fusion glass was selected for development. The principal reason for this selection was the higher reflectance of fusion glass. In addition, fusion glass sheets are presently made in 1.24 m (4 ft.) by 3.1 m (10 ft.) sheets, 0.15 cm (.058 in) thick. When silvered, these mirrors have a specular reflectance of 0.94, although 0.96-0.97 was expected, based on glass transmittance and properties of silver. Low-iron float-glass was recently made for the Barstow plant which exhibits reflectance ranging from 0.907 to 0.931, depending on the mirror manufacturer used for silvering (reference 2-2 ). This experimental run of low-iron float-glass was a nominal 0.32 cm (0.125 in.) thick.

Fusion glass was finally selected for both the front and back skins based on performance, weight and cost, the latter based on a 50,000 heliostat-per-year production rate. However, the design is not restricted to the use of fusion glass. Should events such as lower production rates, supply problems, or improvements in float-glass solar performance occur, the alternate combinations or types of glass can be used with minimal design impact.

### 2.1.1.3 Analyses

A finite element NASTRAN analysis was used to predict the stress state and deflections of the facet under various load conditions. Material tests and industry standards were used to establish acceptable design stress allowables. The results of the analysis, design allowables and margins of safety are presented in Table 2.1-2. It is seen from the table that no deflections occur that exceed the allowable under operating condition, except at 32°F where deflection is approximately 10% in excess of allowed. Several factors of stress margin exist in the skins and core for normal operating conditions. At the 40 m/s (90 mph) (worst case) condition, some margin still exists, although greatly reduced. The latter condition, however, has an extremely low occurrence frequency over the life of the power plant.

A thermal analysis was also performed to evaluate the facet design. The thermal model investigated both steady-state and transient temperature gradients across the panel. The worst thermal case in terms of facet deflection occurred under the following conditions: ambient temperature 0°C, sky temperature -11°C, insolation based on a typical winter day at Albuquerque and zero wind. These assumptions generated a 2.2°C temperature gradient between front and back skins. This differential temperature resulted in a 1 sigma value for the slope error of 0.22 mrad (including gravity effect). Using the same analysis, but allowing a slight wind to be present, drives the temperature gradient to near zero which results in negligible slope errors due to thermal effects.

### 2.1.1.4 Tests

Engineering load tests were conducted on full size facets to verify structural and functional integrity. Coupons representing the facet construction were subjected to temperature, humidity and hailstone testing. Thirty-four facet specimens were tested to establish their modulus of rupture; and several cellular glass core samples were shear tested to establish the core shear allowable. Tests were also conducted to aid in the selection of materials, provide design data, verify design margins or substantiate analytical models. Descriptions and results of these tests are provided in Appendix E.

Table 2.1-2. Facet Stress, Deflections Under Various Conditions

CONDITION	Cond. no.	<span style="border: 1px solid black; padding: 2px;">1</span>	<span style="border: 1px solid black; padding: 2px;">2</span>	<span style="border: 1px solid black; padding: 2px;">2</span>	<span style="border: 1px solid black; padding: 2px;">2</span>
		(m.rad.) $\theta_{Allow}$	$F_t$ (psi) $F_{ref}$	$F_t$ (psi) $F_{back}$	$F_s$ (psi) $F_{core}$
Static $\alpha_0 = 0^\circ$	0 (Ref)	0.20 0.08	—	—	—
27 mph $\alpha = 10^\circ$ $T = 70^\circ F$	1	0.20 0.14	1,000. 220.	1,000. 210.	84. 10.
No-wind $T_{amb} = 32^\circ F$ ( $\Delta T = 4^\circ$ )	3	0.20 0.22	1,000. 300.	1,000. 260.	84. 10.
90 mph $\alpha_0 = 0^\circ$ (Wind $\pm 10^\circ$ )	7	—	2,000. 1,120.	2,000. 1,080.	84. 60.

1 Per error budget (BEC)

2 Per design allowables (BEC)

$F_t = 2,000$ . psi probable minimum (long-time) strength  
 $F_t = 1,000$ . psi working stress in flexure (F.S. = 2)  
 $F_s = 84$ . psi shear (test)

## 2.1.2 Attachment Bracket

### 2.1.2.1 Detail Design Description

The primary functions of the attachment brackets are to provide: load paths between the facets and support structure, adjustment capability for canting of facets, compensation for manufacturing tolerances, and flexibility for absorbing relative motion caused by mismatches in thermal expansion. As a design goal, it was decided to avoid carrying facet loads through bonded joints because of the 30 yr life requirement.

Winds generate pressure gradients both over the surfaces and across the facets. These pressure loads are reacted normal to the facet faces with in-plane facet loads approximately zero. The only in-plane facet loads are due to gravity and earthquake.

Figure 2.1-6 is the detail drawing for the bracket assembly.

Eight different configurations were evaluated based on cost and functional and structural requirements. As a result of this evaluation, a design was selected which consisted of a formed metal C shape with a flat tab for mounting on the frame assembly. Top and bottom plastic pads interface with the facet glass surfaces and transmit loads to the C-bracket through ball joints. Each pad is recessed to accommodate a steel washer. The bottom pad is seated on a steel ball bearing. The ball bearing is press fitted into the bracket. The top pad washer is contacted by a hemispherical-tipped stud which is threaded through the upper leg of the bracket. The threaded stud is used to take up manufacturing tolerances between the facet and the bracket.

A combination of slotted holes in the support structure beams and the bracket allows alignment adjustment capability. Once the facets are oriented, the brackets are secured to the frame beams with bolts, nuts and lock washers.

The primary feature of the reflector assembly is the free-float mount design for the reflector facets. This method of mounting isolates the facets from deflections caused by differential thermal growth between the facets and

support structure. It also eliminates the transfer of moment loads between the facets and the frames, thus reducing combined stresses in the facets and allowing them to act as unrestrained plates.

The advantage of the free-float design is that the effect of frame deflections on the flatness of the facets is minimized. Analysis shows that this method will provide better heliostat performance over a wide range of wind velocities and ambient temperatures as opposed to more rigid mounting.

#### 2.1.2.2 Tests

Tests were performed to aid in the selecting of adequate pad area, and to establish their preferred location relative to the facet edge. A test description and detailed results are provided in Appendix E.

Representative glass reinforced Nylon pads of circular and rectangular configuration were compression loaded onto facet composite panels. Loading was increased until glass failure occurred. Results showed that the (7.6 x 10.2 cm) rectangular pad selected would provide a glass failure design margin of approximately 210%.

## 2.2 FRAME ASSEMBLY

### 2.2.1 Detail Design Description

The frame assembly is illustrated in Figure 2.2-1. It consists of two identical H-frame assemblies which bolt to the gimbal torque tube. An H-frame assembly consists of two deep-section, 7.62 m (25 ft.) long, Z-beams bolted to a 40.6 cm (16 in.) diameter center torque tube. The Z-beams are 14 gage galvanized steel, 48.3 cm (19 in.) deep. Cross braces between the outboard beam ends provide lateral stability. Bolted connections are used throughout the assembly. The bolt flanges on the torque tube are welded to the torque tube prior to galvanizing. All components including nuts, bolts and washers are galvanized for corrosion protection. Weights of individual frame components, single frame and double frame weights are tabulated below.

COMPONENT	WEIGHT	
	KGS	(LBS)
Z-Beams (2)	168	(370)
Braces, Stiffeners, Fasteners	11.3	( 25)
Torque Tube Section (1)	47.6	(105)
Support Brackets (24)	34.1	( 75)
Total(One H-Frame)	261	(575)
Total (Two H-Frames)	522	(1150)

Figure 2.2-2 shows the frame assembly details. Five beam configurations were considered as illustrated in Figure 2.2-3. The various beams represented different shapes and methods of manufacture. Principal comparison criteria included lateral and vertical stiffeners, weight and cost. When these criteria were applied to the optional configurations, the reinforced web, Z-beam proved best and was therefore selected for detail design.



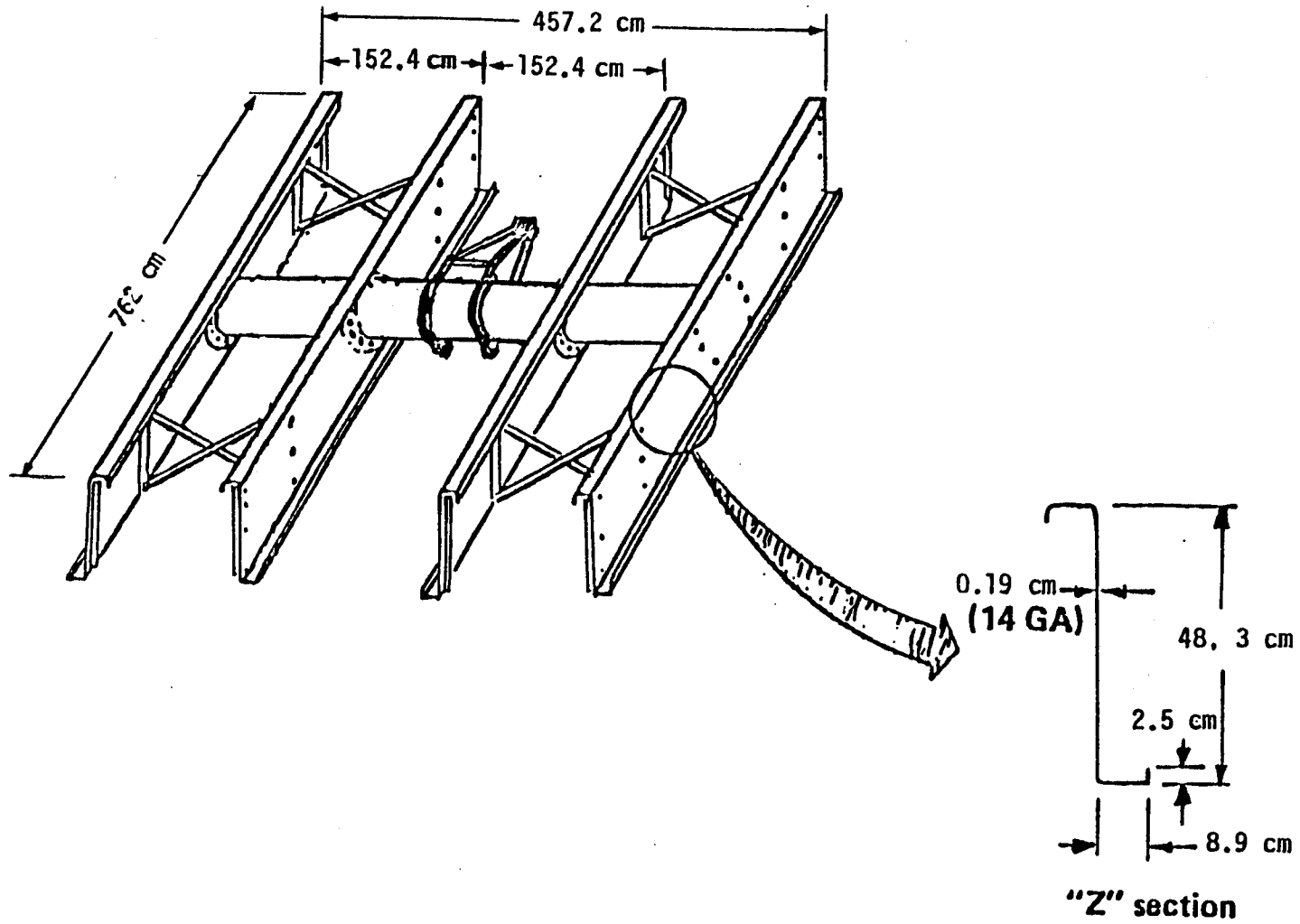


Figure 2.2-1. Reflector Frame Assembly

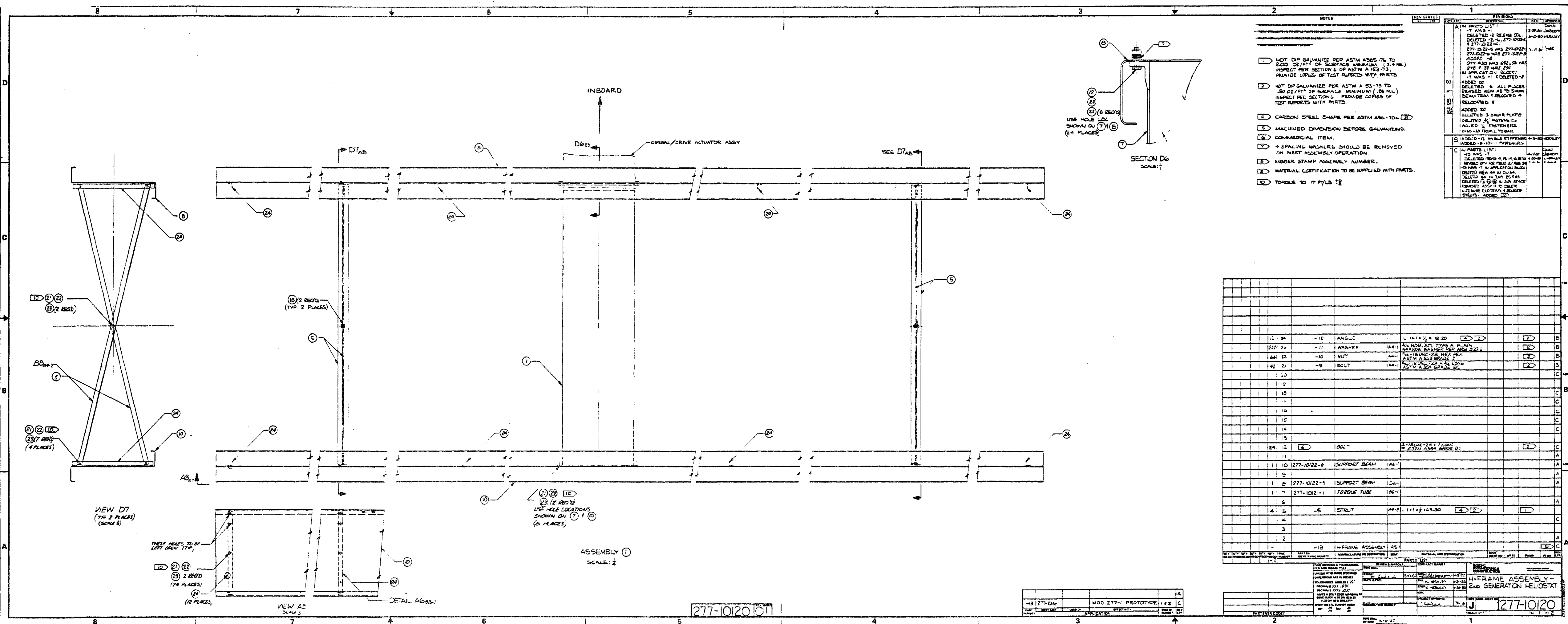


Figure 2.2-2

Figure 2.2-3. Candidate Beam Configurations

	CONCEPT				
	NO. 1	NO. 2	NO. 3	NO. 4	NO. 5
CHARACTERISTIC					
Weight	201.34 lbs	232.0 lbs	155.2 lbs	173.4 lbs	173.4 lbs

A NASTRAN analysis was used to determine the number, size and location of the local web stiffeners which distribute the attachment bracket loads into the Z-beams. The performance of the frame assembly was evaluated under two conditions: deflections under operational conditions, and structural integrity during survival conditions. The NASTRAN finite element model was also used to determine support frame deflections. The model predicted that a 0.76 mrad maximum deflection would occur during 12 m/s ( 27 mph) wind at the outboard end of the outboard beam. Stress analysis at survival conditions resulted in positive margins of safety for all components.

No tests were conducted on the frame assembly by BEC.

## 2.3 Gimbal Actuator

### 2.3.1 Gimbal Actuator Drive Assembly

#### 2.3.1.1 Design Description

The gimbal/actuator drive assembly is the structural/mechanical unit which supports the reflector assembly and provides azimuth/elevation motion. This unit is illustrated in Figure 2.3-1 and consists of three basic subassemblies: gimbal housing and azimuth drive/bearing; elevation arms; and elevation drive.

##### 2.3.1.1.1 Gimbal Housing and Azimuth Drive/Bearing

The gimbal housing and azimuth drive/bearing unit is shown in Figure 2.3-2. The gimbal housing is a compact low cost nodular iron casting providing efficient structural load transfer from the elevation axis to the azimuth drive/bearing assembly. Figures 2.3-3 and -4 illustrate the azimuth drive/bearing assembly, consisting of the input worm speed reducer plus the unique differential planetary drive with integral ball bearing.

The conventional single four-point contact ball bearing provides high stiffness, high reliability, and low friction at low cost since both raceways are simply cut directly into the two drive ring gears. Accurate preloading is economically obtained.

The differential planetary plus worm drive provides a high drive ratio in a compact package. The maximum drive ratio of 52,500:1 has been selected consistent with the slew travel rate and motor RPM, to permit the smallest motor (and lowest operating cost) at negligible cost impact to the drive. The differential planetary drive has inherent high stiffness/strength, low backlash and no backdriving. The unit can be economically mass produced with fairly simple machining, easy assembly, and maximum use of castings. The castings and materials are: upper and lower casting, grey iron; upper and lower ring gear, nodular iron; planetary carrier, grey iron; and three planetary gears, meehanite iron.

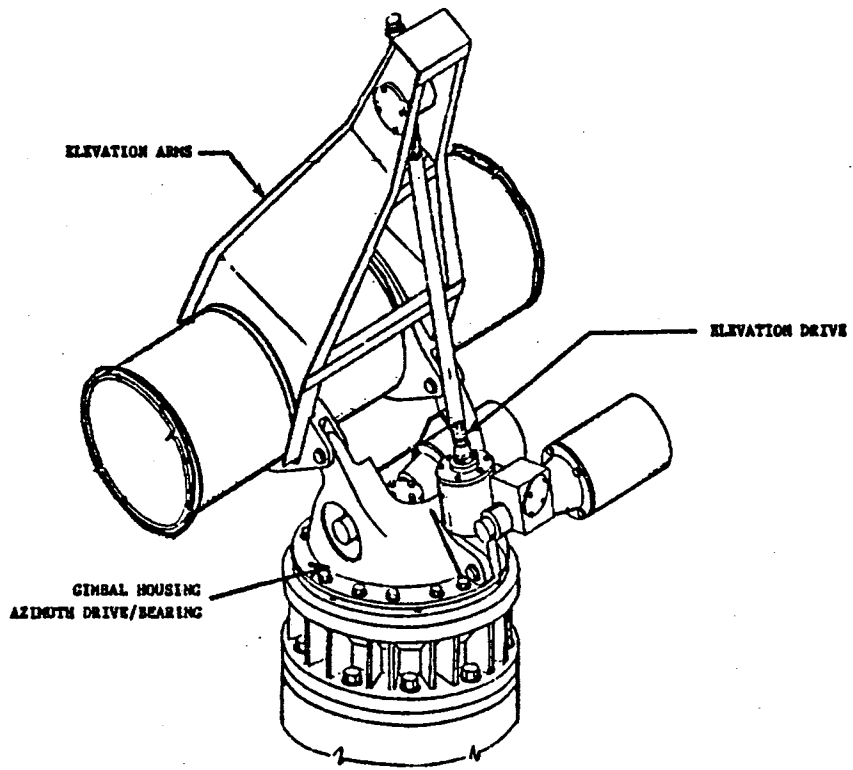


Figure 2.3-1. Gimbal/Actuator Drive Assembly

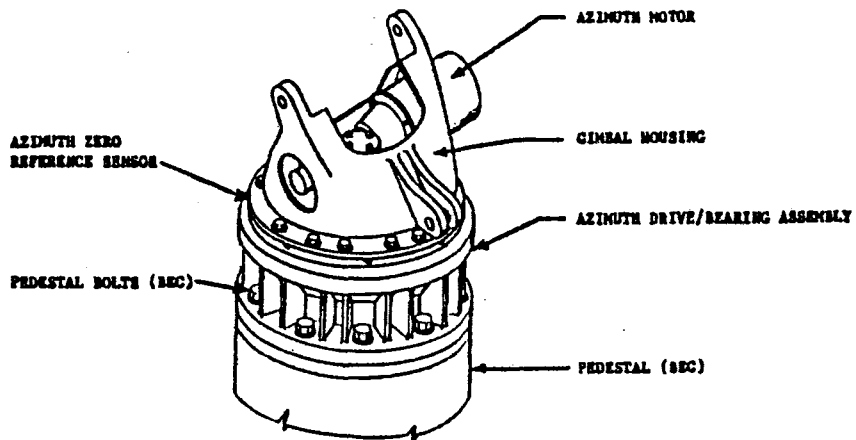


Figure 2.3-2. Gimbal Housing and Azimuth Drive/Bearing Assembly

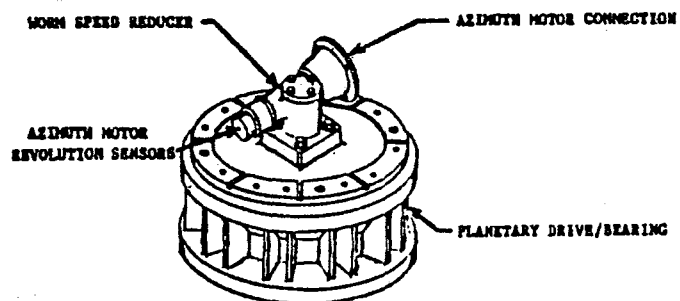


Figure 2.3-3. Azimuth Drive/Bearing Assembly

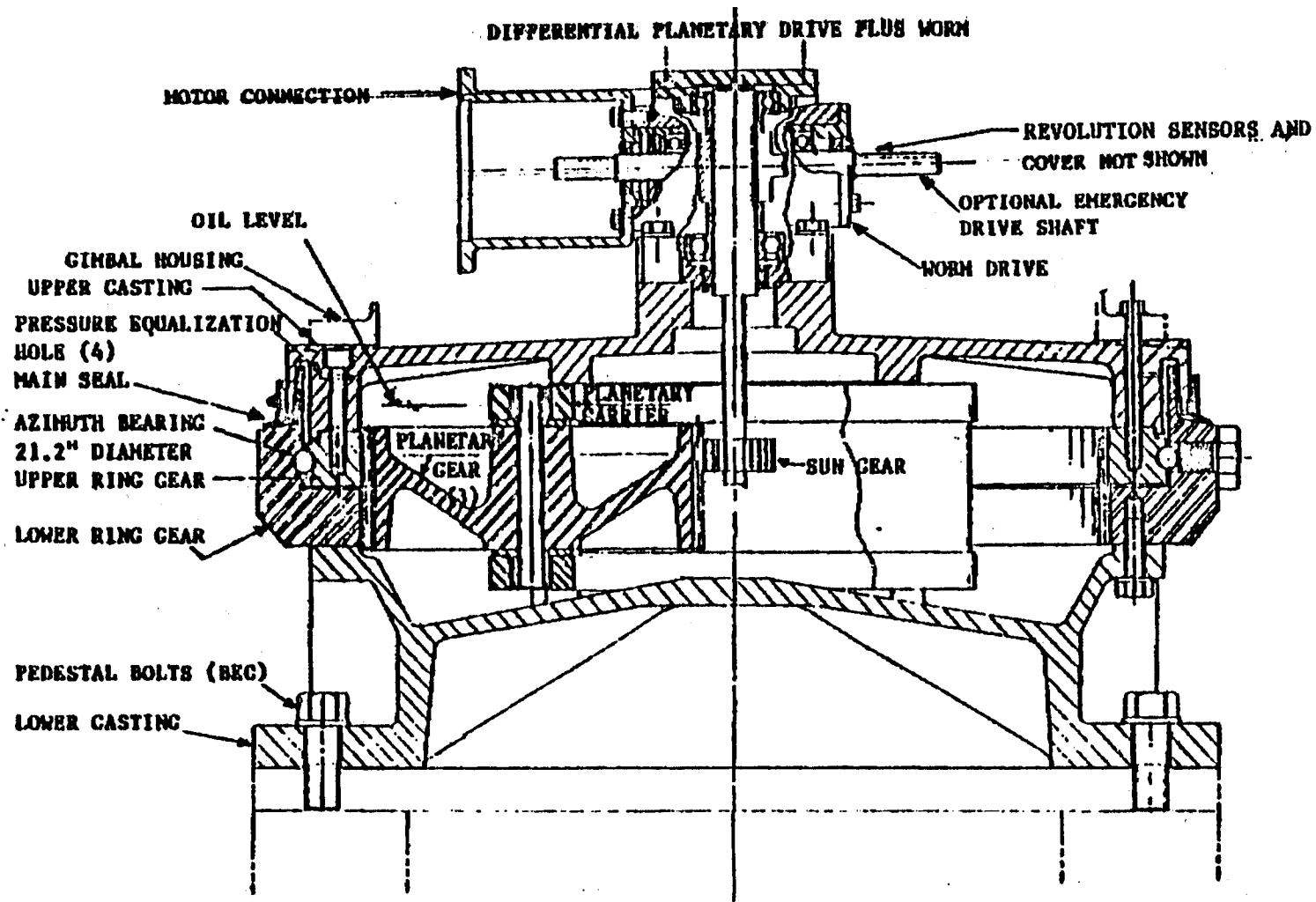


Figure 2.3-4 Cross-Section of Azimuth Drive/Bearing Assembly



The input worm drive and the planetary drive/bearing are each submerged in oil ensuring long and trouble-free life. The main azimuth seal is Viton with a circumferential clamp designed primarily to keep the contaminants out.

#### 2.3.1.1.2 Elevation Arms

The elevation arms, shown in Figure 2.3-5, are shop assembled as an integral unit with the center-section reflector torque tube and attached to the gimbal housing with two elevation bearing pins.

Volume production allows economical use of castings and stampings and accurate tolerances for the critical dimensions. The tube to arms adapters are nodular iron castings, seam welded in complete rings to the torque tube. The arms are stamped 10-gauge steel. Full account has been taken of local buckling in the design details. The entire unit is hot-dip galvanized for low maintenance 30 year life. Each elevation bearing is a self-lubricating teflon filled bushing on a 1 inch (25 mm) diameter stainless steel pin in double shear.

#### 2.3.1.1.3 Elevation Drive

The components of the elevation drive assembly are shown in Figure 2.3-6. Attachment to the arms is by bolted nut retainers and to the gimbal housing with a pivot pin similar to the elevation bearings.

The linear actuator is the most cost effective system to accommodate the 96° of elevation travel. The geometry of the overall gimbal/actuator has been selected so that under normal operating conditions the reflectors' weight always keeps the actuator in tension (under certain wind load conditions, load reversal can occur when the reflector assembly approaches a few degrees of horizontal). This off-center load feature eliminates elevation backlash. The polymeric nut and stainless steel screw do not require lubrication, thus minimizing life cycle costs. (See Section 2.3.1.4.1).

The two-stage worm speed reducer is housed in an integral casting which includes the pivot lug. Its drive ratio is 240:1 for an overall average elevation drive ratio of 101,000:1. This system exhibits high stiffness with no backdriving.

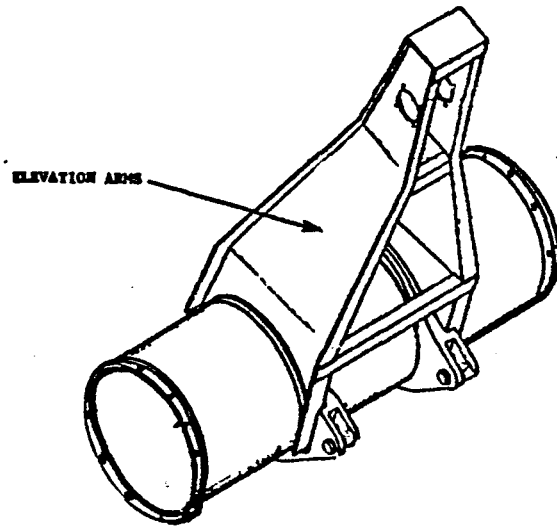


Figure 2.3-5. Elevation Arm and Center Torque-Tube Assembly

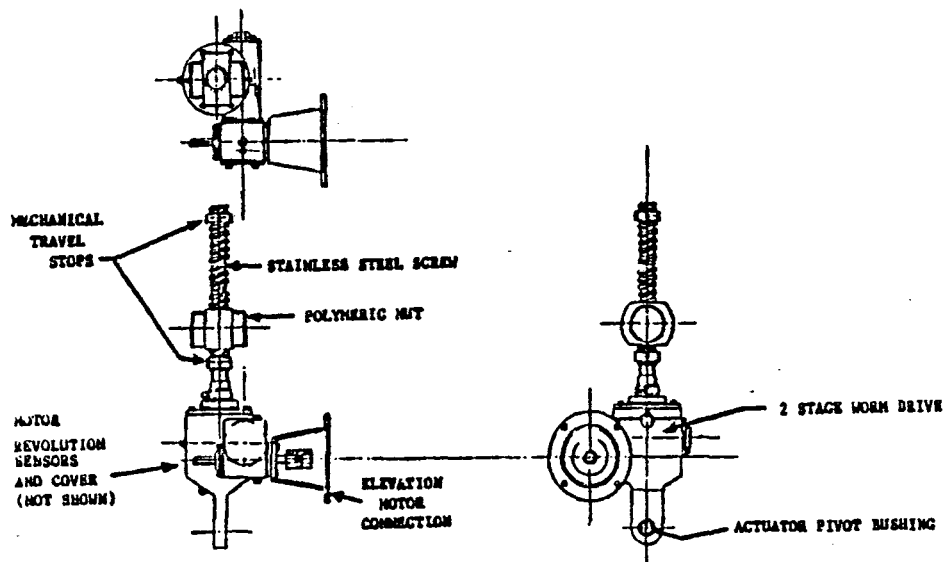


Figure 2.3-6. Elevation Drive Assembly

#### 2.3.1.1.4 Design Drawings

Detail design of the prototype gimbal/actuator drive assembly is depicted in the following drawings, which are submitted separately:

TITLE	DRAWING NUMBER
Gimbal/Actuator Drive Assembly	FACC 531149 (5 sheets)
Interface Control Drawing	FACC 531150
Gimbal Housing	FACC 531146 (2 sheets)
Torque Tube/Arms Assembly	FACC 531147 (2 sheets)
Miscellaneous Details	FACC 531148 (5 sheets)
Azimuth Drive/Bearing Assembly	Winsmith E-651133-60 and D-651133-2
Elevation Drive Assembly	Winsmith C-651140-2 and C-X1002-6

#### 2.3.1.2 Configuration Trades

Various trades were conducted to select preferred design approaches for components of the gimbal actuator.

##### 2.3.1.2.1 Azimuth Drive/Bearing Assembly

Three different types of drive and bearing assemblies were investigated for the azimuth axis. The first of the three designs was a 3-stage worm gear speed reducer; second was a 3-stage simple planetary drive with input worm drive; and third was a one-stage differential planetary drive with input worm drive. A primary consideration for not investigating other possible azimuth configurations was that the three drives considered can accommodate an economical integral ball bearing.

The third drive option, using a differential planetary plus input worm drive, was selected because of its low cost, and because:

- (1) Use of differential planetary plus worm drive produces a high drive ratio in a compact package thus minimizing the material weight of the total component.
- (2) It has high stiffness/strength in both azimuth and elevation axes because all output loads are at a large radius; there are no small diameter shafts subjected to high torque; and torsional loads are shared by three pinions.
- (3) The unit can be economically mass produced since machining and assembly are fairly simple.
- (4) The main drive housing can be designed so that there is no oil leakage path. A main seal can be provided to keep contaminants out, and it is not under oil pressure.
- (5) Use of high ratio differential planetary arrangements precludes backdriving and makes the arrangement self locking.
- (6) Since the loads are shared by three pinions, the pinion teeth are small and accurate. This feature plus the large gear radius results in low backlash.
- (7) The drive uses proven technology based on widely-used designs; this results in a very low risk design.
- (8) The drive uses a single integral four-point-contact ball bearing which does not require any extra races, as both raceways are cut directly into the two ring gears; uses conventional ball bearings, resulting in low friction, high reliability, and economical, accurate preloading; and all the balls are totally submerged in oil, ensuring long and trouble free life.

#### 2.3.1.2.2 Elevation Drive Assembly

The final elevation drive assembly was selected after performing the following trade studies: rotary gear drive vs. linear actuator drive; machine screw vs. ball screw actuator; different actuator arrangements; and plastic nut vs. bronze nut for the actuator. The trade studies considered cost, producibility, performance, and other technical characteristics. (See Volume 1, Appendix II).

The rotary-gear-drive vs. linear-actuator-drive trade study resulted in selection of the linear actuator drive. The machine screw vs. ball screw trade study resulted in selection of the machine screw. The different actuator arrangement trade and the plastic nut vs. bronze nut trade resulted in selection of the non-lubricated, translating plastic nut with a rotating corrosion resistant stainless screw.

#### 2.3.1.2.3 Elevation Bearings

The elevation bearing arrangement trade evaluated rolling element bearings vs. bronze bushings vs. plastic bushings. The result was to select the self-lubricating plastic bushings since rolling element bearings, though they have lower friction, are more expensive and would require periodic relubrication. Bronze bushings were rejected because they have less capacity than high capacity plastic bushings, and depend on high relative velocity for lubrication of the shaft, which is not present in this design.

#### 2.3.1.2.4 Gimbal Housing Structure and Torque Tube/Arms Assembly

Many geometric variations were investigated for the overall drive assembly. The principal considerations were operational pointing error, backlash, survival strength, and cost. These criteria resulted in selection of an efficient, low-cost design for the gimbal housing and torque tube/arm assembly.

### 2.3.1.3 Analysis

The gimbal/actuator drive assembly components were primarily designed for the survival loads and the resulting design was subsequently checked for pointing error requirements. The pointing error for the design based on survival requirements was shown to be within the allowable budget.

#### 2.3.1.3.1 Gimbal Housing and Center Torque Tube/Arms Assembly Structural Analysis

The analysis of the structural components of the gimbal/actuator assembly is included in Ref. 2-5. This analysis includes the stress analysis and compliance analysis for the gimbal housing center torque tube and arms.

#### 2.3.1.3.2 Azimuth Drive/Bearing Analysis

The azimuth drive analysis is included in Reference 2-5. Maximum loads on the azimuth drive are for 22 m/s (50 mph) wind. Actual drive loads were calculated and allowable compliances were established for the budgeted pointing errors. Drive components were then designed to maintain the stress levels and compliances within these established values. The analysis shows that all gearing and azimuth bearing stresses are less than allowable and that the estimated compliances and backlash are less than those allocated.

#### 2.3.1.3.3 Elevation Drive Analysis

The elevation drive analysis is included in Ref. 2-5. This analysis verified that the various components of the elevation drive are adequate for the heliostat application. This analysis also shows how drive compliance is estimated, and confirms that the maximum operating load on the actuator screw is  $3.74 \times 10^4$  N (8400 lbs), which is below the  $4.45 \times 10^4$  N (10,000 lbs) capacity of 3.8 cm (1.5 inch) diameter screw. Maximum static load on the screw is  $9.79 \times 10^4$  N (22,000 lbs) tensile, and the polymeric nut is designed to have a safety factor of more than two for this condition.

The elevation drive uses a 1/3 hp motor and analysis shows that it has adequate capacity to drive to stop against the worst case 22 m/s (50 mph) wind.

Mechanical stops are located at both ends of the actuator travel. In the event of a control failure, the polymeric nut will travel up against a stop and stall the drive motor, which will be automatically switched off as it overheats. This condition has been verified experimentally and analytically.

#### 2.3.1.3.4 Elevation Bearing Analysis

The elevation bearing analysis is included in Ref. 2-5. Bearing loads are calculated in this analysis, based on predicted axis loads. The analysis shows that the elevation bearings have more than adequate capacity to withstand the worst case load, and that the elevation shaft has adequate margin of safety against shear failure. The elevation bearing arrangement is such that the contribution to pointing error is negligible.

#### 2.3.1.3.5 Pointing Error Analysis

The pointing error analysis is included in Ref. 2-5. Pointing error requirements are separated into two parts: no wind pointing error, and 12 m/s (27 mph) wind pointing error. Under the first condition, the allowable pointing error for each axis is 0.5 mrad standard deviation (1 sigma). The analysis shows that the predicted error is within the allowable value.

Under the second condition, the pointing error budgeted is 3.0 mrad (3 sigma), for each axis. The analysis shows that actual error is well within this limit: approximately 1.8 mrad in the azimuth axis (reflector vertical) and 2.2 mrad in the elevation axis (reflector horizontal) in a 12 m/s wind.

#### 2.3.1.4 Tests

Three main types of testing were performed on the gimbal/actuator and components: elevation actuator screw and nut tests; azimuth-drive tests; and gimbal/actuator assembly tests. Detailed results of these are given in Appendices B, C and D.

#### 2.3.1.4.1 Elevation Actuator Screw and Nut Tests

The test procedures for the actuator screw and nut are included in Ref. 2-5. The purpose of these tests was to determine the durability of the stainless steel screw/polymeric nut elevation drive for heliostat application. Two different unlubricated polymeric nuts and unlubricated bronze nuts were tested on a test screw under the load conditions representative of actual life and for a time period that duplicated 30 year life for the actual screw. Also, the actuator screw and nuts were subjected to water spray and sand to simulate actual environmental conditions. At the end of the test, the effects on backlash and friction torque were evaluated to select the best nut material for the application.

#### 2.3.1.4.2 Azimuth Drive Tests

The test procedures for the prototype azimuth drive are included in Ref. 2-5. These tests consisted of:

- (1) Application of survival loads to verify that the azimuth drive could withstand the torque corresponding to a survival wind velocity of 22 m/s (50 mph);
- (2) Checking non-backdriving feature of the azimuth drive to verify that the heliostat would not wander about the azimuth axis due to wind torque;
- (3) Measuring the backlash to verify that the drive backlash was within the budgetary allowance for the azimuth drive; and
- (4) Measuring the torsional stiffness and the moment stiffness to verify that the error resulting due to 12 m/s (27 mph) wind was within the specified value.



#### 2.3.1.4.3 Gimbal/Actuator Assembly Tests

A complete gimbal/actuator was assembled and tested to verify that it met the performance requirements. The test procedures for these tests are included in Ref. 2-5. These tests consisted of:

- (1) Checking and recording non-orthogonality of azimuth and elevation axes;
- (2) Verifying the capability of the azimuth and elevation drive motors to drive against the maximum operational load corresponding to 22 m/s (50 mph) wind;
- (3) Verifying the non-backdriving feature of the elevation drive;
- (4) Application of survival loads, both about elevation axis and azimuth axis to verify that the gimbal/actuator drive assembly could withstand torque corresponding to survival wind of 22 m/s (50 mph) about the azimuth axis, and torque corresponding to survival wind of 40 m/s (90 mph) about the elevation axis;
- (5) Measuring the torsional stiffness about the azimuth axis and the moment stiffness about the elevation axis to verify that the errors resulting due to 12 m/s (27 mph) wind were within the specified value;
- (6) Checking the travel limits to verify that the assembly could travel at least  $\pm 165^\circ$  about azimuth axis and  $-3^\circ$  to  $+93^\circ$  about elevation axis; and,
- (7) Verifying that the elevation drive could be moved to the horizontal position without use of drive motors.

## 2.3.2 Drive Motors

### 2.3.2.1 Detail Design Description

Motors are required to rotate the input drive shafts of the elevation and azimuth assemblies. General design requirements for motors included: sufficient size to satisfy all operational input torque requirements; capability for driving the elevation and azimuth assemblies so as to achieve elevation tracking rates of 6.2°/min; and azimuth tracking rates of 12°/min; and capability for driving the gimbal/actuator through 96° of elevation travel, and azimuth travel of  $\pm 165^\circ$ .

The drive motors are an existing, commercial-grade design and are described by the specifications listed in Appendix F.

Three-phase induction drive motors were selected to provide sufficient power and operate with long life under the intermittent and continuous duty cycles required. Both performance and life cycle cost favored the 3-phase induction motor selection. The elevation motor is 1/3 hp rating in a NEMA 56 frame operating with the overall average drive ratio of 101,000:1. The azimuth motor is 1/6 hp rating in a NEMA 48 frame operating with the overall drive ratio of 52,500:1.

Both motors are 1750 rpm nominal, 208V, 60 Hz, and are totally enclosed (non-ventilated) with a footless C-face mounting. The occasionally severe intermittent tracking duty cycles dictated winding type D and the oversize frame sizes. Automatic reset thermal overload protection is also provided within each motor. The coupling attaching the motor to the drive shaft is resilient, which is dictated by the intermittent duty cycle. A shaft coupling also allows for replacement of a motor.

One cable is attached to each of the two drive motors (azimuth and elevation) and extends through the cable clamp for termination of the pedestal electrical junction box. Each cable is 3-wire plus safety ground (type SJO-4 #18 AWG, 300 volt) complete with a cord grip and four splices at the motor and a cord grip at the heliostat control box. (Motors and cables are illustrated in Figures 2.3-1, -2 and -9, respectively).

### 2.3.2.2 Configuration Trades

To select the lowest-life-cycle-cost motors, several types were investigated; complete discussion of this trade is contained in Ref. 2-5. The types of motors considered were: 1-phase PSC induction motors; brushless DC motors; stepper motors; brush-type DC and AC motors; direct-acting motors such as linear motors and on-axis torquers; and 3-phase induction motors which were selected as having sufficient performance, moderate efficiency, low risk, and low cost.

### 2.3.2.3 Analyses

An analysis was performed to determine the maximum axis torques expected during the drive-to-stow condition which is initiated when the wind velocity exceeds 15 m/s (35 mph).

As shown in Ref. 2-5, the elevation drive motor was selected as 1/3 rated hp based on the drive ratio, a conservative drive efficiency estimate, and the axis torque due to gravity unbalance and worst case wind velocities (without ice or snow). The elevation drive ratio, gravity unbalance and wind torque all vary with elevation axis orientation.

The azimuth drive motor was selected as 1/6 rated hp based on the drive ratio, drive efficiency, and the axis torque due to worst case wind velocity of 15 m/s (35 mph). The azimuth motor will perform in overload capacity during the short time the heliostat drives continuously through even the worst case 22 m/s (50 mph) wind velocity of a "walk-the-wire", drive-to-stow condition.

Larger motors are not desirable since they not only increase life cycle costs, but also result in a worst case condition during normal tracking operating by producing greater heating, and to some extent, produce a larger load condition on the gear system.

In the event of motor overheating, the thermal overheat protection trips and stops the axis motion until the temperature drops; at which time the automatic reset allows the drive to continue.

Since heliostats at certain locations in the field may experience occasionally severe intermittent tracking duty cycles, winding type D and large frame sizes for the motors were selected.

Total motor cycles even for 30 years are not severe and are calculated in Reference 2-5.

Electric drive control configurations were investigated; they are described in Ref. 2-5, including TTL dynamic braking logic, limit circuits, motor and motor control switches, and motor protective devices.

#### 2.3.2.4 Tests

No separate testing of the drive motors was deemed necessary. However, final drive rates under various loads were measured, providing an indirect method of confirming motor selection.

#### 2.3.3 Sensors

##### 2.3.3.1 Detail Design

###### 2.3.3.1.1 Motor Shaft Revolution Sensor

Angular axis position of the heliostat is determined by counting the number of revolutions made by the motor shaft. The incremental sensors used are the Sprague Hall Effect type which respond to a magnetic field. Two sensors are used in order to sense the direction of rotation and one magnet is used to give a count accuracy up to  $\pm 1$  motor shaft revolution. The magnet is bonded to the shaft and the pair of Hall Effect digital switches are mounted on a fixed printed circuit card.

For each axis (azimuth and elevation) two Sprague Electric Company, type UGN 3020T, solid state "Hall Effect" digital switches are mounted on a 3.2 cm (1-1/4") x 5 cm (2") printed circuit card. One magnet, Hitachi Magnetics Co., Hicorex 90B, 0.20 cm (.080") x 0.64 cm (.250") x 0.10 cm (.040") thick, is bonded to a holder attached to the motor shaft and is environmentally enclosed. The mounting arrangement is shown in Figure 2.3-7; detail mounting is illustrated in Figure 2.3-8.

#### 2.3.3.1.2 Zero Reference Sensor

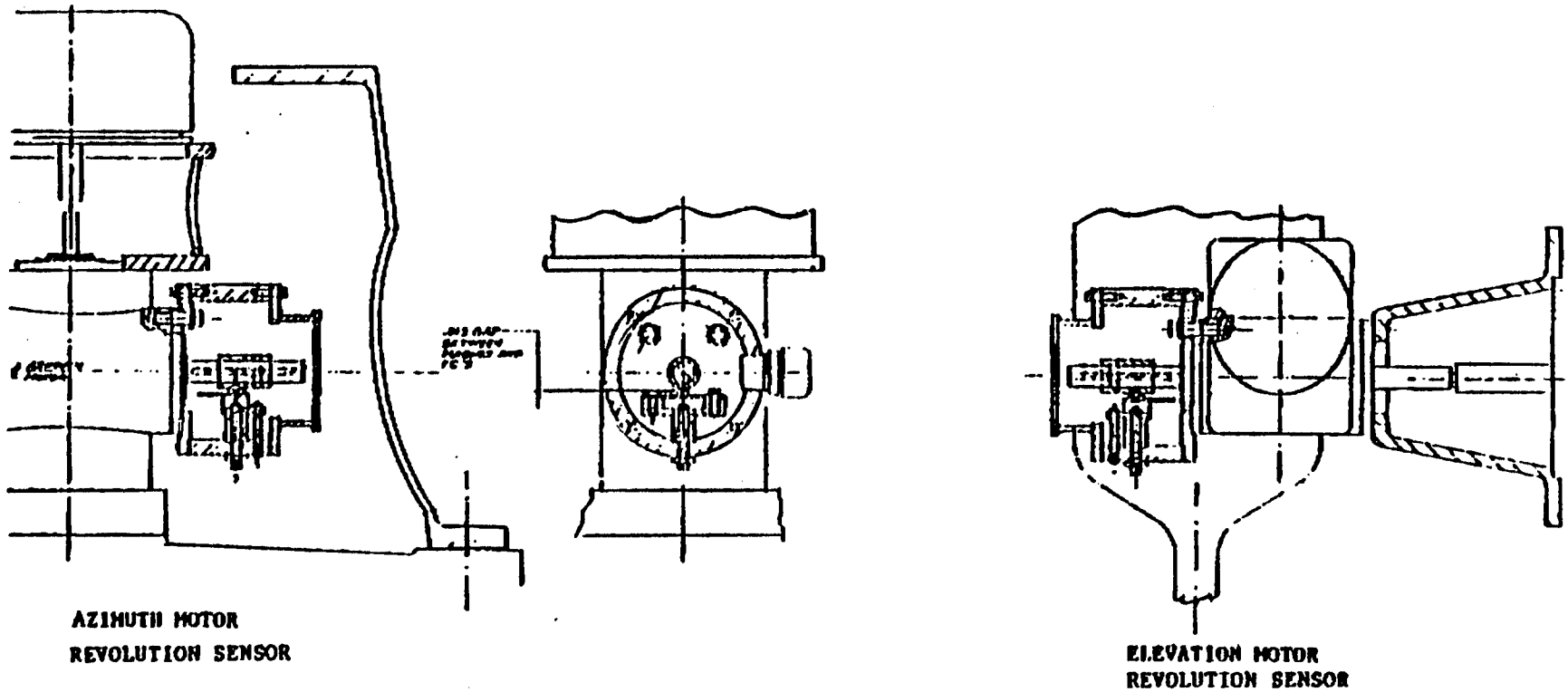
To provide a daily reference point for the incremental motor shaft revolution sensors, a zero reference sensor is mounted on each axis (azimuth and elevation). A similar Hall Effect sensor is used in this application. To obtain an improved sensitivity drift, the Microswitch Hall Effect sensor was selected.

Only a single magnet sensor is required per axis. For the azimuth axis, supporting brackets are provided between the fixed lower ring of the azimuth drive and the rotating gimbal housing. For the elevation axis, brackets are provided between the fixed gimbal housing and the rotating torque tube at the arms ring.

For each axis (azimuth and elevation) one Microswitch "Hall Effect" position sensor, type 513SS16, is mounted on the rotating bracket. One magnet, Hitachi Magnetics Co., Hicorex 908, 0.20 cm (.080") square x 0.10 cm (.040") thick, is mounted on the fixed bracket.

#### 2.3.3.1.3 Electrical Wiring for Sensors

One cable is attached to each of the two motor revolution sensor cards (azimuth and elevation) and extends through cable clamp for termination at the control box. Each cable is a 4-wire (type 2#20SSJ plus 2#20SC with a neoprene jacket) complete with a cord grip, three ferrules, and seven ring lug terminals at the sensor card and a cord grip at the control box.



**AZIMUTH MOTOR  
REVOLUTION SENSOR**

**ELEVATION MOTOR  
REVOLUTION SENSOR**

*Figure 2.3-7. Motor Shaft Revolution Counter Mounting Arrangements*

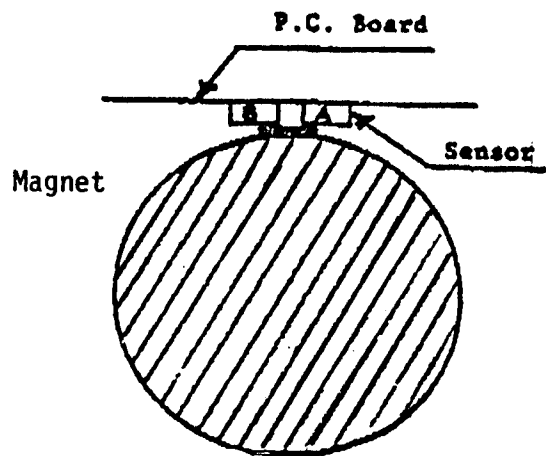


*Figure 2.3-8. Counter Mounting Detail*

One cable is attached to each of the two zero reference sensors (azimuth and elevation) and extends through the cable clamp for termination at the control box. Each cable is 3-wire (type 3#20SC/OASJ) complete with a cord grip, ferrule, ring lug terminal and three shrink tubings at the sensor and a cord grip at the control box.

Figure 2.3-9 shows the wiring route and clamp supports.

### 2.3.3.2 Configuration Trades

Various devices available in the market were explored to find suitable sensors for the revolution count measurements and the zero reference sensor. They were analyzed for measurement accuracy, applicability and cost. The complete investigation is reported in Ref. 2-5. The following sensor categories were investigated: optical encoders; proximity switches; and Hall Effect sensors which respond to a magnetic field. The latter were selected as least cost, and further analyzed and tested for performance.

### 2.3.3.3 Analysis

Various Hall Effect devices from four manufacturers were analyzed (see Ref. 2-5 for use as the revolution and zero reference sensors. The Sprague and Microswitch types were selected for testing over the F.W. Bell and Xolox Corp. Sensor arrangements, sensor/magnet mounting tolerances, warning time, incremental pulse width, sensitivity drift due to age and temperature variation, and supply voltage were investigated. Rare earth samarium cobalt target magnets from Hitachi Magnetics Corps and Indiana General were also analyzed.

### 2.3.3.4 Tests

Two Hall Effect sensors (Microswitch #513SS16 and Sprague #UGN 3020T) were tested in conjunction with a Hitachi samarium cobalt permanent magnet (0.20 cm (0.08 inch) square x 0.10 cm (0.04 inch) thick). The change in the operate and release points due to the change in power supply voltage, distance between sensor and magnet, and lateral offset distance between sensor and magnet were studied. The magnet was moved via a jig-bore machine past each fixed Hall

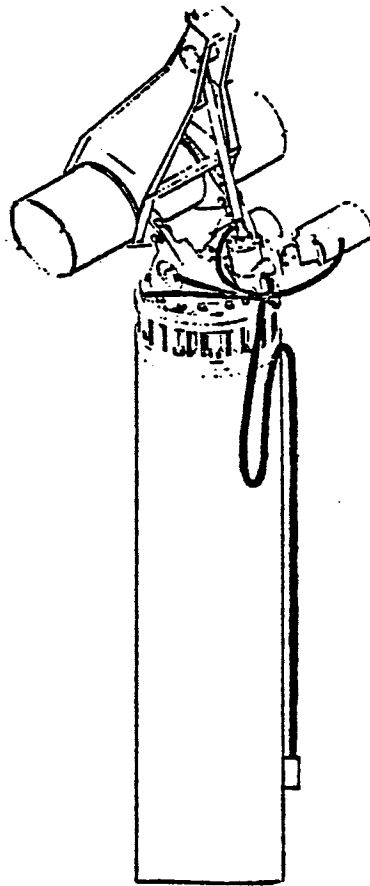


Figure 2.3-9. Wire Routing



Effect sensor. All test methods, equipment, data, results and recommendations are reported in Ref. 2-5.

Since resolution and repeatability are only secondary considerations for the incremental revolution sensors, the studies and test results indicated that the Sprague #UGN 3020T can be effectively employed. The benefits of their lower cost and compact package can also be realized. The tests also showed that the Microswitch sensors are preferable for the zero reference sensors.

## 2.4 Pedestal/Foundation

### 2.4.1 Detail Design

The pedestal assembly is an available commercial pre-stressed concrete pile. Consequently, only slight modifications are required to meet performance and design requirements. The primary change consists of adding a steel pile-end-cap with a bolt pattern which interfaces with the gimbal drive assembly. The pedestal assembly is illustrated in Figure 2.4-1; additional design details are shown on Figure 2.4-2.

### 2.4.2 Configuration Trades

The pedestal/foundation design selection is somewhat sensitive to plant site characteristics. The primary variables involve materials availability and costs at the site; local labor costs and skills; weather conditions; production rates and schedules; and soil conditions.

It was evident early in the trade study phase that slight changes in the above variables could lead to selection of different designs. However, the Sandia specification (Reference 3-1) established soil conditions for the design, thus allowing design configurations to be evaluated in terms of structural and functional characteristics.

Table 2.4-1 lists the preliminary configurations considered and compares their costs. From this initial list, three final configurations were selected; they are listed in Table 2.4-2. The prestressed concrete pile was ultimately selected over the two other candidates for cost, and manufacturability reasons. The prestressed pile was spun-cast to provide a more uniform density, higher strength, and higher modulus (stiffness) than a comparable poured concrete foundation. Also because it is manufactured within a factory, quality control is superior and field cure time is not required. The installation problems associated with drilling, form building, etc., are eliminated. Pile driving equipment and crews are all that is required after minimal field preparation as compared against the greater amount of field preparation and types of equipment and labor skills associated with poured foundations.

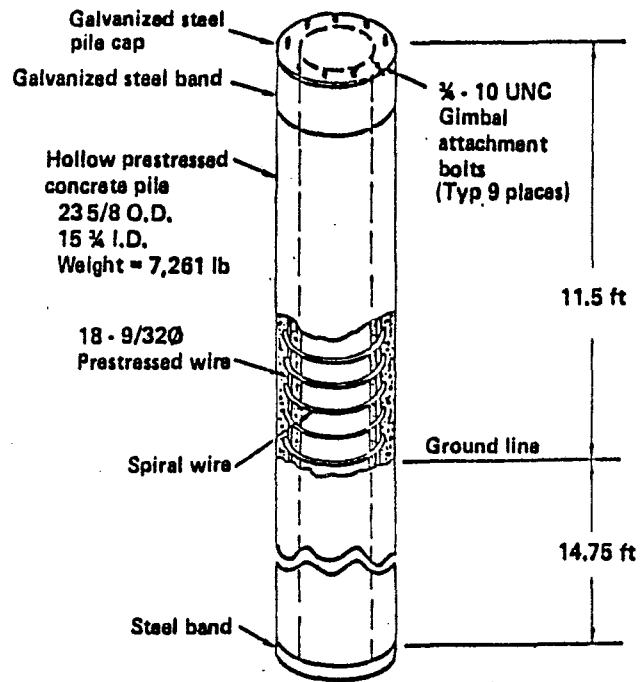
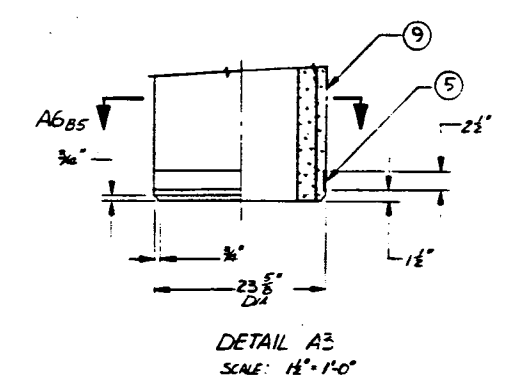
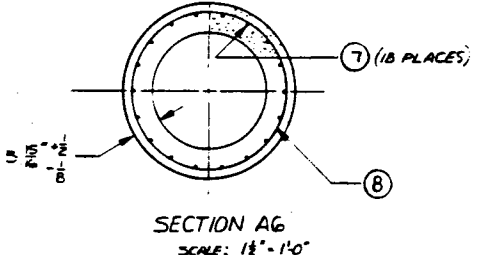
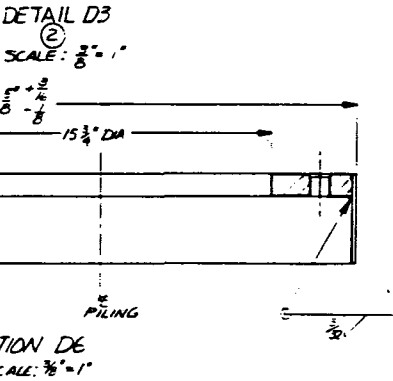
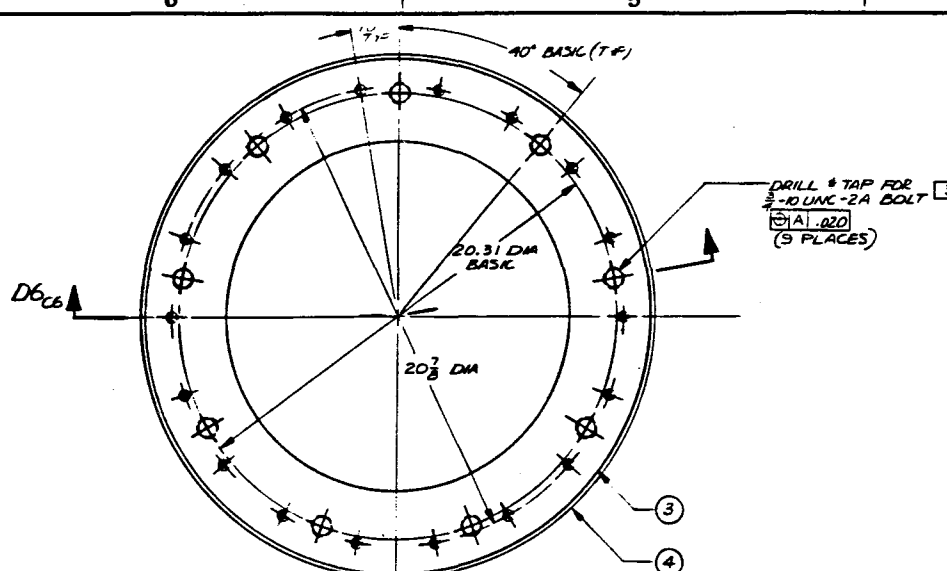
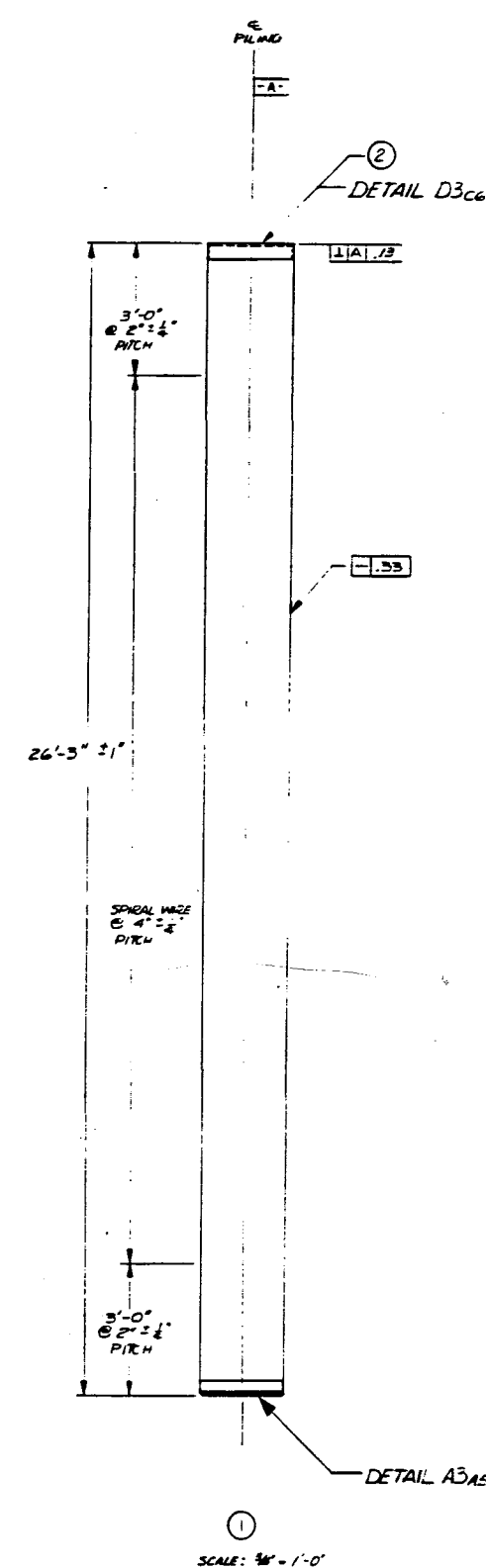


Figure 2.4-1. Pedestal-Foundation Pile Assembly

STL-10124



APPROVED SOURCE OF SUPPLY			
SPECIFICATION NUMBER	SUPPLIER	CODE IDENT.	SUPPLIER NAME & ADDRESS
277-10124-1	Q-1B13A		



PART NUMBER	REV	DESCRIPTION	DATE	BY	CHKD
-1	277-10123	MOD 277-1 PROTOTYPE			

- NOTES**
- GALV. PER ASTM A123
  - ASTM C150 TYPE I GRAY CONCRETE W MOLD FINISH #11;  $f_c @ 28$  DAYS = 7000 PSI
  - USE TAPPED HOLES FOR PRETENSIONING BOLTS. END OF PRETENSIONING BOLTS TO PROJECT MINIMUM OF 1/2" BELOW BOTTOM OF (3) DURING CONCRETE EMPLACEMENT & SET.
  - ALL WELDING SHALL BE IN ACCORDANCE WITH CURRENT REQUIREMENTS OF AWS D.1.
  - TOLERANCES UNLESS OTHERWISE SPECIFIED  $\pm 1/16"$ .
  - CENTRECON INC. 1200 NORTON AVE., EVERETT, WA. 98206 MAILING P.O. BOX 28
  - QUALITY CONFORMANCE INSPECTION AND APPROVAL PROCEDURE SHALL BE PER CENTRECON SPECIFICATION FOR SPUN PRESTRESSED CONCRETE PILES.
  - ONLY THE ITEM DESCRIBED ON THIS DRAWING WHEN PROCURED FROM THE VENDOR LISTED HEREON IS APPROVED BY BOEING ENGINEERING & CONSTRUCTION FOR USE IN THE APPLICATION DESCRIBED HEREON. A SUBSTITUTE ITEM SHALL NOT BE USED WITHOUT PRIOR TESTING AND APPROVAL BY BEC.

REV	STATUS	DESCRIPTION	DATE	APPROVED		
A1	REVISED	1. PARTS LIST DELETED (C) WITH (2) & (3) ADDED (3). 2. ZU, DS, (A) (B) (C) (D) (E) (F) (G) (H) (I) (J) (K) (L) (M) (N) (O) (P) (Q) (R) (S) (T) (U) (V) (W) (X) (Y) (Z) (AA) (AB) (AC) (AD) (AE) (AF) (AG) (AH) (AI) (AJ) (AK) (AL) (AM) (AN) (AO) (AP) (AQ) (AR) (AS) (AT) (AU) (AV) (AW) (AX) (AY) (AZ) (BA) (BB) (BC) (BD) (BE) (BF) (BG) (BH) (BI) (BJ) (BK) (BL) (BM) (BN) (BO) (BP) (BQ) (BR) (BS) (BT) (BU) (BV) (BW) (BX) (BY) (BZ) (CA) (CB) (CC) (CD) (CE) (CF) (CG) (CH) (CI) (CJ) (CK) (CL) (CM) (CN) (CO) (CP) (CQ) (CR) (CS) (CT) (CU) (CV) (CW) (CX) (CY) (CZ) (DA) (DB) (DC) (DD) (DE) (DF) (DG) (DH) (DI) (DJ) (DK) (DL) (DM) (DN) (DO) (DP) (DQ) (DR) (DS) (DT) (DU) (DV) (DW) (DX) (DY) (DZ) (EA) (EB) (EC) (ED) (EE) (EF) (EG) (EH) (EI) (EJ) (EK) (EL) (EM) (EN) (EO) (EP) (EQ) (ER) (ES) (ET) (EU) (EV) (EW) (EX) (EY) (EZ) (FA) (FB) (FC) (FD) (FE) (FF) (FG) (FH) (FI) (FJ) (FK) (FL) (FM) (FN) (FO) (FP) (FQ) (FR) (FS) (FT) (FU) (FV) (FW) (FX) (FY) (FZ) (GA) (GB) (GC) (GD) (GE) (GF) (GG) (GH) (GI) (GJ) (GK) (GL) (GM) (GN) (GO) (GP) (GQ) (GR) (GS) (GT) (GU) (GV) (GW) (GX) (GY) (GZ) (HA) (HB) (HC) (HD) (HE) (HF) (HG) (HH) (HI) (HJ) (HK) (HL) (HM) (HN) (HO) (HP) (HQ) (HR) (HS) (HT) (HU) (HV) (HW) (HX) (HY) (HZ) (IA) (IB) (IC) (ID) (IE) (IF) (IG) (IH) (II) (IJ) (IK) (IL) (IM) (IN) (IO) (IP) (IQ) (IR) (IS) (IT) (IU) (IV) (IW) (IX) (IY) (IZ) (JA) (JB) (JC) (JD) (JE) (JF) (JG) (JH) (JI) (JJ) (JK) (JL) (JM) (JN) (JO) (JP) (JQ) (JR) (JS) (JT) (JU) (JV) (JW) (JX) (JY) (JZ) (KA) (KB) (KC) (KD) (KE) (KF) (KG) (KH) (KI) (KJ) (KK) (KL) (KM) (KN) (KO) (KP) (KQ) (KR) (KS) (KT) (KU) (KV) (KW) (KX) (KY) (KZ) (LA) (LB) (LC) (LD) (LE) (LF) (LG) (LH) (LI) (LJ) (LK) (LL) (LM) (LN) (LO) (LP) (LQ) (LR) (LS) (LT) (LU) (LV) (LW) (LX) (LY) (LZ) (MA) (MB) (MC) (MD) (ME) (MF) (MG) (MH) (MI) (MJ) (MK) (ML) (MM) (MN) (MO) (MP) (MQ) (MR) (MS) (MT) (MU) (MV) (MW) (MX) (MY) (MZ) (NA) (NB) (NC) (ND) (NE) (NF) (NG) (NH) (NI) (NJ) (NK) (NL) (NM) (NN) (NO) (NP) (NQ) (NR) (NS) (NT) (NU) (NV) (NW) (NX) (NY) (NZ) (OA) (OB) (OC) (OD) (OE) (OF) (OG) (OH) (OI) (OJ) (OK) (OL) (OM) (ON) (OO) (OP) (OQ) (OR) (OS) (OT) (OU) (OV) (OW) (OX) (OY) (OZ) (PA) (PB) (PC) (PD) (PE) (PF) (PG) (PH) (PI) (PJ) (PK) (PL) (PM) (PN) (PO) (PP) (PQ) (PR) (PS) (PT) (PU) (PV) (PW) (PX) (PY) (PZ) (QA) (QB) (QC) (QD) (QE) (QF) (QG) (QH) (QI) (QJ) (QK) (QL) (QM) (QN) (QO) (QP) (QQ) (QR) (QS) (QT) (QU) (QV) (QW) (QX) (QY) (QZ) (RA) (RB) (RC) (RD) (RE) (RF) (RG) (RH) (RI) (RJ) (RK) (RL) (RM) (RN) (RO) (RP) (RQ) (RR) (RS) (RT) (RU) (RV) (RW) (RX) (RY) (RZ) (SA) (SB) (SC) (SD) (SE) (SF) (SG) (SH) (SI) (SJ) (SK) (SL) (SM) (SN) (SO) (SP) (SQ) (SR) (SS) (ST) (SU) (SV) (SW) (SX) (SY) (SZ) (TA) (TB) (TC) (TD) (TE) (TF) (TG) (TH) (TI) (TJ) (TK) (TL) (TM) (TN) (TO) (TP) (TQ) (TR) (TS) (TT) (TU) (TV) (TW) (TX) (TY) (TZ) (UA) (UB) (UC) (UD) (UE) (UF) (UG) (UH) (UI) (UJ) (UK) (UL) (UM) (UN) (UO) (UP) (UQ) (UR) (US) (UT) (UU) (UV) (UW) (UX) (UY) (UZ) (VA) (VB) (VC) (VD) (VE) (VF) (VG) (VH) (VI) (VJ) (VK) (VL) (VM) (VN) (VO) (VP) (VQ) (VR) (VS) (VT) (VU) (VV) (VW) (VX) (VY) (VZ) (WA) (WB) (WC) (WD) (WE) (WF) (WG) (WH) (WI) (WJ) (WK) (WL) (WM) (WN) (WO) (WP) (WQ) (WR) (WS) (WT) (WU) (WV) (WW) (WX) (WY) (WZ) (XA) (XB) (XC) (XD) (XE) (XF) (XG) (XH) (XI) (XJ) (XK) (XL) (XM) (XN) (XO) (XP) (XQ) (XR) (XS) (XT) (XU) (XV) (XW) (XZ) (YA) (YB) (YC) (YD) (YE) (YF) (YG) (YH) (YI) (YJ) (YK) (YL) (YM) (YN) (YO) (YP) (YQ) (YR) (YS) (YT) (YU) (YV) (YW) (YZ) (ZA) (ZB) (ZC) (ZD) (ZE) (ZF) (ZG) (ZH) (ZI) (ZJ) (ZK) (ZL) (ZM) (ZN) (ZO) (ZP) (ZQ) (ZR) (ZS) (ZT) (ZU) (ZV) (ZW) (ZX) (ZY) (ZZ)				

SOURCE CONTROL DRAWING

QTY	QTY	QTY	QTY	QTY	QTY	QTY	QTY	QTY	QTY	QTY	QTY	QTY	QTY	QTY	QTY	QTY	QTY	QTY	QTY
REQD	REQD	REQD	REQD	REQD	REQD	REQD	REQD	REQD	REQD	REQD	REQD	REQD	REQD	REQD	REQD	REQD	REQD	REQD	REQD

**FASTENER CODES**

**PARTS LIST**

CONTRACT NUMBER: **277-10124**

BOEING ENGINEERING & CONSTRUCTION

PROJECT APPROVAL:

DATE: **11/17/81**

SCALE: **AS SHOWN**

277-10124

Figure 2.4-2

DO NOT SCALE FROM THIS DRAWING

STL-10124

Table 2.4-1. Preliminary Pedestal-Foundation Candidates



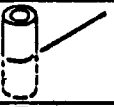
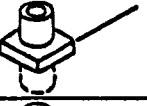
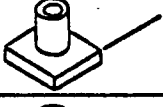




	Configuration	Relative cost
Steel driven piles	Cylindrical 	1.5
	H-beam 	2.4
Prestressed concrete piles	Unrestrained 	1.0
	Restrained 	1.2
Formed reinforced concrete foundations	Spread with prestressed concrete pedestal 	1.6
	Caisson 	1.1

Table 2.4-2. Final Pedestal-Foundation Candidates

Configuration	Foundation		Pedestal	Founda- tion/ Pedestal	Pedestal/ Gimbal	Transpor- tation	Total
	Material	Installation					
• 23 5/8 in OD x 15 3/4 in ID Prestressed driven concrete piling foundation/ pedestal 	355	67	329	-	63	76	890
• 30 in OD poured caisson foundation 30 in OD x 1/4 in wall steel pipe pedestal 	338	147	439	126	63	-	1,113
• 30 in OD poured caisson foundation 30 in OD poured column pedestals 	338	147	708	-	63	-	1,256

### 2.4.3 Analysis

A preliminary analysis based on Brom's methods was used to size the pedestal/foundation. A soils consultant (Roger Lowe Associates) was retained who used the Reese method to determine the size. It was concluded that the initial size of pedestal/foundation of 49.8 cm ( 19-5/8 inches) was marginal. Therefore, the size was increased to 60 cm ( 23-5/8 inches) and a new analysis performed by the consultant which indicated its adequacy. The analysis indicated that the design is deflection limited. At the maximum loading condition of a 40 m/s ( 90 mph) wind with 10° angle of attack, margins of several factors exist between the loads and strength allowables. (Axial bearing load of  $2.65 \times 10^4$  N (5944 lbs), allowable of  $1.67 \times 10^6$  N (374,600 lb); moment load  $8.82 \times 10^4$  Nm ( 64,800 ft. lb), ultimate allowable of  $2.54 \times 10^5$  Nm (187,000 ft. lb.))

The predicted deflection at the top of the piling under a 12 m/s ( 27 mph) wind at the worst reflector orientation (axial load of  $1.57 \times 10^4$  N ( 3538 lbs.), drag load of  $4.15 \times 10^3$  N (932 lbs) and moment load of  $1.14 \times 10^4$  Nm (8380 ft. lb.)) is 0.82 mr. The predicted torsional deflection under 27 mph and the worst orientation (not concurrent with worst orientation for drag and moment loading) is 0.15mr. Neither of these exceeds the budgeted error of 0.9mr.

Soil conditions in the Southwest U.S. make pile-driven concrete pedestals an economically attractive choice for many prospective solar plant sites. It is recognized, however, that driven piles may not be the best choice where highly solidified subsoil conditions exist. At those locations, alternative foundation designs will have to be utilized.

### 2.4.4 Test

No tests were conducted by BEC on the pedestal.

## 2.5 Control System

The prototype control and data distribution components have been configured to demonstrate the heliostat control functions at minimum cost. The prototype design combines heliostat array controller (HAC), field controller (HFC) and the two heliostat controller (HC) functions into one microcomputer. To provide design flexibility through software changes and to most nearly simulate production control system characteristics, the motor control communications between the computer and the heliostat are implemented as discrete (i.e. on-off) signal lines. The prototype heliostat electronics box contains motor control and sensor processing circuits similar to those planned for the production (HC); however, it does not contain a microprocessor which would be used in a production system. Design and development of a production control system capable of handling a large field of heliostats and interfacing with a plant controller, was beyond the scope of the present contract.

There is no data distribution network involved in the prototype controls design except for the communication link between the microcomputer and the heliostats. Serial data lines are provided at the Sandia Central Receiver Test Facility to transmit absolute position encoder information from the heliostats to the computer. (Absolute encoders were installed on heliostats for instrumentation purposes only during pre-delivery checkout, and were removed prior to delivery of heliostat to Sandia).

### 2.5.1 Prototype Heliostat Control Hardware

#### 2.5.1.1 Detail Design Description

##### 2.5.1.1.1 Overview

A top level block diagram of the control system used for prototype heliostats is shown in Figure 2.5-1. Figure 2.5-2 shows a block diagram of the heliostat motor control processes and indicates those processes implemented in hardware and software. The hardware implementation was kept to a minimum to best duplicate the low cost design using a microprocessor. The computer calculates the desired motor positions and then compares the desired position



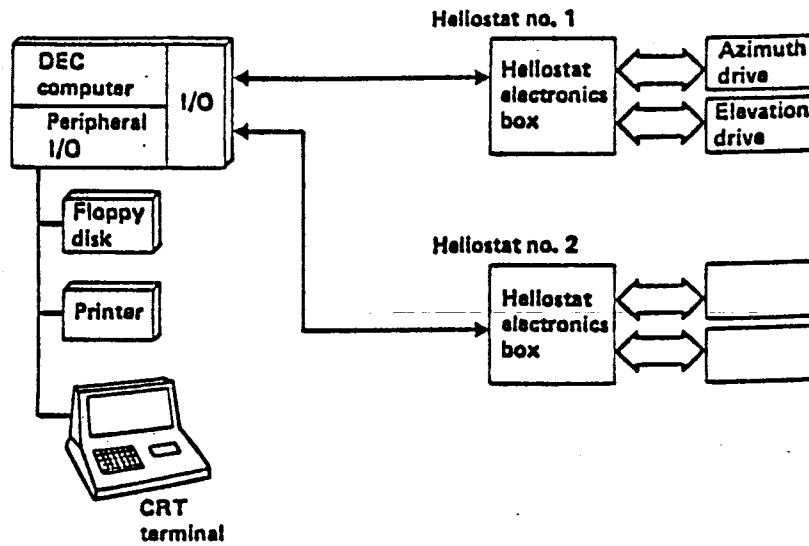


Figure 2.5-1. Top Level Block Diagram of Prototype Central System

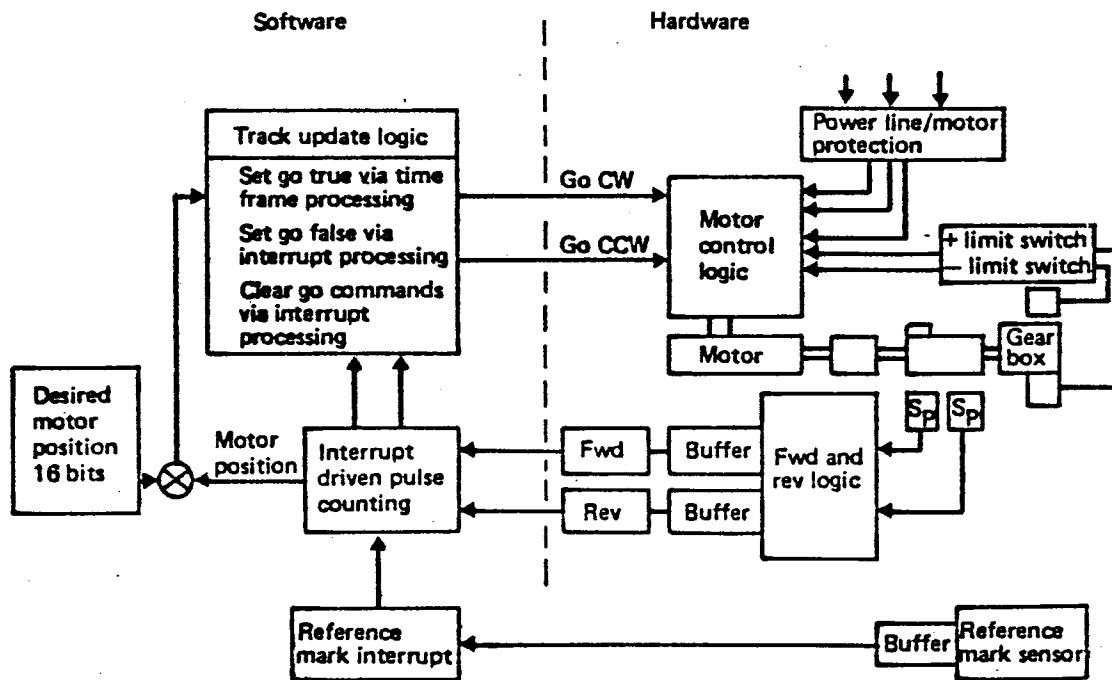


Figure 2.5-2. Block Diagram of Heliostat Motor Control Process

to the actual motor position to determine the control error. If the control error is larger than half the allowed step size, then a motor go command is set true to run the motor in a direction to reduce the error. The motors are 3 phase induction motors that run at a near constant speed of 1750 RPM. Each rotation of the motor shaft is sensed by a magnet passing by two low-cost Hall effect switch sensors. The Hall effect switch outputs are processed by a simple hardware circuit which outputs either a forward pulse or a reverse pulse, depending on the direction of motor shaft rotation. The motor pulses are counted in the computer via two interrupt driven software routines to keep track of motor position.

The motor go commands are set true by a timer interrupt driven software module. The go commands are set to the false, i.e. not-go condition by the interrupt service routine which counts the motion pulses.

A reference mark sensor is mounted on the azimuth and elevation axes to provide a means of setting or checking the position count maintained in the computer. When in the reference mark locating mode, the interrupt from the reference mark Hall effect switch will set the motor position count to the correct value.

Limit switches are provided to cut the motor power when limits are exceeded at either end of the travel range. The limit switch circuits are designed so the controls can command the motor to back away from the limit after the switch has stopped the motor travel.

#### 2.5.1.1.2 Motor Control Circuits

The motor control circuit cards contain all card-mounted circuits necessary for motor control.

##### (1) Motor Control Circuit

A detailed schematic of the baseline motor control circuit is shown in Figure 2.5-3. The go-forward (GO-FWD) and go-reverse (GO-REV) commands are transmitted from the computer over twisted, shielded pairs of wires. The signal-path electrical specifications conform to the RS 422 specifications.

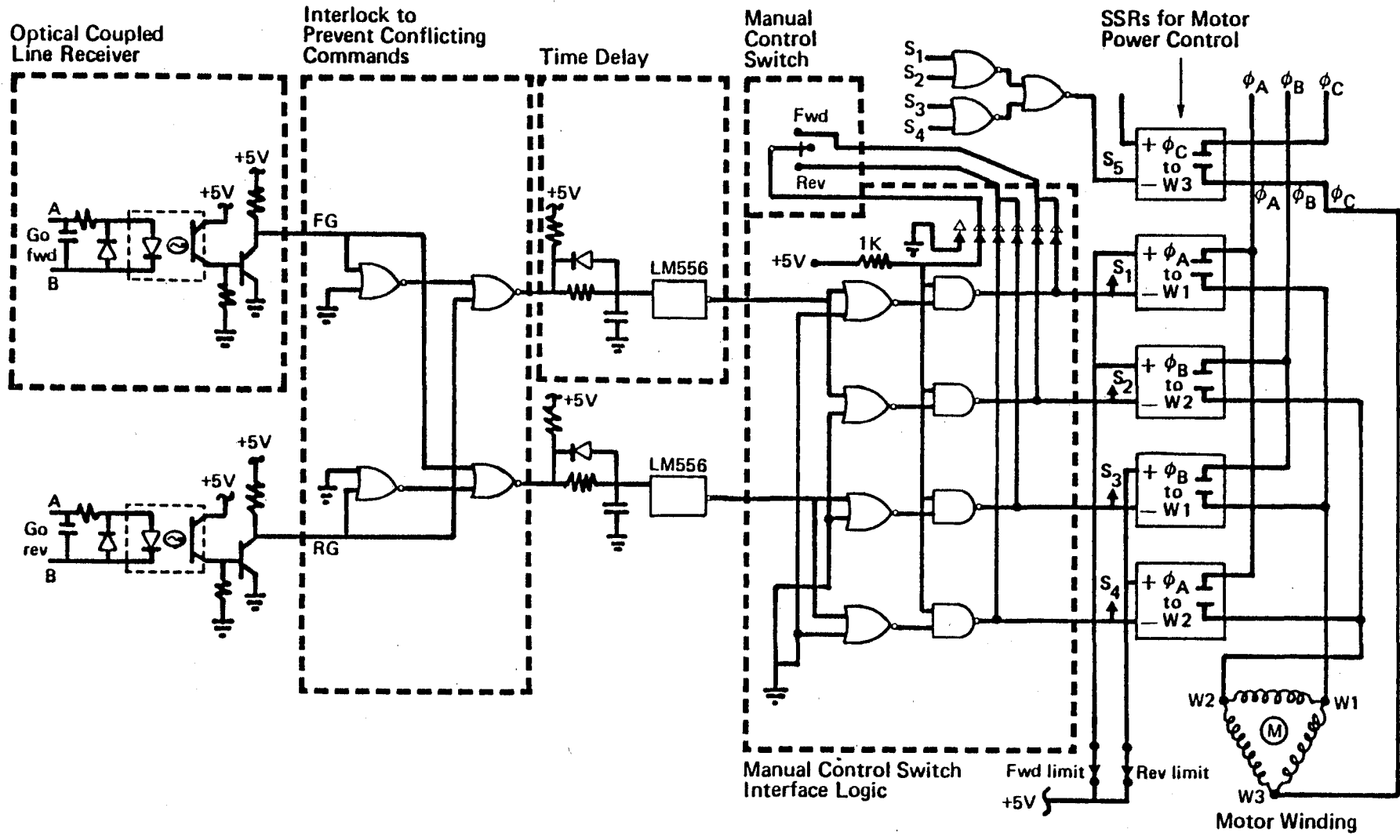


Figure 2.5-3. Schematic of Baseline Motor Control Circuit

Optical isolators are provided at the inputs for lightning surge protection. The four NOR gates shown immediately after the inputs provide an interlock so the down stream signals cannot both be true at the same time. This interlock protects against software errors and computer output circuit failures which might cause motor control circuit failures.

The R-C network with the diode, in conjunction with the LM 556 chips provide time delays of approximately 21 milliseconds in the turn-on of a motor go-command. They cause no delay in the turn off of the motor go-command. The time delays are necessary to prevent turn-on of the go-reverse commands while the solid state relays (SSR's) are still conducting in the go-forward path and vice versa.

The power switching for the motor control is done by SSR's. The SSR's have the very desirable characteristics of turning on only when the voltage across their output terminals is near zero and turning off when current through the output terminals is near zero. Thus, the SSR's minimize the surge voltages that occur with the switching of inductive loads.

The SSR's are turned on by applying 5 volts across the input terminals which lights an LED in an optical coupling and enables the SSR to be in the conducting state. The SSR's are turned on (i.e. put in conducting state) by the signals from the LM556 chips going low thus applying 5 volts across the LED in the SSR input.

The NOR and NAND gates between the LM556 and the SSR inputs are for the manual override switch. The manual override switch is a small hand held switch box with a 15 foot cord. The connector on the cord is plugged into the bottom of the heliostat electronics box. The act of inserting the connector disables the go-signal paths from the computer and enables the manual switch by shorting to ground the 5 volt enabling signals into the NAND gates. With the NAND gate output forced high, the manual switch can command the motor by shorting the NAND gate outputs to ground.

The limit functions are implemented by simple low cost switches which open the 5 volt supply to the inputs of the SSR's which are driving the motors against the limit. This location for the limit switches protects against all upstream hardware and software failures and yet provides a very simple and low cost limit.

The only failures in which the limit switches would not limit motor travel are failures in the SSR's. It is not expected that a short in one SSR will cause a motor to run even if the third leg of the motor winding is connected to the power line. However, a short in one SSR may cause a motor coil to burn out after repeated cycling of the thermal cut out in the motor winding.

A fifth SSR was added to cut power to the third leg of the motor to prevent a single SSR failure from burning out a motor coil. This was considered a requirement for the prototype to prevent a potential long delay in the test program. The fifth SSR may not be recommended for the production design.

## (2) Motor Motion Pulse Circuits

The motor motion pulse circuit schematic is shown in Figure 2.5-4. The shaft motion sensor in each axis contains two Hall effect switches which are actuated by a single magnet. The Hall effect switches are identified as being a primary switch (P) and a quadrature switch (Q). The switch mountings are staggered so the center of the quadrature pulse is located approximately at the edge of the primary pulse when the motor shaft is moving in the clockwise (CW) direction. The primary pulse feeds into a delay circuit which shifts the P signal about 250 microseconds and inverts it to give a signal  $\overline{Pd}$ . The clockwise (CW) motion pulse is basically  $P \cdot \overline{Pd}$  where the "AND" function is performed in the line driver. The counterclockwise (CCW) pulse is basically  $\overline{P} \cdot Pd$ . Figure 2.5-5 shows a timing diagram for the CW and CCW pulses. The Q pulse is used to exclude the possibility of noise on the P signal line from producing pulses except when the Q signal is low.

A pulse enabling signal is also fed into the line drive "AND" gates. The purpose of the pulse enabling signal is to assure that erroneous motion pulses are not transmitted at power up and power down. At power up there is a delay in the pulse enabling signal going high (true) until all the gates have had

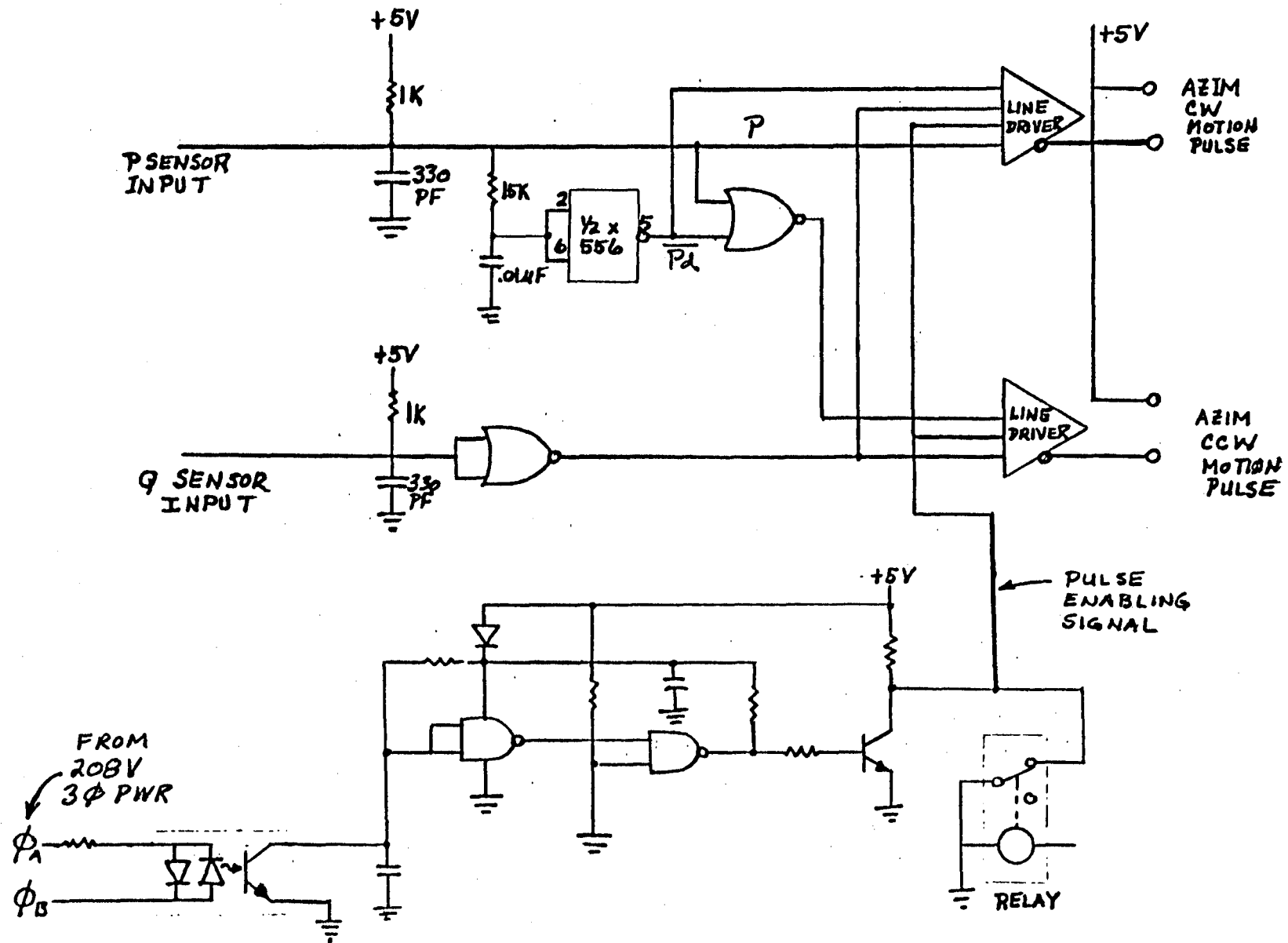


Figure 2-4. Schematic of Motor Motion Pulse Circuits

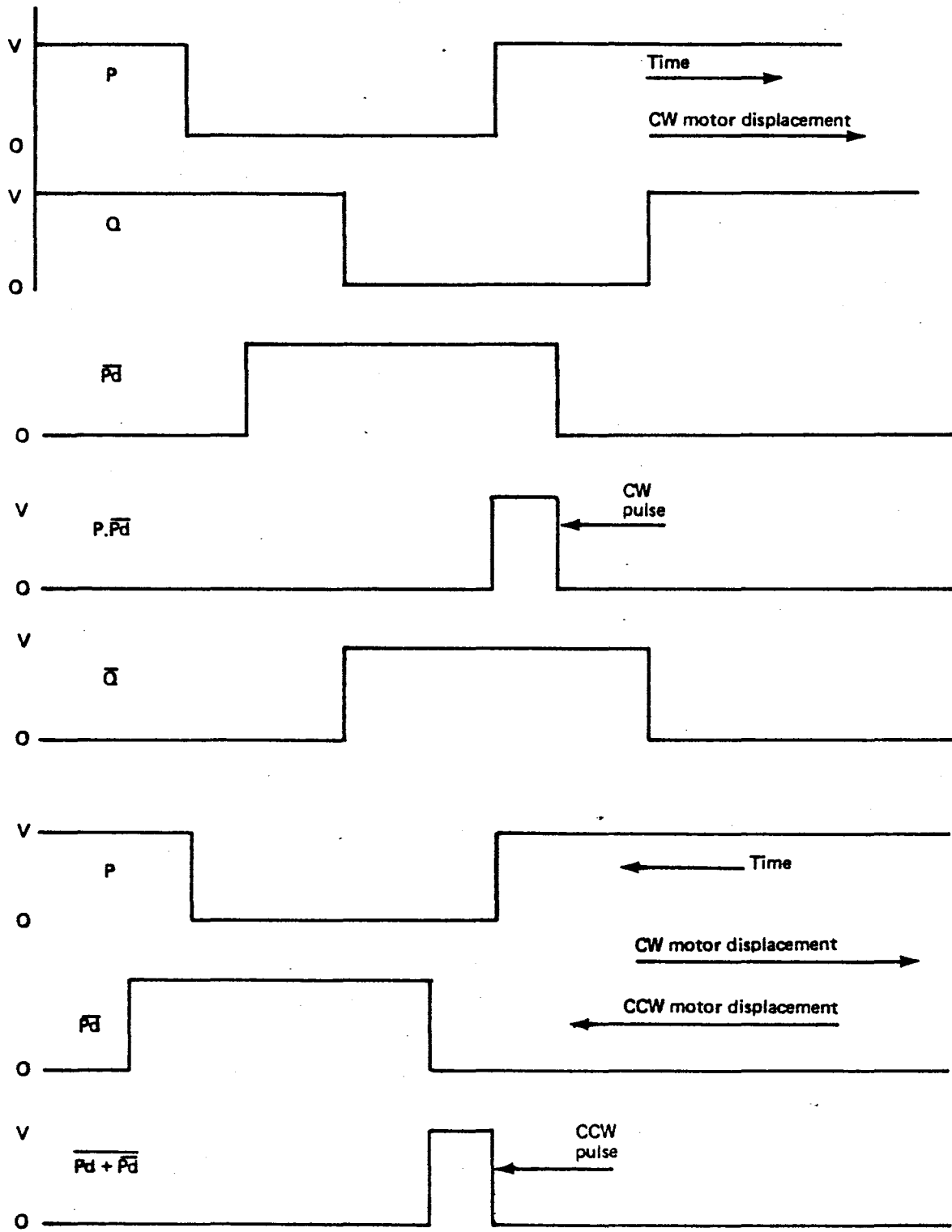


Figure 2.5-5. Timing Diagram for Generation of Motor Motions Pulses.

time to stabilize. At power down, the loss of A.C. power is sensed, and the pulse enabling signal goes low while the 5V power supply is still holding all the logic gates stable. Thus, the line drivers are shut off during the periods when erroneous pulses could be generated by logic gates changing with power up or power down.

This circuit was selected for its high noise immunity after it was determined there is no tendency for the motor shafts to back up when stopping.

### (3) Reference Mark Circuits

Reference mark switches are essential to provide a means of initializing the motor position count at a known location. The only circuits required for the reference mark switches are line drivers.

#### 2.5.1.1.3 Serial Data Circuit

The serial data card (also referred to as the position encoders circuit card) takes parallel data from the absolute position encoders and then transmits the data over an asynchronous serial data line. The serial data is for instrumentation only and therefore the circuits are put on a separate card so they may be removed from the heliostat electronics box and for spare-parts consideration. The data line drivers and receivers conform to RS-422 specifications. A schematic of the serial-data-card circuit is shown in Figure 2.5-6.

The inputs from the 15 bit encoders come into 3 tristate buffer chips (MM80C95). The circuit handles 2 encoders (1 for elevation axis and 1 for azimuth axis). Each tristate buffer chip has 6 inputs and handles five encoder bits with one bit tied off to either 5 volts or ground. The contents of each 6 bit buffer constitute the data bits of a six-data-bit character on the asynchronous serial data line. The first character of the 6 characters required for a reading of both encoders is identified by having it's first bit tied to ground. The first bit of the next five characters is tied to five volts. A seventh character of all 1's is sent to aid in rapid synchronization.



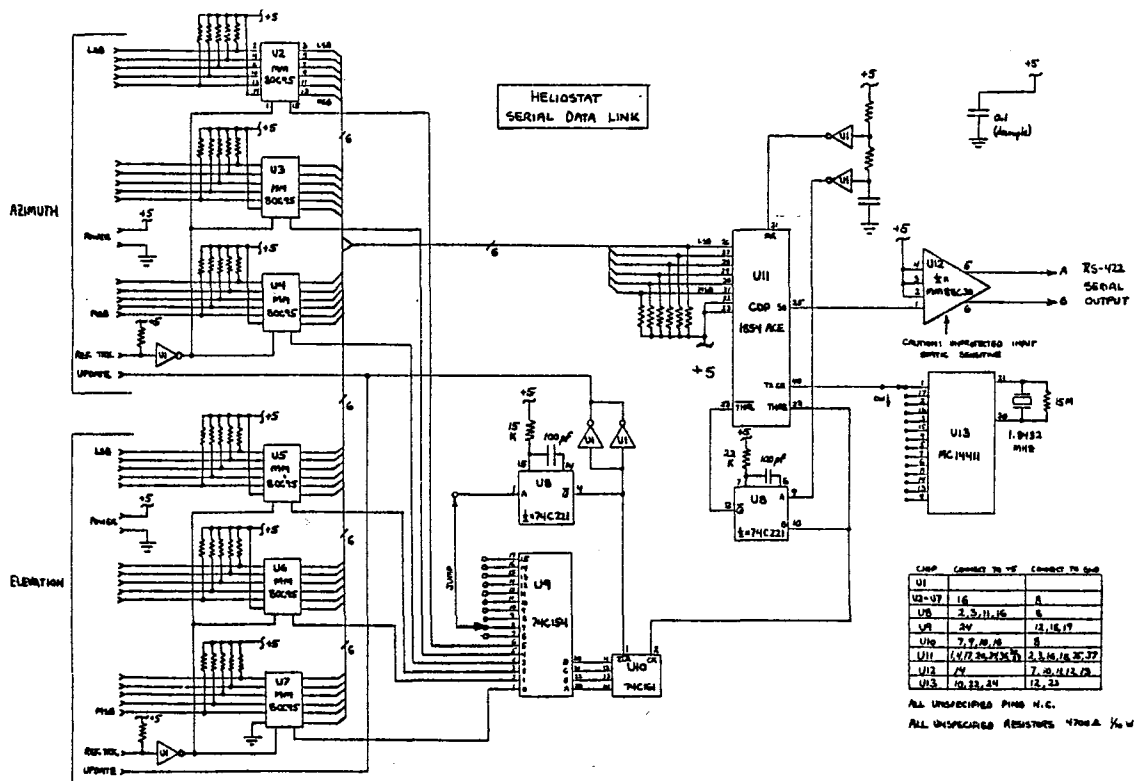


Figure 2.5-6. Schematic of Serial Data Transmitting Circuits for Instrumentation Position Encoders

The contents of the six buffer devices are sequentially enabled onto the six bit input to the universal asynchronous receiver and transmitter (UART, U-11). For the seventh character, no input is enabled, so the pullups on the input to the UART sends all ones. The UART transmits the character through the RS-422 drive amplifier and then increments a four bit counter (U10) through the "transmission complete" signal (THRE).

The outputs from the counter control a sequence selector (U9) which places the next character of data on the UART input bus. After allowing a 2.2 microseconds delay for input data to settle, the UART triggers its own start transmission line (THRL). When the last character of a message has been transmitted, the sequential selector steps to its next state which is jumped to reset the selector counter and send a pulse to the encoder update input (i.e. gating input) to latch in current data. Then transmission resumes starting with character 0 (from U7).

At power up, the UART requires a high pulse on its "master reset" (MR) input followed by a low pulse on the "start transmission" (THRL) line. This sequence is accomplished by two gates of U1 providing abrupt edges from a charging capacitor.

The UART is clocked by the U13 device. The selected band rate is 2400 baud but can be changed at U13 by changing a wire wrap jumper.

The asynchronous serial character format is six data bits, even parity, and two stop bits.

#### 2.5.1.1.4 Heliostat Electronics Box

Figure 2.5-7 shows the arrangement of the heliostat electronics box. The CR's are control relays (i.e. the solid state relays -SSR's). The 10 SSR's and two power supplies are mounted directly against the sides of the box for conduction cooling. Four current limiting resistors were also mounted on the side of the box for cooling. These resistors protect the SSRs from overcurrent if they are triggered by  $dv/dt$  at power up. Figure 2.5-10 shows their circuit location. The two circuit cards are mounted against the back of the box with stand out mounts. All connectors come through the bottom of the box .

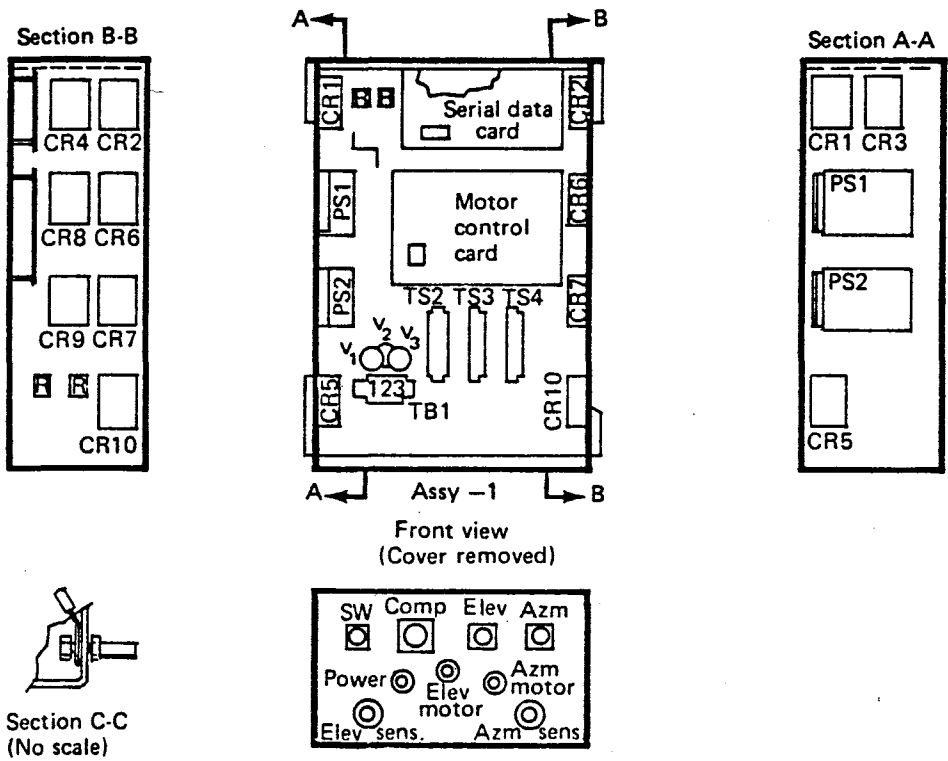


Figure 2.5-7. Heliostat Electronics Box Arrangement

The connectors and their functions are listed below.

- J1 - Manual Control Switch
- J2 - Computer Interface
- J3 - Elevation Axis Position Encoder
- J4 - Azimuth Axis Position Encoder

Only connector J1 above would be contained in the production design. In the production design, the computer interface would be only two wires and a lower cost method of connection would be selected.

Mil-Spec. quality external connectors may not be cost-effective for the production designs. Therefore, the power line connections to the electronics box and the connections between the electronics box and the gimbal actuator assembly were chosen to provide a test of a low cost means of connection that could be used in the production design.

There was insufficient time to do an exhaustive search to find the optimum low cost connectors presently available. The means selected was to use terminal blocks with a snap in connector for each wire. The terminal blocks and wires were labeled for easy identification. Each wire bundle comes through a separate hole with a grommet to hold the wire. The grommets can be easily unscrewed to remove a wire bundle to change a sensor. The power wires come into terminal block 1 where the varistors V1, V2 and V3 are installed to attenuate lightning surge voltages.

Connector J1 must be a convenient weather proof connector to allow quick connection of the manual control switch box. The manual control switch box can be held in one hand. It has separate center loaded switches for the elevation and azimuth axis. The box circuitry is shown in Figure 2.5-3.

Figure 2.5-7 shows power supply 1 (PS1) and power supply 2 (PS2). All circuit cards and the motor motion sensors are powered from a 5 volt power supply (PS1). A second 12V power supply (PS2) was added to power the reference mark sensors. The 12 volt supply should not be part of a production design; it became part of the prototype design because the reference mark sensors selected for testing showed optimum repeatability with a supply

voltage between 9 and 12 volts. In addition, there was not sufficient time or budget to test and verify other sensors which will probably show just as good a repeatability with a 5 volt power supply.

The power switch is contained in a separate small box below the heliostat electronics box so that power can be completely removed from the heliostat electronics box for safe removal or repair in place. The switch box is a standard design with fuses mounted in it.

Figure 2.5-8 shows the pedestal mounting of the heliostat electronics box. The mounting is tilted 5° so all moisture that condenses in the box will run to the lower front edge and drain out of screened drain holes in the corners of the box.

#### 2.5.1.1.5 Heliostat Electronics Lightning Protection

The most important part of the heliostat lightning protection is a good grounding system. Figure 2.5-9 shows how the electronics box interconnects with the grounding system. A number 2 copper ground cable comes up from the underground counterpoise (grounding grid) system to about six inches below the bottom edge of the electronics box. A number 2 ground wire which grounds all metal parts on the mirror frame and gimbal actuator assembly comes down the opposite side of the pedestal from the electronics box. The ground wires were kept on the opposite side of the pedestal to minimize the probability of lightning energy branching through the electronics box. The electronics box is connected to the ground cable by a number 6 ground wire going half way around and at least 12 inches down the pedestal to enter the same clamp which ties the gimbal actuator ground and counterpoise wires together. The electronics box should not have any other grounds except the one connected to the counterpoise system to minimize the probability that lightning will branch through the electronics box. This conduit coming up from the ground will be terminated at least 12 inches below the electronics box. The conduit for the power wires will be terminated at the power switch. Conduit for the computer communications cable will be terminated with a cable clamp and water sealing putty 16 inches below the electronics box.

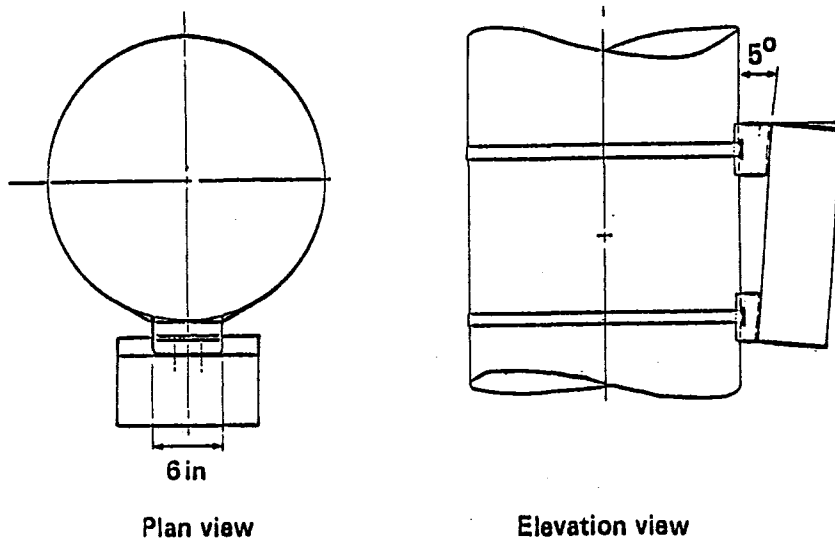
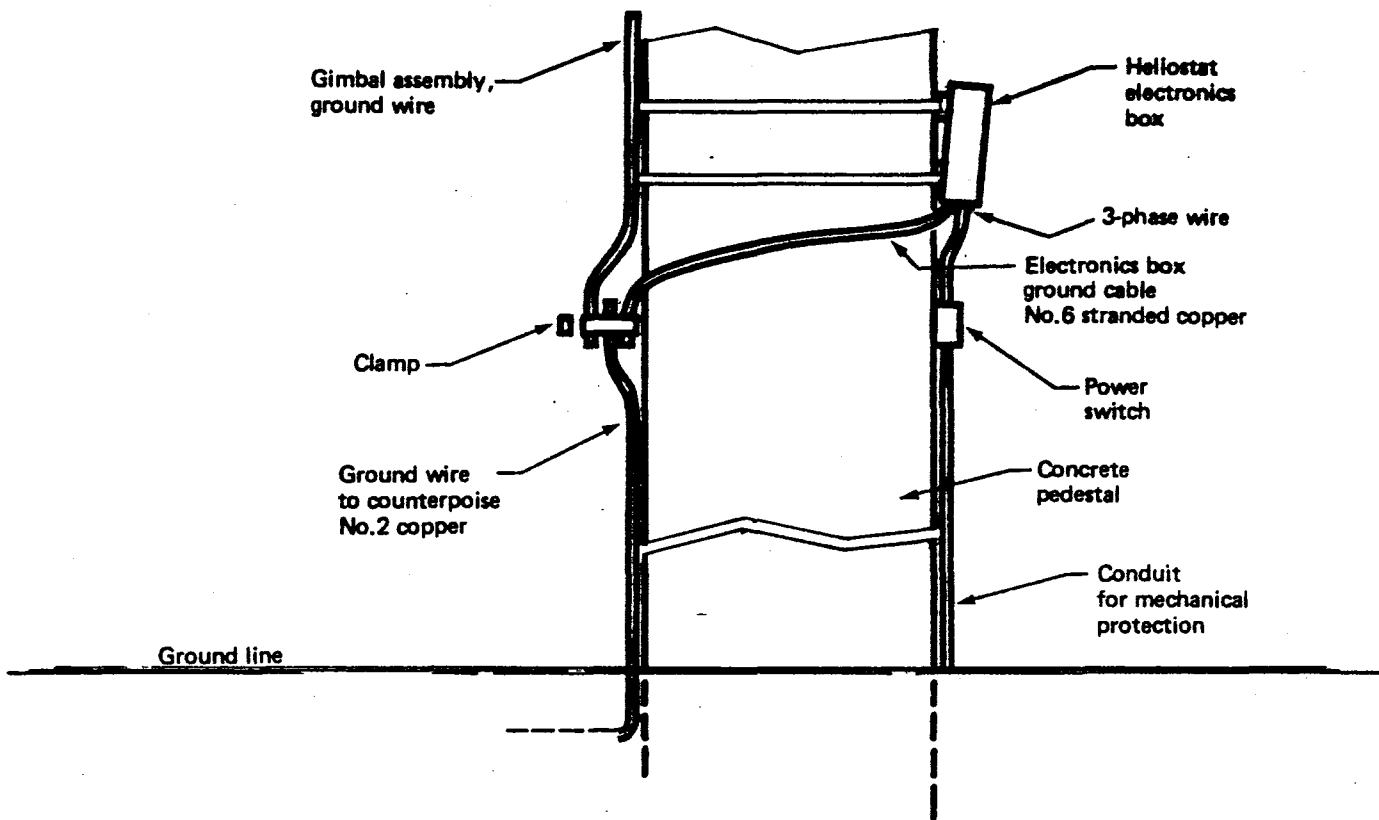


Figure 2.5-8. Pedestal Mounting of Heliostat Electronics Box



*Figure 2.5-9. Heliostat Electronics Grounding*

The gimbal assembly ground wire should avoid metal to metal contact with the clamps used to attach the electronics box to the concrete pedestal. This was accomplished by slipping 5 inch lengths of grey polybutylene tubing over the #2 ground wire where the electronics box clamps cross over it to clamp it to the pedestal.

The grounding system minimizes the probability that lightning strikes on a heliostat will put large surges of energy into the electronic power or communication cables connected to the heliostat. Additional protection against moderate amounts of surge energy is provided by the following:

1. All the computer communication lines have optical isolators in the receiving ends of the lines.
2. The power lines into the heliostat have varistors connected line-to-line and fuses upstream of the varistors to protect against differential surge voltage coming into the heliostats from lightning strikes on adjacent heliostats. The circuit diagram for the varister and fuse connections is shown in Figure 2.5-10. The fuses are sized to take continuously the maximum current that both motors can draw.

#### 2.5.1.1.6 Heliostat Electronics EMI Protection

EMI protection is provided by individual shielding on each signal line. All communications between the heliostat and the computer use twisted shielded pairs. The shields are grounded at the computer end by a direct tie to the green ground wire on the 115 volt power receptacle. All sensor signal lines at the heliostat are individually shielded, and the shields are grounded at the sensors to minimize the number of connector pins necessary at the heliostat electronics box.

The heliostat electronics box is a galvanized steel box which provides an EMI shield for electronics in the box.



R = 1.6Ω 15 watt  
current limiting resistor

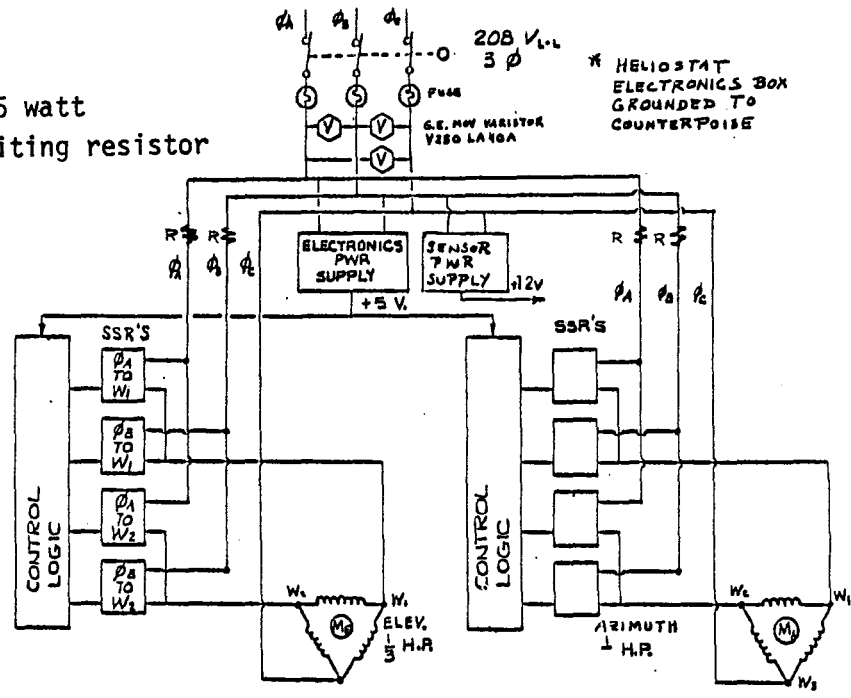


Figure 2.5-10. Circuit Diagram of Heliostat Interface to Power Lines.

#### 2.5.1.1.7 Computer Hardware

##### (1) General Equipment Selection

The computing equipment was selected to satisfy functional and performance requirements at lowest cost consistent with the program schedule.

A Digital Equipment Corporation (DEC) LSI 11/2 processor and memory was selected since it met all requirements, and an in-house BEC computer could be used for early development work.

The ADAC Corporation 1000M computer chassis, backplane and power supply was selected because it was a competitively-priced, well-designed chassis that would allow for growth, and take both half-quad and full-quad cards. Also ADAC manufactures a large selection of interface cards to meet the I/O requirements and would provide consultation and rapid repair/support.

The ADM 3A CRT was selected because it was compatible with the ADAC equipment and it is a reliable, low-cost unit.

The Data Systems floppy disk was also compatible with the ADAC equipment, and had been previously evaluated at BEC. Its unique features of hardware-write protection for system disks, and indicator lights to show when the disk is being accessed are useful features.

A DEC LA-120 keyboard printer was selected because its high-print rate (up to 180 characters per second) is important for fast printout of files during software development.

The DELTEC Model DLC 1260 line voltage regulator was selected because of its outstanding regulating and voltage surge suppression characteristics, and it is a convenient rack-mountable unit.

A CABTRON equipment rack was selected for mounting the equipment.

## (2) Computer Card Selections

Computer interface cards were selected to be compatible with the major computer hardware.

An ADAC 1750 dual channel serial data card was selected to provide the interfaces to the CRT and keyboard printer. A second ADAC 1750 card was selected to receive the serial absolute position data from the heliostat. (The two ADAC 1750 cards were selected after it was determined the 4 channel DEC DLV11J card could not be obtained on a satisfactory delivery schedule).

An ADAC 1616 MIC card was selected to provide the vectored interrupt inputs. It provides for 16 optically isolated interrupt inputs .

An ADAC 1601 GPT (general-purpose-timer) card was selected to provide the precise program controlled timer interrupt capability. The card can also be used for precise measurement of the processing time for software modules. It is a half-quad card as opposed to the DEC KVV11-A timer card which requires a full quad space.

A TCU-50 calendar clock card from Digital Pathways was selected to provide a precise time source that runs independent of computer power. The TCU-50 card has battery back-up-power built into the card. It can be read to 1 second increments set as accurately as one can anticipate the beginning of a one second interval. The quad size of the card was selected because it provides room for modifications which might be desirable at a later date. The TCU-50 clock was set by manually reading a WWV time clock.

An ADAC 1664 TTL card was selected to provide the discrete inputs and outputs. The 1664 card provides 64 I/O lines which can be designated as input or output in banks of 8. It is designed to be compatible with TTL circuitry. In order to provide the required lightning protection and the ability to drive over the line distances from computer to heliostat, it was necessary to provide line drivers and optically isolated receivers to buffer the 1664 card interfaces to the heliostat.

Drawing 277-10134 shows schematics of the circuits on the BEC designed buffer card. All inputs except those going to the 1616 MIC interrupt card are brought into optical isolators on the buffer card. The discrete outputs from the 1664 card are routed through RS-422 line drivers on the buffer card. If the line drivers are blown by a high differential surge voltage from a lightning strike they can be easily replaced. The line drivers will greatly reduce any surge voltage that might propagate onto the computer card, thus protecting against long down time failures and expensive repairs.

### (3) Computer Card Installation

The computer card installation in the computer chassis is shown in Figure 2.5-11. The sequence of card installation determines the priority of interrupts. The sequence was chosen to establish the following interrupt priority: first, the 1616 MIC interrupt input card; then the 1601 GPT (timer interrupt) card; then the CRT and keyboard printer serial data card; then the HelioStat Serial Data card; and finally, the floppy disk interface.

The TCU 50 calendar clock card and the I/O buffer card have no interrupt capability and were installed at the bottom. The I/O buffer card can be moved down to provide more space if necessary.

Top priority was given the interrupt card to ensure that a motor motion pulse would never be lost. The timer interrupt was given the next highest level of priority because it is necessary for correct program timing. The CRT and keyboard printer interrupts have no time-critical requirements in the real time program. Likewise, the servicing of the heliostat serial data receiver can be delayed without any risk to correct program functioning. The floppy disk interface interrupts only need to function at program startup and shutdown so they can function with a very low priority.

The card installation was established after evaluating the interrupt priorities. However the available time is such that the system would probably work with almost any order of card installations, i.e., there appears to be plenty of time to do all interrupt tasks between the highest rate of occurrence of any interrupt. The important requirement is to design the software so the service time required for each interrupt is as short as

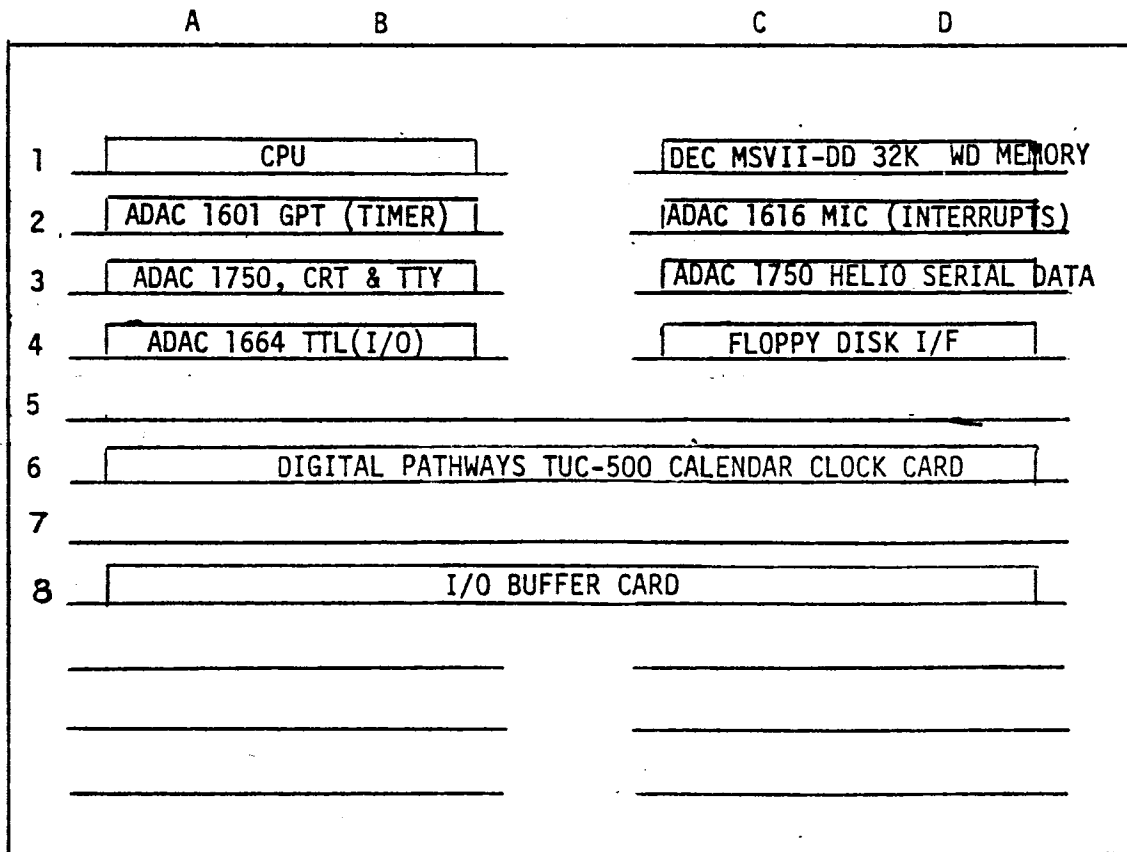


Figure 2.5-11. Computer Card Installation

possible. This minimizes the risk that interrupts could ever stack up to prevent proper service.

#### 2.5.1.1.8 HelioStat Control Cable Interface To Computer

The heliostat control cable must interface with the computer so as to provide test access to each signal. A reliable, low cost design is essential, and must include cable supports and clamps to prevent stress on pin connectors.

The design chosen mounts a terminal block in the back of the equipment rack which interfaces the cables to the computer cards and provides test access to each signal.

#### 2.5.1.2 Design Analysis and Trades

Several trade studies and analyses were conducted to select the preferred design approaches and hardware configurations.

##### 2.5.1.2.1 Time Source Selection

A study was conducted to select a source of time information. Sources considered were an IRIG B line time reader with a computer interface which would allow the computer to read WWV time, and the TCU-50 calendar clock card which would give an accurate time read out from its own clock. The cost of an IRIG B line reader would have been over \$1,200 compared to the TCU 50 cost of about \$325. An error analysis showed that a one second-of-time error could be tolerated and the TCU 50 could be set accurate to 1/2 second. Thus, the TCU 50 was selected.

##### 2.5.1.2.2 Signal Transmission Specifications

A study was conducted to determine what electrical specifications should govern the design of the signal lines between the heliostats and the computer. The specifications considered were: RS-423, RS-422 and 20 ma current loop for the serial data. It was assumed a heliostat may be located as far as 305

meters from the computer. The RS-422 specification was selected because it has a safe margin for communication for longer distances and it did not cost significantly more than it would to design to a lesser specification.

#### 2.5.1.2.3 Operator Communications

A study was conducted to determine if there was a need for any special hardware to handle mode control requests or displays. It was concluded that it was feasible to handle all operator communications through the CRT. Using the CRT was also the least cost approach for the prototype. Thus, no requirements for mode control or mode annunciation hardware were established.

#### 2.5.1.2.4 Mode Selection and Naming

Mode selection and naming constituted part of the software development. Principal considerations were operator participation requirements; automatic or manual mode-to-mode transition; and control simplicity and safety.

#### 2.5.1.2.5 Control Step-Size Selection

Heliostat power consumption and wear on the gear box and motors are a function of the number of start-stop cycles required to perform the tracking task. As control step size increases, the number of start-stop cycles decreases, but the RMS value of the aiming error increases. Tracking is accomplished by moving the reflected beam a specific step size in one axis each time a motor is turned on. The beam movement step size was tentatively selected to be two milliradians in each axis. The beam movement axes are elevation and cross-elevation. The beam movements are approximately twice the mirror elevation and cross-elevation movements. The cross-elevation movement is the azimuth axis movement multiplied by the cosine of the elevation angle. Thus, the mirror step sizes are 1 milliradian in the elevation axis and  $1/(\cos \text{ elevation angle})$  milliradians in the azimuth axis. The step sizes can be increased if the total pointing errors are below the specification allowances.

#### 2.5.1.2.6 Update Time Frame Requirements

The heliostat axis rates required to hold the beam on the receiver vary as a function of: the heliostat position relative to target, the time of year, and the time of day. A nominal update rate requirement can be established from analysis of sun travel rates. The sun's apparent motion across the sky is at a nominal rate of 0.073 milliradians per second. If the mirror is stationary, the reflected beam will move at the same rate as the sun. The nominal time for the beam to move two milliradians is  $2/0.072 = 27.8$  seconds. Thus, on an average basis, updates will need to occur about every 28 seconds. The computer frame time was selected to be four seconds which will allow track updates to occur at a rate seven times faster than the nominal requirements.

#### 2.5.1.2.7 Control System Error Analysis

The aiming errors analysis allocated a 0.4 mrad mirror-positioning error per axis to the control system. The control system error analysis shows that it will easily comply with this requirement.

Time readings accurate to less than  $\pm 1$  second are easily achieved by the TCU-50 time clock card. The time error would consist of a setting error and a drift error. The setting error will generally predominate. The error over many settings should have a Gaussian distribution. A conservative estimate for the one sigma value of the time error is 1/2 second. Considering the sun's travel rate of 0.073 milliradians per second, the equivalent beam error from the time error would be about  $\pm 0.036$  milliradians. The mirror normal pointing error is approximately half the beam error or 0.018 milliradians. A conservative value of 0.02 milliradians per axis was thus used for the error analysis.

In addition to time error, there is also an error in the Ephemeris data. The nautical almanac states that errors in declinations and the Greenwich hour angle (GAA) may exceed 0.014 milliradians for one third of the time. To be conservative, it was assumed the error may have a one sigma value of 0.02 milliradians per axis.



Computational errors are also introduced. The command calculations will be done in floating point arithmetic, thus, the most significant computation errors will occur in the granularity of the fixed point arithmetic necessary for the motor controls. The granularity is determined by the design which makes the least significant bit (LSB) of the command word equal to one motor revolution.

The azimuth axis gear ratio is 52,426 to 1, so the LSB value is  $\frac{2\pi}{52,426} = .12\text{mrad}$

The elevation axis gear ratio is approximately twice the azimuth axis ratio so the LSB value is 0.06 milliradians.

The floating point commands will be truncated to produce fixed-point commands so the granularity error will have a uniform distribution from 0 to 1 LSB. The one-sigma value for each axis is, therefore: 0.07 milliradians in azimuth, and 0.035 milliradians in elevation. The azimuth axis value is multiplied by  $\cos 20^\circ$  to get a cross elevation estimate. Thus, the cross elevation value is 0.066 mrad.

Errors also are affected by step size. The baseline step size is 1 mrad. The error will be uniformly distributed about zero, so the one sigma value is or 0.29 milliradians in each axis.

Refraction corrections for a standard day must also be included in the control algorithms. These corrections will be adjusted for the altitude at the test site. Refraction errors must be estimated for non-standard days under various conditions.

For a temperature range between  $0^\circ\text{C}$  and  $50^\circ\text{C}$ , the refraction correction factor varies from 1.04 to 0.88, respectively. For a pressure variation ranging from 775mm ( 30.5 inches) of Hg to 660 mm ( 26 inches) of Hg, the refraction correction factor varies from 1.03 to 0.88 respectively.

It is not likely that the combinations of a high temperature near  $50^\circ\text{C}$  and a low pressure near 660 mm ( 26 inches) of Hg would occur on an operating day. It is assumed the worst case variations from combined temperature and pressure effects would result in a refraction equal to 0.84 times the standard

refractions, i.e., the refraction error would be  $1-.84=0.16$  times the standard refraction.

The standard refraction varies from 1.03 milliradians at 15 degrees of sun elevation, to zero degrees at 90° of sun elevation. For most of the operating day the sun would be above an elevation of 30°; the standard refraction at 30° is 0.48 milliradians. Thus, for most of the day the refraction error would be less than  $.16 \times 0.48 = 0.08$  milliradians. A conservative estimate for the one sigma value of the refraction error is therefore, 0.04 milliradians. The refraction error will have a significant effect only on the elevation axis errors.

The net effect of the foregoing errors are tabulated for each axis in Table 2.5-1. The root sum square of the individual calculated errors is 0.3 milliradians in each axis, compared to the budgeted value of 0.4 milliradians. This leaves a comfortable margin for errors which may not have been considered. If testing shows the heliostat has smaller errors than the specification requirements, then the control step sizes can be increased, which will decrease the heliostat power consumption.

## 2.5.2 Control Software

### 2.5.2.1 Software Design Description

#### 2.5.2.1.1 General

A top level flow chart used for software development is shown in Figure 2.5-12 a and b . The main program was written in Fortran to gain the advantages of a high level language.

The heliostat control program begins with the startup initialization block. This block takes care of all startup tasks which only need doing at startup or once a day. Some of the more obvious of these tasks are described below.

Table 2.5-1. Tabulation of Control Errors and RSS Results

Source	Value	Effect (milliradians)	
		Elevation	Cross Elevation
Clock time	$\pm 1$ sec.	0.02	0.02
Ephemeris data	$\sigma = .03$	0.02	0.02
Off-nominal refraction 0° to 50°C 980 to 1,040 millibars	$\sigma = .04$	0.04	0
Computation	LSB	0.04	0.05
Step size, 1 MR	$\pm .5$ MR	0.29	0.29
Root sum square average		0.30	0.30
Budget		0.4	0.4

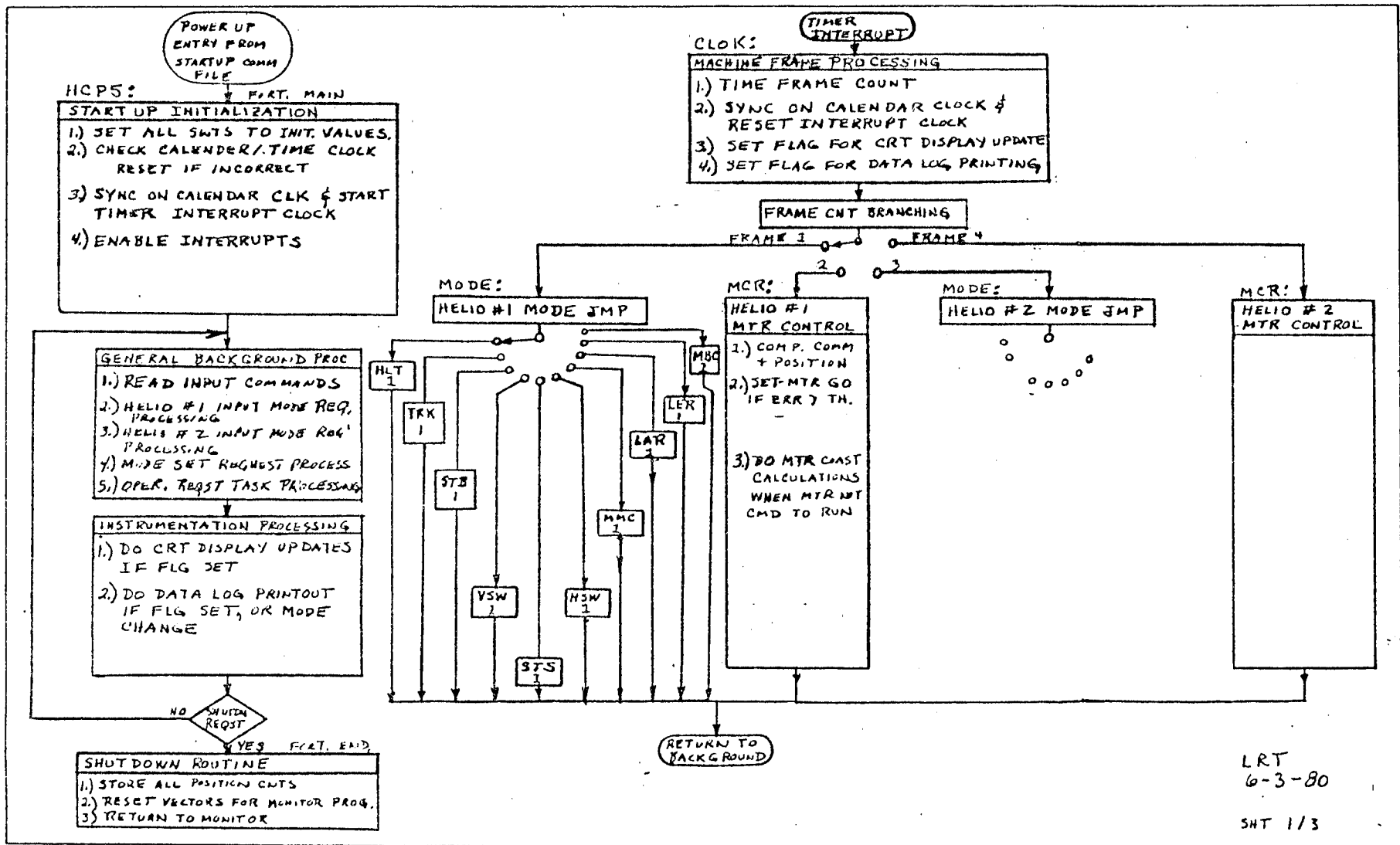


Figure 2.5-12a. Top Level Flow Chart for Software Design

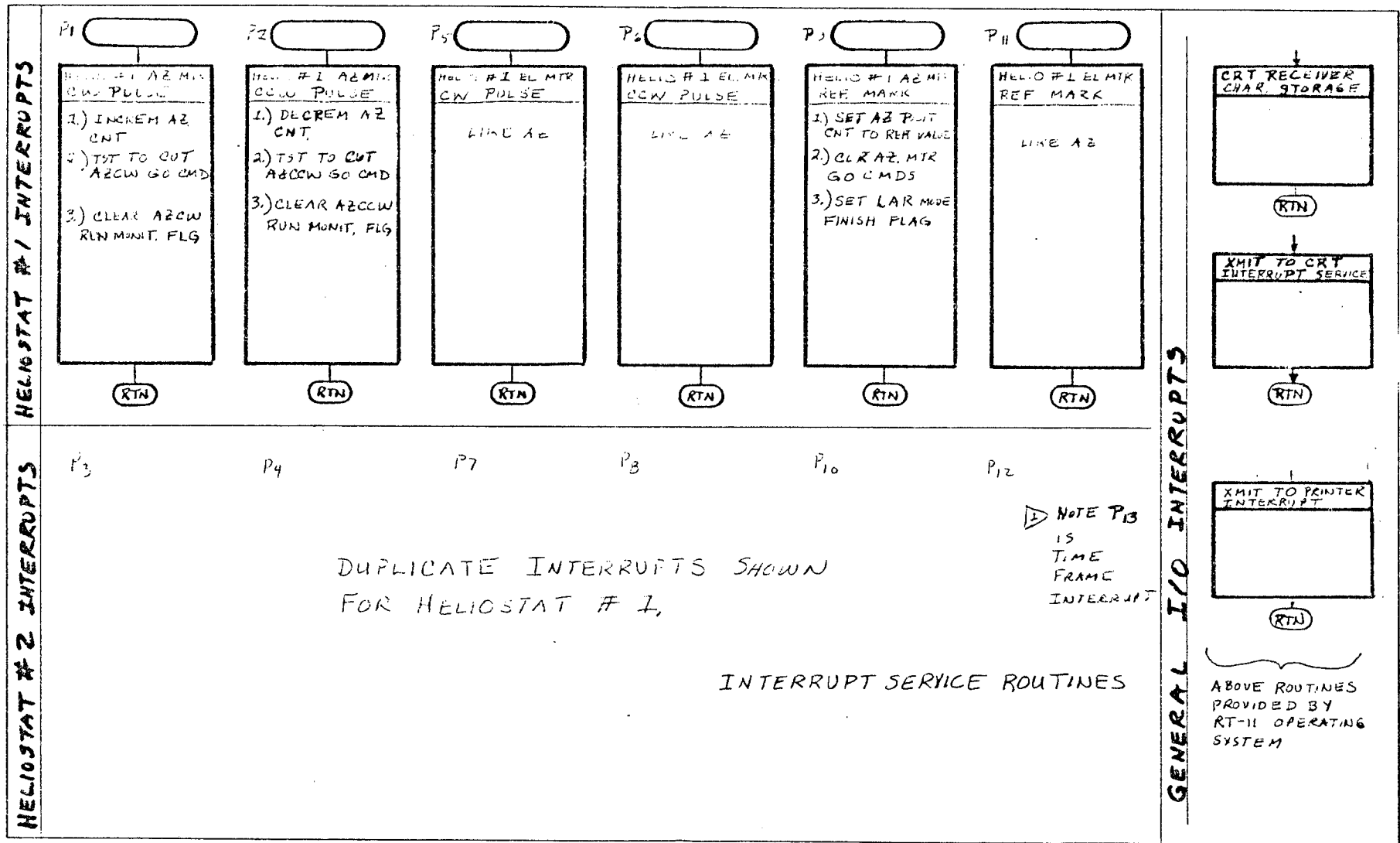


Figure 2.5-12b. Top-Level Software Flowchart,

Data is read from the disk. All program switches such as the frame count and mode jump switches are set to initial values, e.g., the mode switches are set to the halt mode. All counts are set to initial values. Next the system displays the calendar clock time and asks the operator to approve it or correct it. The calendar clock time is displayed to the nearest second. After approval, the seconds past midnight count is determined from the calendar clock reading. Next, it examines the calendar clock until it detects the seconds change and then starts the timer interrupt clock. Last, all the regular program interrupts are enabled, and the processor starts executing the background program.

The processor continues to loop through the background program until a time interrupt occurs. The time interrupt will pull the processor out of the background program and start it processing at the beginning of the timer interrupt routine.

The time frame counter counts the number of timer interrupts for a time count in seconds past midnight. The timer interrupt from the ADAC 1601 GPT card is set to occur slightly less than one second after it is started counting. The "SYNCH ON CALENDAR CLOCK" routine then watches for a change in the seconds readout of the calendar clock and resets the interrupt when the seconds change. Then a flag is set to cause the background program to update the CRT modes and positions displays (once per second) and seconds are counted to set a flag for the data log print out if it is enabled.

The timer interrupt routine then jumps to one of four branches on a sequential and continuous basis. The timer-interrupt occurs on one-second intervals to produce a machine-frame time of one second but the software computation frame-time is four seconds. Each of the four machine frames performs separate functions.

In frame 1, the processor executes the instructions for the mode requested for heliostat number 1. In frame 2, the processor executes the motor control instructions for heliostat number 1. In frames 3 & 4, the processor services heliostat number 2.

After the timer interrupt service is completed, the processor returns to the background program at the point from which it was interrupted.

Other interrupt service routines have also been written and are indicated in Figure 2.5-12b. These are interrupt routines which count the motor motion pulses and do the reference mark detection processing. In addition to the interrupt service routines which were written, the heliostat control program uses interrupt service routines in the RT-11 single job monitor program to handle the CRT and keyboard printer communication interrupts.

The background processing is divided into the general background processing and the instrumentation processing (i.e., data logging on request) handles the printout of mode operating history and instrumentation data on the printer. The general background processing handles all operator communications with the CRT and the mode logic and mode setup tasks.

The software is structured to keep all interrupt service routines including the timer interrupt service as short as possible. The background is designed to avoid any program hangups so the processor cycles through the background on a rapid basis and the operator does not notice any delay between typing characters on the CRT keyboard and seeing them echoed from the computer to the CRT screen.

The shutdown task assures the heliostats are halted and then stores the motor position counts on the disk and returns to the operating system monitor program. On next startup the motor position counts will be loaded with no need to execute the locate reference marks routine.

#### 2.5.2.1.2 Data Base Structure Modification and Examination

Most of the data which controls the operation of the control program, or is of significance for understanding and troubleshooting it, is contained in two arrays - an integer array - K1 to K120; and a floating point array - F1 to F240. While the program is running, any element of these arrays can be examined or changed using the CRT terminal. The elements of these arrays are identified in (Appendix H). To examine an element of the integer array,

type Kn,Pcr in which n is a number indicating the desired element and cr is a carriage return. For the floating point array, use F in place of K. To replace an element with a new value type Kn,Lm cr or Fn,Lm cr, in which m is the value desired. It must be written with a decimal point for either the K or F array. All the requests must have more than 4 characters or else the program will try to interpret it as a mode request. Hence, single character numbers must be typed with a preceding zero for display.

This capability to examine and change elements of these arrays is not needed during normal operation. It is needed during initial setup and alignment of a heliostat, to enter ephemeris data for another month, for manual control of mirror and beam position, and for changing various operating parameters such as the stow and standby positions.

#### 2.5.2.1.3 Automatic Data Logging

The automatic data logging provides the operator with the options of printing out any parameter in the data base. When enabled, it automatically prints a record of all mode changes and the time of mode change.

The data printout time interval can be selected to be any integer number of seconds less than 256.

#### 2.5.2.1.4 Selected Modes and Processes

The mode transitions map for the prototype heliostat controls is shown in Figure 2.5-13. The three letter mnemonics are the mode call letters. The normal daily mode transition would be from one of the two stow positions, up through track and back.

For vertical stowing, at power up the system always comes up in the halt (HLT) mode. The halt mode means the mirror will receive no commands to move. When ready for the mirror to go to standby position the operator should request the stow-to-standby (STS) mode which will take the mirror to standby position. When the standby position is reached the system automatically changes to standby (STB) mode and holds the reflected beam at the standby position. A track (TRK) mode request will then move the reflected beam onto the receiver



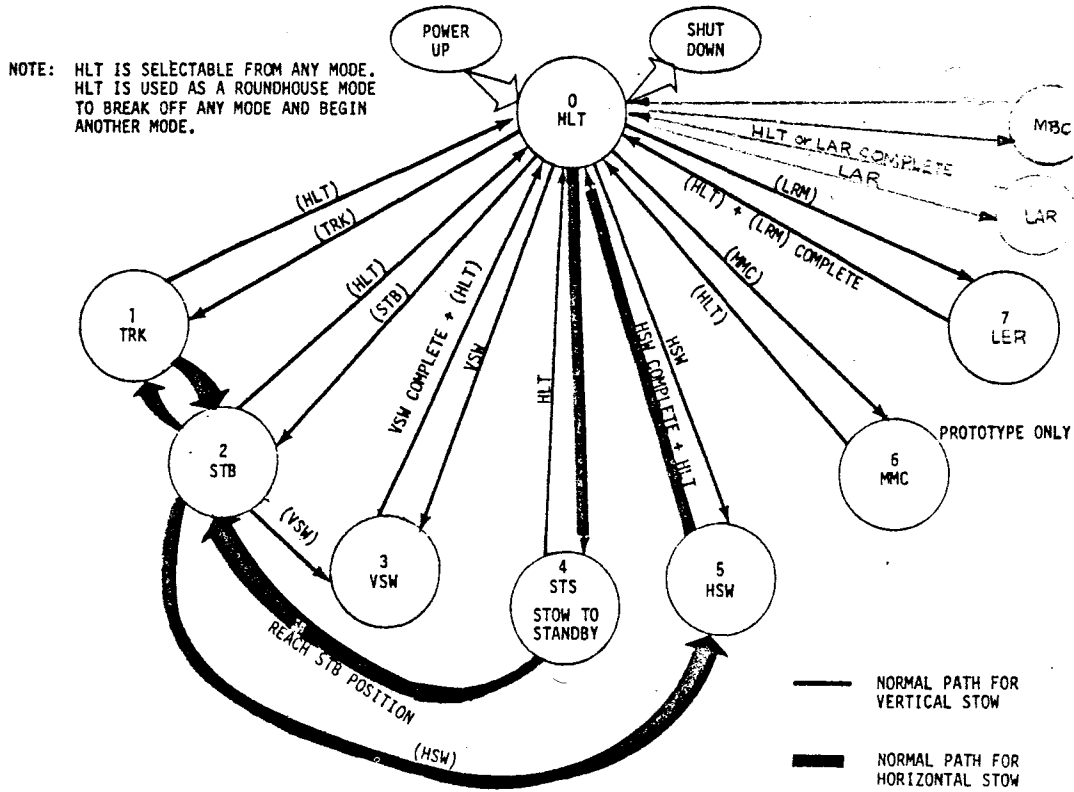


Figure 2.5-13. Mode Transitions Map

and hold it there throughout the day. When through tracking, the standby mode can be requested to move off target and hold the reflected beam at the standby position. From standby one can request either vertical stow (VSW) or horizontal stow (HSW). The stow modes will move the reflected beam from the standby position along a prescribed path and leave the mirror in the stow position. The sequence for horizontal stow would be the same except the HSW mode would replace the VSW mode in the sequence of calls.

In addition to the normal daily operating modes, a manual mirror control (MMC) mode is provided to allow manual control of the mirror to any position. The LER and LAR modes are provided to locate the elevation and azimuth reference marks. A manual beam control (MBC) was added as a possible aid to the alignment task. It allows the operator to move the designated target coordinates while tracking.

Only the transitions shown on the mode transition map (see Figure 2.5-13) will be allowed by the mode logic. The mode logic will allow any mode to be requested from the halt mode, or the halt mode can be requested from any mode. Thus, the halt mode can be used as a 'round-house' or intermediate mode to achieve any transition.

The modes were defined so each mode performs a simple well-defined function. Appendix G provides detailed descriptions of mode operations and software organization.

### 3.0 COLLECTOR SUBSYSTEM

This section provides a description of the overall collector subsystem (heliostats, controls, peripheral equipment, site preparation and documentation), and discusses its performance and operational characteristics.

#### 3.1 SUBSYSTEM DESCRIPTION

The production collector subsystem includes a field of 6914 heliostats, as shown in Figure 3.1-1. The field is controlled by a computerized, digital electronic system, which is, in turn, an integral part of the overall plant control system.

The 1.268 Km<sup>2</sup> field assumes a 1.5 solar multiple, design point of day 81, noon, and a nominal reflective area per heliostat of 44m<sup>2</sup>. The Sandia DELSOL computer program was used for the field analysis. (Reference 3-2)

Figure 3.1-2 shows all the elements that are normally delivered with a collector subsystem. This includes, in addition to heliostat hardware, maintenance support, personnel, subsystem integration and technical publication elements. The classification of elements is in accordance with the Sandia Cost Breakdown Structure provided under the contract.

#### 3.2 PERFORMANCE ANALYSIS

The primary purpose of the collector subsystem is to deliver reflected sunlight to an elevated receiver. The ability to perform this function was evaluated at two levels; the individual heliostat, and the collector subsystem field.

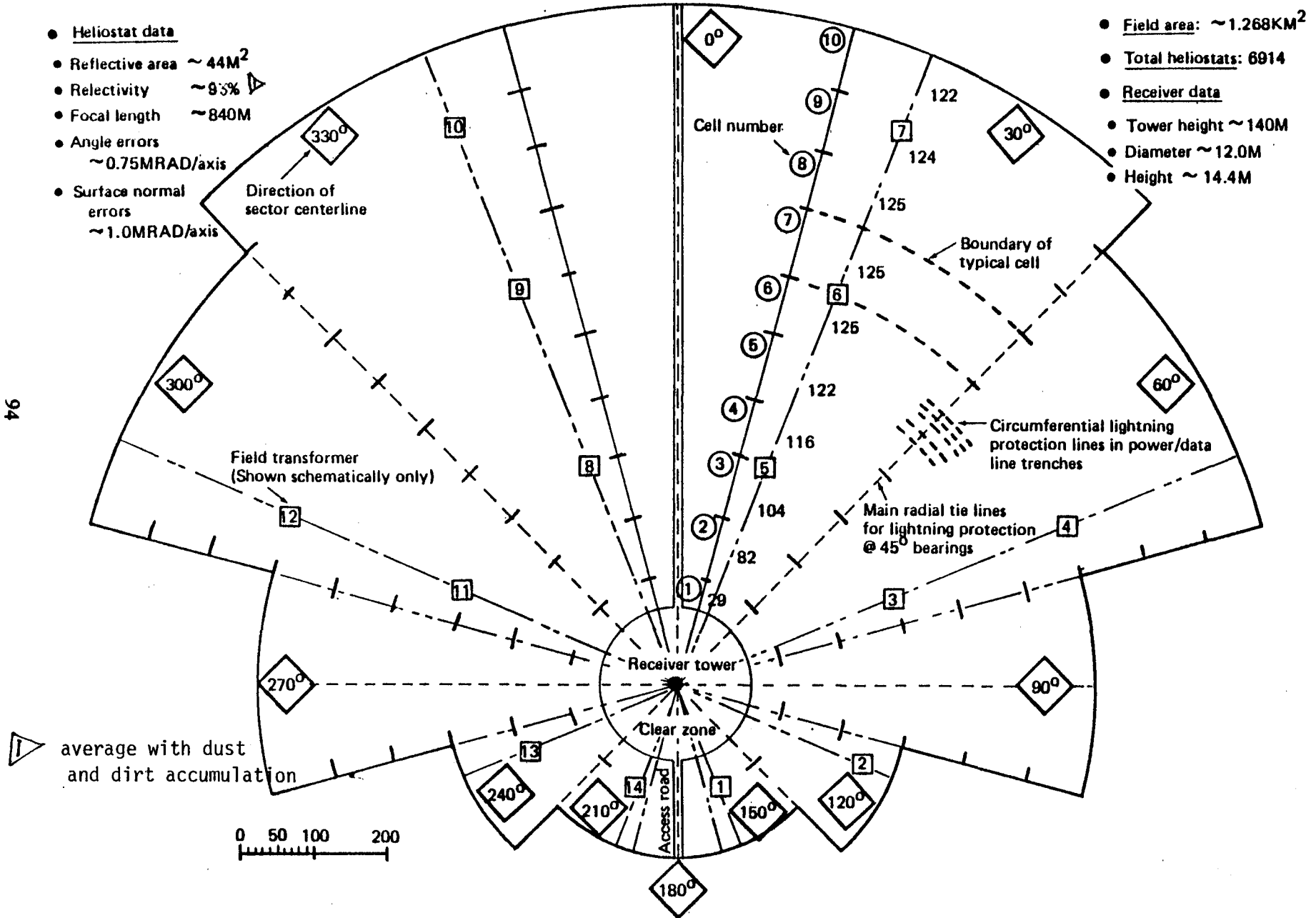


Figure 3.1-1. Collector Subsystem, General Field Layout, 50 MW Solar-Electric Plant

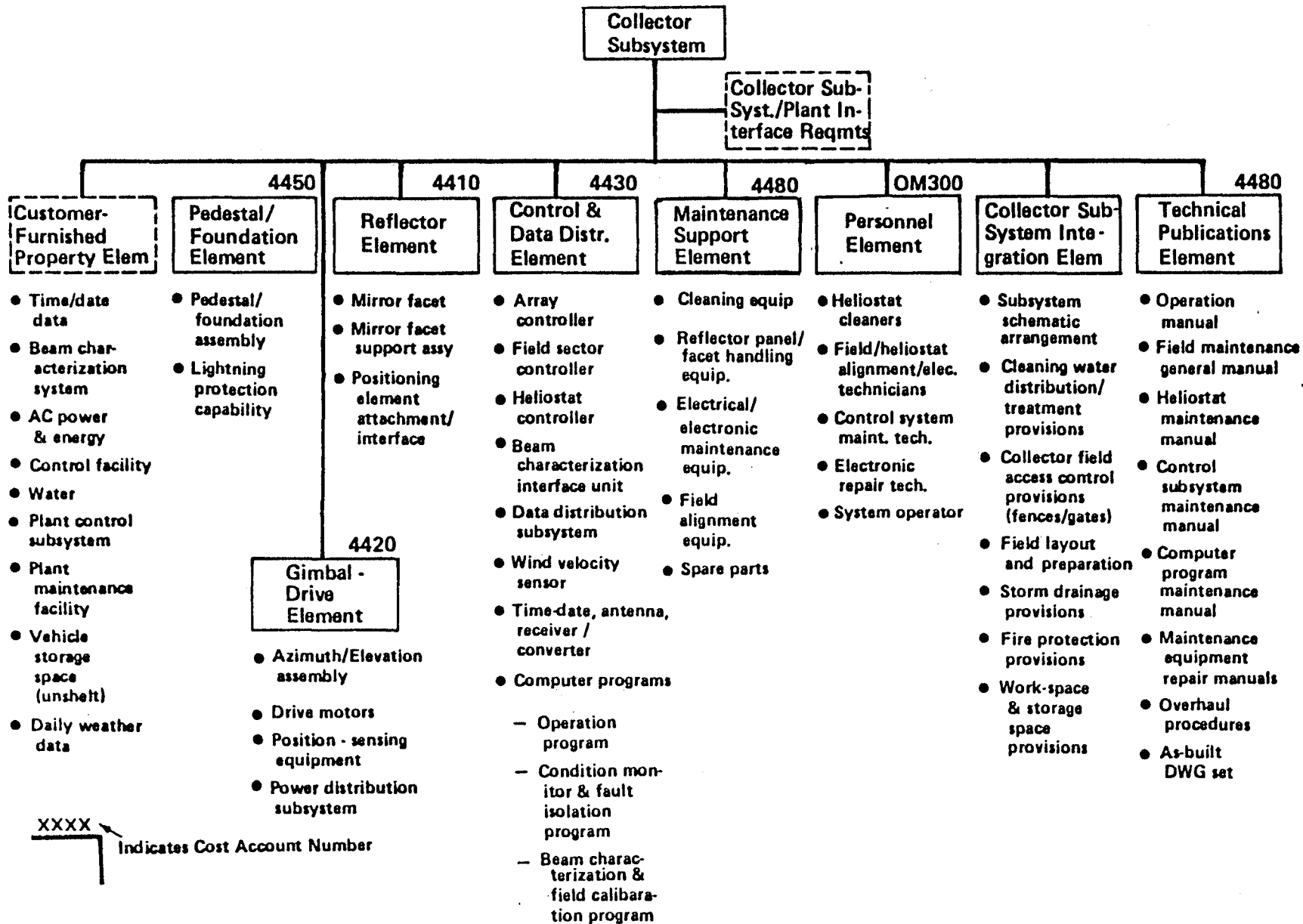


Figure 3.1-2. Major Elements of the Collector Subsystem

### 3.2.1 Reflected Energy From Single Heliostat

Paragraph 3.2.1b of the Sandia Specification (Reference 3-1) requires not less than 90% of the solar energy reflected from a single heliostat to fall within the heliostat's theoretical beam shape\* plus a 1.4 milliradian fringe at target slant range.

The performance of the BEC heliostat was analyzed by the Sandia HELIOS (Reference 3-3) computer program. The theoretical image (facets canted for 921 m range, perfect glass) reflected to a flat, normal, target on the summer solstice is shown in Figure 3.2-1; with a 1.4 milliradian fringe. The outer boundaries of the energy reflected from the heliostat when certain errors were modelled was determined by the DELSOL computer program (Reference 3-2); the result for noon on the summer solstice is shown in Figure 3.2-2. Analysis of the data from the two computer programs showed that the reflected image energy requirement could be met for combined random errors up to approximately 1.1 milliradians. The analysis is summarized graphically in Figure 3.2-3.

### 3.2.2 Collector Subsystem Efficiency and Power Output

The DELSOL computer program was used to evaluate the collector subsystem average annual efficiency based on a generalized insolation model; the results are shown in Figure 3.2-4. Starting with an average reflectance of 0.92, the losses due to cosine, shading, blocking, atmosphere attenuation and receiver overflow result in an average efficiency of 67.9%

With a field of approximately 6914 heliostats, the DELSOL computer program predicted that 210 MW of thermal power are delivered to the receiver at noon on the design day. The field provides sufficient thermal energy on an annual basis for an average of 2.7 hours of storage for a 50 MWe electric plant; this yields an expected capacity factor for such a plant of about 40%

---

\*The theoretical beam shape was determined by a Sandia computer program, HELIOS (reference 3-1).

Summer Solstice

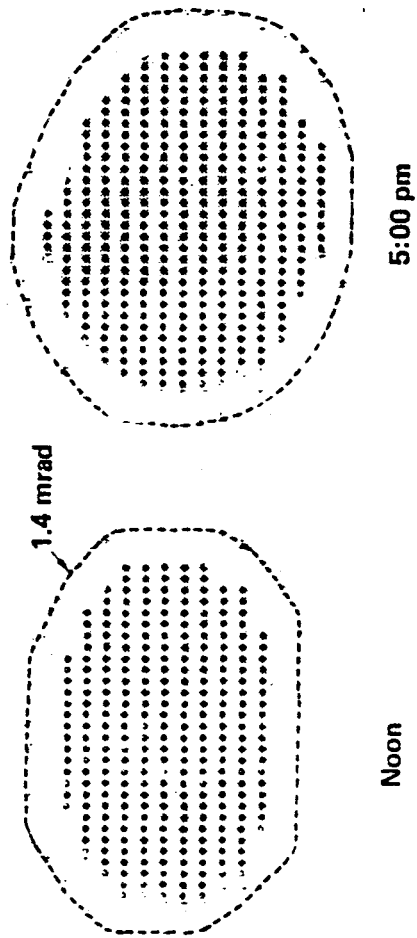


Figure 3.2-1. Theoretical Image with 1.4 Milliradian Fringe

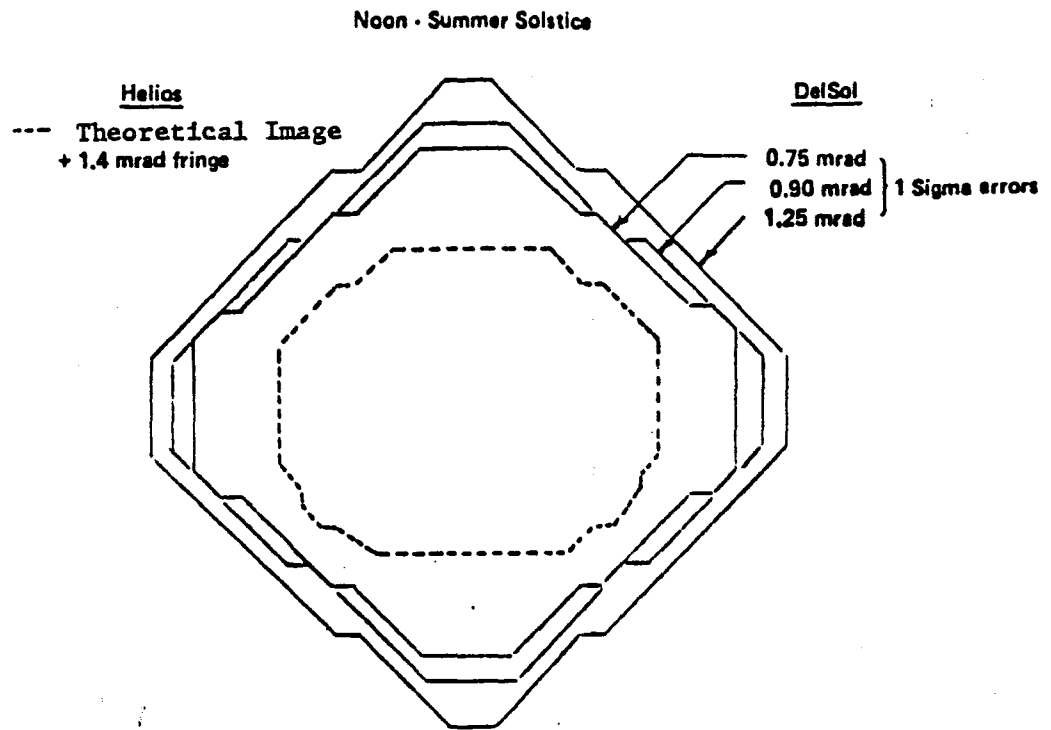


Figure 3.2-2. Theoretical Reflected Image and Boundaries of Reflected Energy when Errors are Present

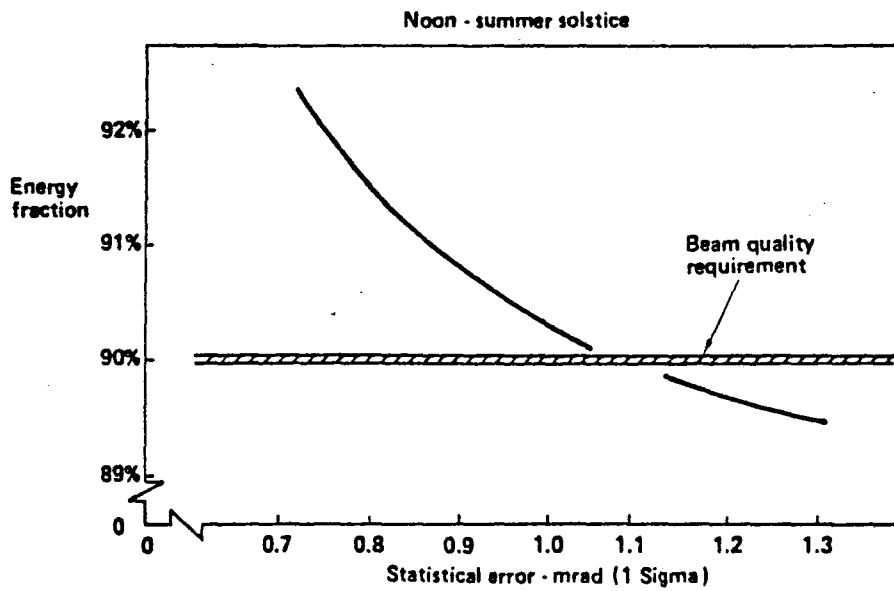


Figure 3.2-3. Fraction of Reflected Energy within 1.4 Milliradian Fringe when Errors are Present



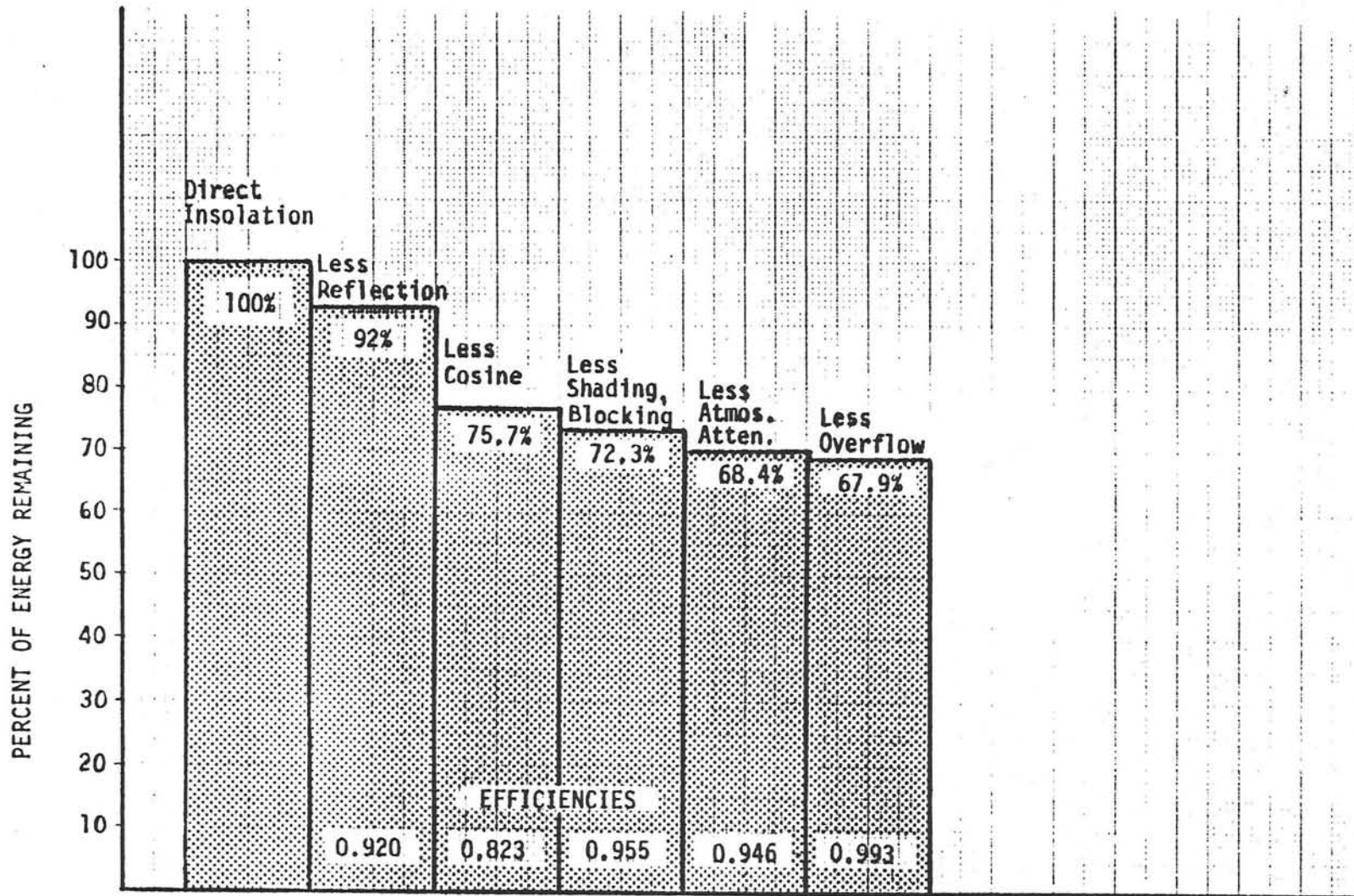


Figure 3.2-4. Collector Subsystem Average Annual Loss Sources and Values

### 3.2.3 Availability

#### 3.2.3.1 General Considerations

Economic production of electricity by solar-thermal conversion processes requires reliable and maintainable equipment. This is especially true for the collector subsystem due to the variable nature of insolation from both diurnal and weather effects.

The collector's reliability and maintainability attributes are combined in an availability measure, which we define as the (long-term) probability that it will be able to perform a programmed (daily) dispatch, given that adequate insolation is present. This probability may be quantified by taking the ratio of the system 'up-time' to some total time, in this case, 24 hours\*.

A 24-hour period will normally include both a daily dispatch and quiescent, or nighttime collector operations. In the latter period, only a few of the collector subsystem elements will be functioning. Thus, it is appropriate to separate these periods in the availability model. This is accomplished by constructing an availability expression for the 24-hour time period as:

$$A_{\text{SUBSYS}} \equiv A_{\text{DISPATCH}} \times A_{\text{QUIESCENT}} \quad (3.1)$$

-----  
\*A 24-hour period was selected because repairs can be made on 2nd or 3rd shifts, and because some collector elements operate 24 hours per day. In addition, a solar-electric plant would naturally be subject to a repetitive daily dispatch.

This expression is appropriate because the two time periods may be considered as statistically independent. We may then use a general availability expression for the  $i^{\text{th}}$  element, taking account of the appropriate times in each period; thus we have:

$$A_i = \frac{MTBF_i}{MTBF_i + MTTR_i + MDT_i} \quad (3.2)$$

where  $A_i$  = the availability of the  $i^{\text{th}}$  element

and  $MTBF_i$ ,  $MTTR_i$  and  $MDT_i$  are the mean time between failure, mean repair time, and mean delay time (if applicable) of the  $i^{\text{th}}$  element.

The availability of each ( $i^{\text{th}}$ ) element may then be combined to determine the collector's availability in each time period. In general, we have:

$$A_{\text{subsys}} = \left[ A_{\text{ped found}} \right] \times \left[ A_{\text{gimb-drive}} \right] \times \left[ A_{\text{reflec.}} \right] \quad (3.3)$$

$$\times \left[ A_{\text{cont. \& data dist.}} \right] \times \left[ A_{\text{maint. suppt.}} \right] \times \left[ A_{\text{pers.}} \right]$$

where  $A_{\text{subsys}}$  = the subsystem availability

and  $A_{\text{ped found}}$ , etc., are the individual element availabilities

This expression is perfectly general and is applicable to either dispatch or quiescent modes when account is taken of operating and non-operating failure rates and the expected length of each time period.

### 3.2.3.2 Expected Values For Dispatch and Quiescent Time Periods

Because the availability of the collector subsystem is to be evaluated over the long term, say one year, it is necessary to determine the expected values of the dispatch and quiescent times. This is accomplished by considering collector/plant use in both peak and off-peak months.

The number of operating days per month and the average daily operating times throughout the year are shown in Table 3.2-1. Weighting the average daily time (the difference between "collector stop" and "collector startup" in Table 3.2-1) by the number of days in each month, the average time for the

Table 3.2-1. Shift Time Requirements for Operation and Maintenance Personnel

Month	Days		Average Daily Time For ①						Shift Times For				
	Per Mo.	Operating ①	Collector Startup	"Sunrise"	Gen. Brkr. Close	"Sunset"	Collector Stop	Gen. Brkr. Open	Operation Personnel			Maintenance Personnel	
									1st	2nd	3rd ②	1st	2nd ③
Jan	31	23	0730	0836	0900	1524	1600	1630	0700-1530	1500-2330	-	0730-1600	1600-2400
Feb	28	20	0700	0803	0830	1557	1700	1730	0630-1500	1430-2300	-	0730-1600	1600-2400
Mar	31	21	0615	0715	0745	1645	1730	1800	0545-1415	1345-2215	-	0730-1600	1600-2400
Apr	30	22	0545	0642	0715	1718	1800	1830	0515-1345	1315-2145	-	0730-1600	1600-2400
May	31	23	0530	0621	0700	1739	1815	1900	0500-1330	1300-2130	-	0730-1600	1600-2400
Jun	30	30	0500	0609	0645	1751	1845	2000	0430-1300	1230-2100	-	0730-1600	1600-2400
Jul	31	31	0530	0621	0700	1739	1815	1900	0500-1330	1300-2130	-	0730-1600	1600-2400
Aug	31	31	0545	0642	0715	1718	1800	1830	0515-1345	1315-2145	-	0730-1600	1600-2400
Sep	30	30	0615	0715	0745	1645	1730	1800	0545-1415	1345-2215	-	0730-1600	1600-2400
Oct	31	23	0700	0803	0830	1557	1700	1730	0630-1500	1430-2300	-	0730-1600	1600-2400
Nov	30	21	0730	0836	0900	1524	1600	1630	0700-1530	1500-2330	-	0730-1600	1600-2400
Dec	31	22	0745	0342	0915	1518	1600	1630	0715-1545	1515-2345	-	0730-1600	1600-2400

- Notes: ① Assume summer-peaking load.  
 ② Based on 1976 Barstow insolation.  
 ③ No operator required on 3rd shift for collector subsystem; may be required for other power plant subsystems.  
 ④ Shorter shift time reflects wage differential.

year is 11.1 hours\*, or, approximately 11 hours/day. The balance of the time (13 hours), the subsystem is (on the average) in a quiescent mode, with only portions of some elements operating.

With the time periods in each mode determined we can now evaluate the reliability and maintainability characteristics, and hence, the availability of the collector subsystem.

### 3.2.3.3 Reliability Evaluation

To determine the reliability of the collector subsystem, we assume that failures are independent events characterized as a Poisson process with constant event rates, and exponentially distributed times between failure. This assumption leads to a straight forward expression of reliability, namely

$$R = e^{-\lambda t}$$

Where:  $\lambda$  = Failure Rate (3.4)

t = Time

However, for availability analysis, we need not determine the component or subsystem reliabilities, but can deal, instead, with their failure rates or their reciprocals, mean times between failure (MTBF).

Each of the collector subsystems elements was evaluated to determine the expected mean time between failure, where "failure" was defined as the inability of the element to perform its intended function. The estimated MTBF's are summarized in Table 3.2-2. Due to contract budgetary limitations the scope of the effort was limited. Consequently, these estimates are considered to be conservative.

-----  
\*Note: The average time does not include scheduled power-plant downtime; the inclusion of this factor would not change the expected value significantly.

Table 3.2-2. MTBF, Failure Rates, MTTR and Availability Estimates for the Collector Subsystem Elements and Components

ELEMENT OR COMPONENT	NUMBER PER SUBSYSTEM	ESTIMATED UNIT VALUES			AVAILABILITY	
		MTBF, HOURS	FAILURE RATE x 10 <sup>6</sup>	MTTR HOURS	DISPATCH (11 HOURS)	QUIESCENT (13 HOURS)
Ped.-Foundation Ele.	1	-	-	10.00	0.999999	0.999999
Pedestal Assy.	6,400	876,000	1.14	10.00		
Lightning Prot. Sys.	1	150,000	6.67	50.00		
Gim.-Drive Ele.	1	-	-	8.95		
Gimbal Assy.	6,400	28,725	34.81	3.07	0.996403	
Azimuth Gear Box	6,400	100,000	10.00	60.00		
Elevation Drive	6,400	150,000	6.67	30.00		
Motors ①	12,800	200,000	5.00	8.00		
Wiring & Switches	6,400	150,000	6.67	8.00		
Structure	6,400	675,000	1.48	25.00		1.0
Pwr Distribution Substations	1	2,700	371.19	9.39	0.996534	
Power Cable Net	5	200,000	5.00	16.00		
Switch Boxes	1	350,000	2.86	40.00		
Misc. Components	50	150,000	6.67	10.00		
Reflector Element	1	100,000	10.00	20.00		
Facet Assy. ②	1	26,900	37.20	5.71	0.990813	0.990813
Frame Assy.	76,800	750,000	1.33	NR ③		
Bracket Assy.	6,400	500,000	2.00	24.00		
Con. & Dat. Dis. Ele.	307,200	2,500,000	0.40	NR ④		
Array Controller	1	-	-	2.55	0.960182	-
Field Sector Cont.	1	20,000	50.00	24.00	0.999001	0.999001
Heliostat Controller	16	25,000	40.00	16.00	0.999988	-
BCS Interace Unit	6,400	25,000	40.00	16.00	0.964424	-
Data Dist. System	1	20,000	50.00	48.00	0.997606	-
Wind Vel. Sensor	1	150,000	6.67	24.00	0.999840	-
Time-Date Recvr.	1	50,000	20.00	16.00	0.999680	0.999680
Computer Programs	1	50,000	20.00	16.00	0.999680	0.999680
Mainten. Support Ele.	1	500,000	2.00	100.00	0.999800	0.999800
Cleaning Equip.	1	-	-	47.69		
Facet Handlg. Fixt.	3	10,000	100.00	40.00	0.988095	0.988095
Reflect. Aling. Fixt.	2	100,000	10.00	8.00	0.999840	0.999840
BCS Set	2	100,000	10.00	8.00	0.999840	0.999840
Misc. Elec. Repr. Equip.	1	50,000	20.00	48.00	0.999041	-
Personnel Elem.	1	100,000	10.00	500.00	0.995025	0.995025
Operator	1	-	-	13.80		
Cleaners	2	50,000	20.00	8.00	0.999200	0.999200
Repair Tech.	15	30,000	33.33	16.00	0.992034	0.992034
	6	40,000	25.00	8.00	0.998801	0.998801

Notes: ① Includes active repair time only, but includes delay times, e.g., overnight waits,

② "NR" - Not repairable

③ Approx. fail rate from CRTF:  $4.93 \times 10^{-6}$

④ Approx. CRTF fail rate:  $0.4 \times 10^{-6}$

#### 3.2.3.4 Maintainability Evaluation

Each of the elements of the subsystem were reviewed to determine their expected repairability and mean repair time. Since the repair capability for the collector subsystem will be integrated with the general maintenance/repair capability for the power plant, it is not practical to attempt detailed repair/discard, or optimal-repair-level analyses. It is, however, possible to make estimates of the feasibility of repairing various components, and to establish estimated repair times; these estimates are shown in Table 3.2-2.

#### 3.2.3.5 Availability

As noted above, the availability of the various elements in each mode can be determined by the expression shown in equation 3.2; they are shown in Table 3.2-2. In some cases, however, it is necessary to carefully define "failure" in order to calculate an availability for an individual element or component. This is true for the gimbal-drive reflector, and control and data distribution elements, and results from their large numbers of individual components, e.g., gimbal assemblies, reflector assemblies, heliostat controllers.

To establish an effective MTBF for these three elements, it was assumed that a "failure" had occurred in the collector field when more than 0.1% of the heliostats were simultaneously out of commission. To determine these effective MTBF's, the probability of a single component (e.g., gimbal) failure was calculated from the Poisson probability mass function. Using this probability, the expected (average) number of failures during the dispatch or quiescent periods were determined based on the population of the various components. A new cumulative probability was then calculated (again using the Poisson pmf) for the event which corresponds to not more than 0.1% of the heliostats out of commission. Using this cumulative probability as the

equivalent of element (or sub-element) reliability\*, it was then possible to derive an equivalent MTBF by simply solving equation 3.4 for  $\lambda$  (since  $t$  and  $R$  were known).

Based on the element availability shown in Table 3.2-2, the predicted availability for the collector subsystem in the dispatch and quiescent modes are 0.918 and 0.962, respectively; this gives a combined daily availability of 0.883.

-----  
\*Recall that 'reliability' is normally stated as a conditional probability, i.e., given a system is good at some time  $t$ , the probability that it will perform without failure over some interval  $t, t+\Delta t$  is the systems reliability.



### 3.2.4 Safety

Paragraph 3.2.3 of Sandia Specification A10772D established three major safety requirements for the collector subsystem:

- a. emergency detargeting of the heliostat images from the receiver to less than 3% of an initial value within 120 seconds;
- b. heat fluxes on the receiver tower and unirradiated portions of the receiver are to be 25 kW/m<sup>2</sup> or less;
- c. the reflected sunlight beams control strategy and equipment are to be controlled so as not to endanger personnel and property within and outside the plant boundary, including air space.

#### 3.2.4.1 Emergency Detargeting

The emergency detargeting requirement is satisfied by the control element issuing commands to the heliostat controllers, and applying power to the drive motors, thus removing the images from the receiver. The drive-rate capability of the motors (12°/minute, azimuth; 6.2°/minute, elevation) in any wind up to 16 meters per second is sufficient to move the image from the nearest and farthest heliostats to a standby position near the receiver within the prescribed time. Table 3.2-3 shows the results of the calculations. The data shows that the average time of the nearest (worst case) heliostat is 15 seconds, after communication and command.

#### 3.2.4.2 Flux Spillage and Beam Control

Some redirected sunlight could illuminate portions of the receiver and tower not intended to be irradiated. This might result from unfocused energy from individual heliostats; from beam travel during normal startup and shutdown functions; or during emergency detargeting (e.g., required due to a generator trip, etc.).

Since the production control element will include computer program subroutines to startup and detarget the field in a controlled manner,

Table 3.2-3. Heliostat Range and Image Size, Displacement and Elapsed Times to Standby Position

Field Location	Slant Range, Meters, From Receiver	Approximate Image Size, Meters at Slant Range ①		Maximum Azimuth Displacement Of Reflected Image Degrees, Receiver to Standby ①	Average ② Time to Move Reflected Image, Minutes, Receiver to Standby ③
		Width	Height		
Nearest Heliostat	108	4.0	2.2	~ 6°	0.25
Farthest Heliostat	1200	13.5	11.7	~ 1.2°	0.05

- Notes: ① Assumes image energy centroid is centered on receiver, and outer fringe of image is swung left or right until it is 10 meters away from receiver.
- ② Times shown are expected values: Assume a standard deviation of 0.5 minutes and 0.25 minutes respectively for the nearest and farthest heliostats. If the specified value (120 seconds) is a 99 percentile time, the requirement is met for both heliostats, i.e., the 99 percentile times (mean + 2.33 sigma), are approximately 1.42 and 0.63 minutes, respectively.
- ③ Heliostat is required to move 1/2 of image displacement; time is based on maximum slew rate in azimuth and elevation as required to place field in standby in 0 to 16 m/s wind conditions.
- ④ Calculated from mirror dimensions, slant range and solar subtenue angle

undesired illumination of the tower is not expected to be a problem. During startup, for example, heliostats will be oriented so as to position their images in the space near the receiver, prior to receiver heatup. A feasible approach might be to pre-position the heliostats, and begin them tracking, so that the first sunlight is redirected to the standby region; this prepositioning could be done prior to sunrise. The reverse procedures can be followed for sunset.

In the case of emergency detargeting to the standby position, the reflected images will be steered to the space surrounding the receiver according to a standard computer subroutine. It may also become necessary to drive the heliostats to the high-wind stow position. In such a case, a subroutine will steer the images in such a way that they achieve a vertical orientation without generating regions of high flux concentration.

#### 4.0 PROTOTYPE FABRICATION, CHECKOUT AND INSTALLATION

#### 4.1 FABRICATION

##### 4.1.1 Reflector Facets

The reflector facets were manufactured by the Pittsburgh Corning Co. at Port Allegany, Pennsylvania, using the Foamsil-75 cellular glass produced at their Sedalia, Missouri plant. The Code 0317 fusion glass for facets was manufactured by Corning Glass Works at their Blacksburg, Virginia plant. The silver reflective coating was applied by Falconer Glass of Falconer, N.Y. The following steps were performed per drawings 277-10117 (Figure 2.1-5) and 277-10118 in the assembly of each facet. By necessity, tooling for fabricating prototype facets dictated a labor intensive assembly operation. For moderate production quantities automated tooling would be used for trimming, handling and bonding core blocks.

- (1) Layout core blocks on flat surface table, arrange and trim per fabrication drawing.
- (2) Transfer blocks to temporary storage table, being careful to retain configuration.
- (3) Place reflective glass sheet, with silvered side up, on flat surface table.
- (4) Prepare and position clear glass sheet on handling equipment.
- (5) Apply adhesive to core blocks, reflective glass sheet and clear glass sheet.
- (6) Position core blocks on reflective sheet in configuration determined in Step 1.
- (7) Position clear glass sheet on core blocks.

- (8) Vacuum bag and cure at ambient temperature.
- (9) Apply edge sealant and cap strips per drawing.
- (10) Paint glass back skin and cap strips.

Figure 4.1-1 illustrates the assembly sequence graphically. Following assembly, 16 facets were inspected for surface waviness and flatness using a precision electronic level, which traversed the facet surface in a prescribed path (Moody method). During the inspection for flatness it was discovered that the facets were being produced with a slightly negative radius of curvature (convex) in the long dimension. Table 4.1-1 lists the serial numbers of the facets that were flatness tested, along with their respective curvature values. In all cases the curvature is due to cylindrical curvature about the short axis of the facet and is expressed in Table 4.1-1 in terms of distance between parallel planes containing the curvature. Time and budget constraints prevented ascertaining and correcting the cause for the curvature. Consequently, all facets have negative radii of curvature. It is believed that the problem can be corrected by proper retention of the flat tooling surface during vacuum bagging.

Facet fabrication inspection records are contained in Reference 4-1.

#### 4.1.2 Attachment Brackets

The attachment brackets were fabricated by M and M Fabrication Company of Yakima, Washington, and the nylon pads by the Fleck Company of Auburn, Washington, per drawing 277-10119 (Figure 2.1-6). The bracket was formed by bending a steel bar into a "U" shape and welding a steel plate on one side of the "U". The weldment was then hot dip galvanized. The support pads were made from 0.95 cm ( 3/8") thick, 30% glass fiber reinforced type 6 nylon. One minor deviation from the drawing exists in the prototype hardware. This is discussed in Section 4.2.3.3 of Assembly and Checkout.

● Block production

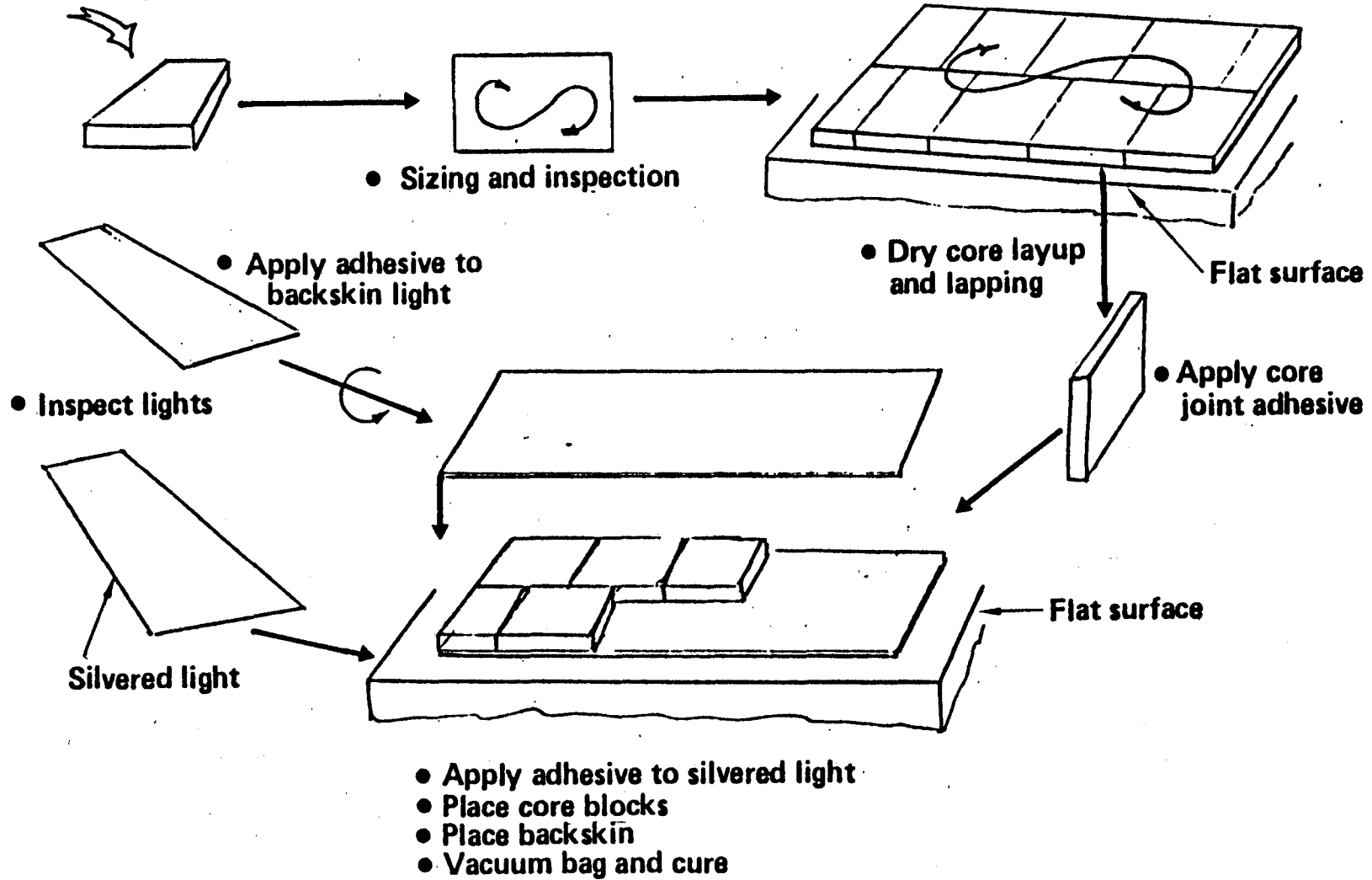
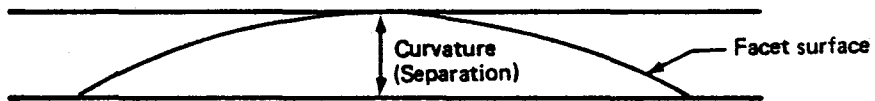


Figure 4.1-1. Facet Preparation Sequence

**Table 4:1-1. Prototype Facet Curvature**

<b>Serial number</b>	<b>Curvature (Parallel plane separation) inches</b>
1	.0438
2	.0388
3	.0400
5	.0341
6	.0227
8	.0296
9	.0360
10	.0465
11	.0314
12	.0397
14	.0397
15	.0367
17	.0385
18	.0248
19	.0274
20	.0508



#### 4.1.3 Frame Assembly

The H-frames and torque tubes were manufactured by Steel-Fab of Everett, Washington, per drawing 277-101120 (Figure 2.2-2), 277-101121 and FACC drawing 531147. The "Z" beam portion of the H-frame was made by brake forming galvanized, 14 gage sheet steel. The torque tube portion of the H-frame (outboard torque tube) was fabricated by welding flanges, made from steel plate stock, to 40.6 cm (16 inch) diameter x 0.27 cm (0.105 inch) wall steel pipe. Lateral stiffening struts between Z beams and vertical stiffeners on Z beam webs were made of galvanized 2.54 cm (1 in) x 2.54 cm (1 in) x 0.32 cm (1/8 in) steel angle material. H-frame parts were assembled with 5/16" -18 fasteners.

The inboard torque tube was fabricated in a similar fashion to the outboard torque tubes, with the addition of the elevation arm. Cast nodular steel ring adapters were welded to the tube. The elevation arm assembly was in turn welded to the ring adapters. The weldment was hot dip galvanized prior to final machining.

#### 4.1.4 Gimbal Actuator

The gimbal actuator was fabricated by Ford Aerospace and Communications Corporation (FACC) Western Development Lab in Palo Alto, California. Under subcontract to FACC, the gearboxes were provided by Winsmith of Springfield, New York. The 3 Phase, 208 volt, AC, induction motors were supplied by Bodine Electric Company of Chicago, Illinois. Fabrication was per design drawings listed in paragraph 2.3.1.1.4.

The azimuth drive/bearing assembly was assembled (and tested) at the Winsmith plant in Chicago. This unit along with the elevation drive assembly was sent to FACC in Palo Alto for integration with other components built by FACC.

#### 4.1.5 Pedestal Foundation

The pedestals were manufactured by Centrecon, Inc. of Everett, Washington. They were fabricated by a standard process used by Centrecon in the



manufacture of commercial poles and pilings. A steel wire cage, composed of wires running axially as well as circumferentially, is positioned in a cylindrical form. Axial wires are hydraulically pretensioned in the form. The form is rotated while the concrete is fed in and partially cured. A steam cure cycle follows the spinning operation. This fabrication process was selected because it produces a hollow, prestressed, high density/high modulus concrete pile.

Galvanized steel bands at the top and bottom of the pile provide reinforcement during driving operations. The steel gimbal interface plate at the top of the pile anchors axial prestressing wires.

A drawing of the pedestal is shown in Figure 2.4-2.

#### 4.1.6 Control Fabrication

The controls fabrication required building the following items:

1. 2 heliostat electronics boxes.
2. 3 motor control cards (1 for spare)
3. 2 serial data cards.
4. 1 computer buffer interface card.
5. 2 cables for encoders.
6. 1 terminal board to interface central cables from heliostats to computer.
7. 1 octopus cable assembly to connect computer cards to terminal board.
8. 1 cable to interface the ADAC 1616MIC card to the terminal board.

Items 6, 7, & 8 above were built at BEC, and items 1 through 5 were fabricated at Syntix Industries, Inc., Redmond, Washington.

Several modifications were made to electronic hardware as a result of assembly/integration testing. In addition to the above, controls fabrication, assembly and checkout was performed on all computer equipment. This involved:

1. Changing switches and wire jumpers to properly configure each computer card, and installing the cards in the ADAC computer chassis.
2. Setting up the communication options on the CRT and keyboard printer.

## 4.2 ASSEMBLY AND CHECKOUT

This section of the document presents results of tests performed on selected assemblies and integration and checkout tests performed during build up in Seattle prior to installation of the prototype heliostats at the CRTF in Albuquerque.

### 4.2.1 Life-Cycle/Wear Testing of Elevation Actuator Screw and Nut

A test loading frame was fabricated and set-up at the FACC lab in Palo Alto, CA. The loading frame had provisions to perform accelerated endurance testing under simulated loading and environmental conditions. Candidate materials were axially preloaded and cycled up and down the stainless steel screw. Figure 4.2-1 is a photograph of the test set up.

Tests were performed on three candidate materials for the non-lubricated nut of the elevation drive. Bronze (Dynalloy) and 2 polymers (Delrin 'AF' and Turcite 'A') were tested on a 304 stainless steel screw. Appendix A contains the complete test report, while a summary is presented here.

After testing the equivalent of 45 days the bronze nut showed 0.20 cm (.080 inches) of wear and had severely damaged the stainless steel screw threads. It was removed from test at that point. The sharp corners of the threads were rounded and bronze particles were bonded to screw threads due to excessive heat generated by friction. The Turcite "A" polymeric nut failed in shear after the equivalent of 20 years of testing. At the time of failure, the Turcite nut had worn by 0.23 cm (0.090 inches). Delrin "AF" survived the equivalent of 30 years of service with only 0.10 cm (.040 inches) of wear. The stainless steel screw showed no wear under clean test conditions and only visual wear from sand tests after testing the polymeric nuts. Figure 4.2-2 is a plot of wear versus linear travel for the polymeric nuts.

Actual service nut wear values are expected to be less than test results for the following reasons:

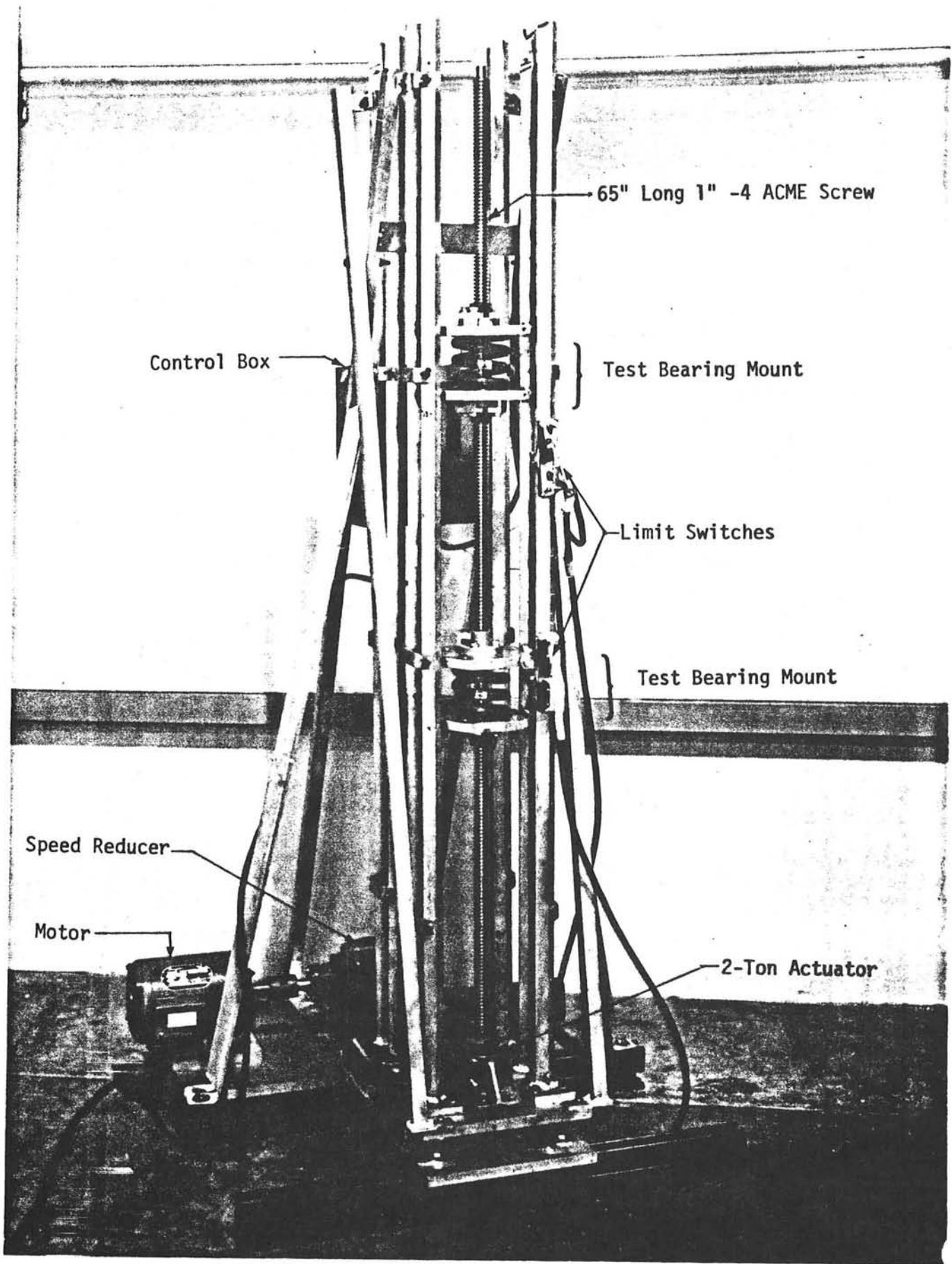


Figure 4.2-1. Test Setup

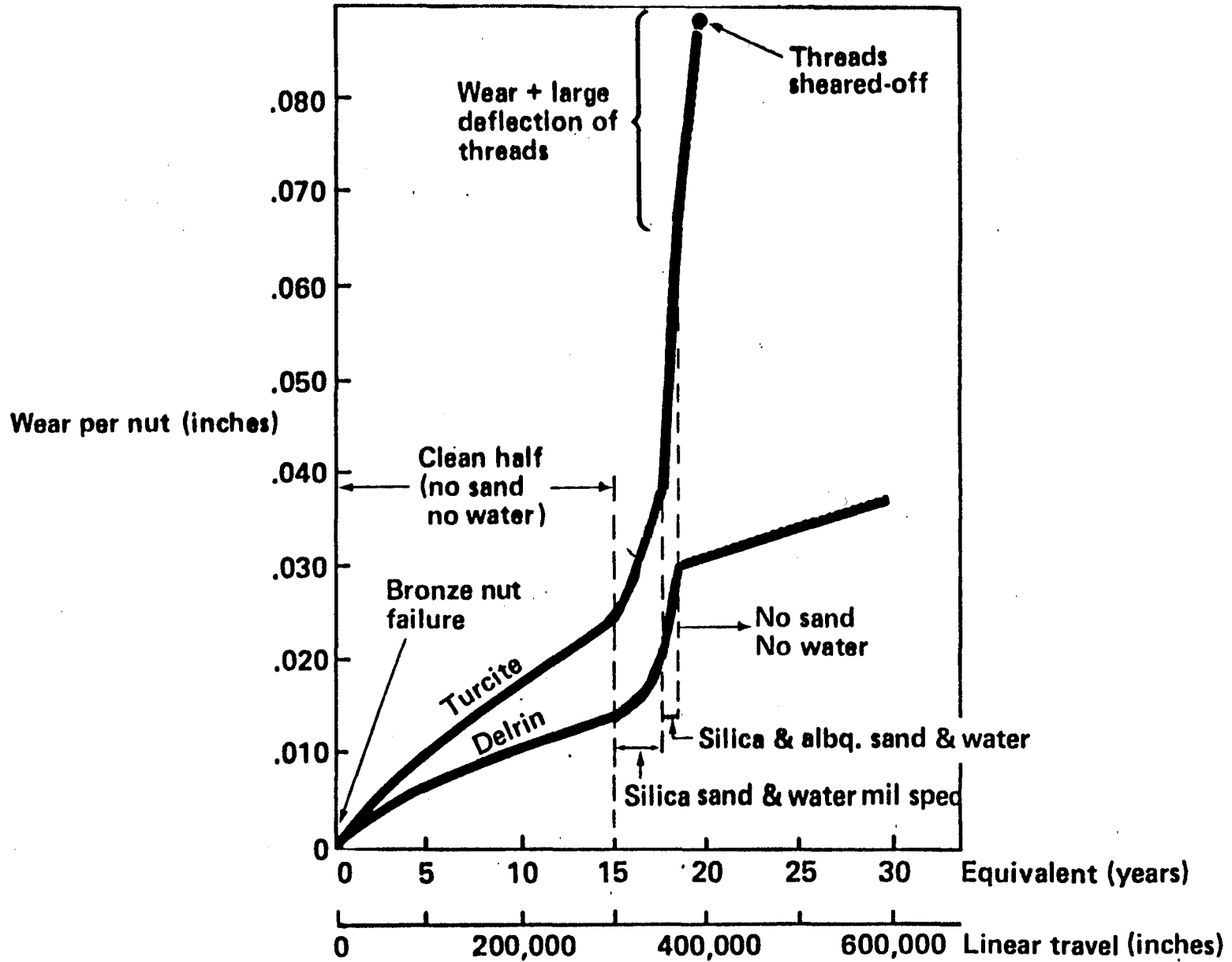


Figure 4.2-2. Nut Wear vs. Life

- (a) The pitch line velocity for the thread in actual operation is about 1/5 of the test case. Therefore, the generated heat due to friction will be less and the screw and nut materials will be operating at a much cooler temperature, allowing polymeric nuts to operate within their specified temperature range. (Preliminary data from an ongoing subsequent test has verified an approximate 50% reduction in wear rate associated with a lower pitch line velocity).
- (b) The actual load on the nut thread will not be constant as simulated in the test (maximum gravity condition). Therefore, threads will see less average pressure than was subjected during testing.
- (c) The water and sand slurry applied for about 4 equivalent years is believed unrealistically harsh compared to field grit and dust.

As a result of these tests the Delrin "AF" material was selected for use in the Second Generation Heliostat prototypes.

#### 4.2.2 Gimbal Tests

This section summarizes the results of in-plant testing by FACC on the Gimbal/Actuator Drive Assembly. Appendices B and C contain detailed test results and photographs.

The assembly is shown in Figure 4.2-3 and consists basically of:

Center torque tube to which the heliostat reflector assembly is mounted at the torque tube flanges.

Elevation arm

Elevation drive assembly

Gimbal housing

Azimuth drive/bearing assembly which will bolt to the top of heliostat pedestal.

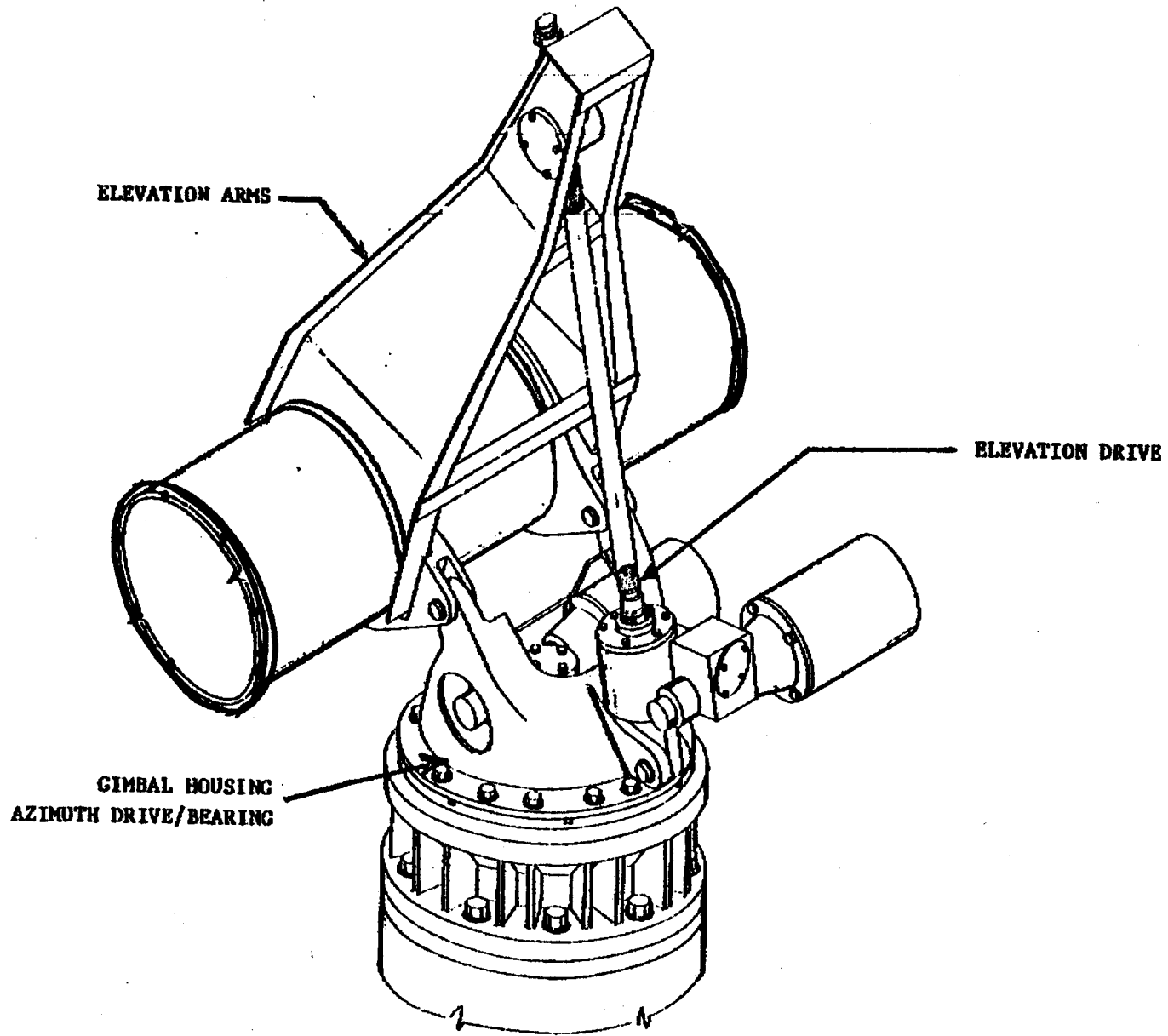


Figure 4.2-3. Gimbal Actuator Drive Assembly

Testing was performed in two stages. Two units of the azimuth drive/bearing assembly (Figure 4.2-4) were initially tested at the Winsmith facility. Then one entire gimbal/actuator was tested by FACC.

#### 4.2.2.1 Load Tests

##### Azimuth Survival Load Tests

Survival of the entire assembly was verified by applying the maximum specified azimuth torque. This torque was 10,608 Nm ( 7800 ft. lbs.) applied to the torque tube flanges with the reflector assembly at the vertical position, corresponds to a 22 m/s ( 50 mph) wind load. No failure of any part, and no torque tube flange slippage occurred. The assembly was rotated about the azimuth axis subsequent to this load application to verify that there was no internal damage.

Azimuth survival torque loads of 10,608 Nm ( 7800 ft. lbs.) were also applied to both azimuth drive/bearing assemblies during Winsmith tests.

##### Elevation Survival Load Tests

Survival of the entire assembly was verified by applying the maximum specified elevation torque. This torque was 27,200 Nm ( 20,000 ft. lbs.) applied to the torque tube flanges with the reflector assembly at the horizontal position and corresponds to a 40 m/s ( 90 mph) at 10° attack angle wind load. Torques were applied to simulate both front and rear wind conditions. No failure of any part and no torque tube flange slippage. The assembly was rotated about the elevation axis subsequent to these load applications to verify that there was no internal damage.

##### Stiffness Tests

The requirement established for pointing error of the gimbal/actuator drive assembly due to 12 m/s ( 27 mph) operational wind velocity, is not to exceed 3.0 mrad peak (3σ) for either axis under the worst conditions of wind direction and heliostat orientation. The peak pointing error about the



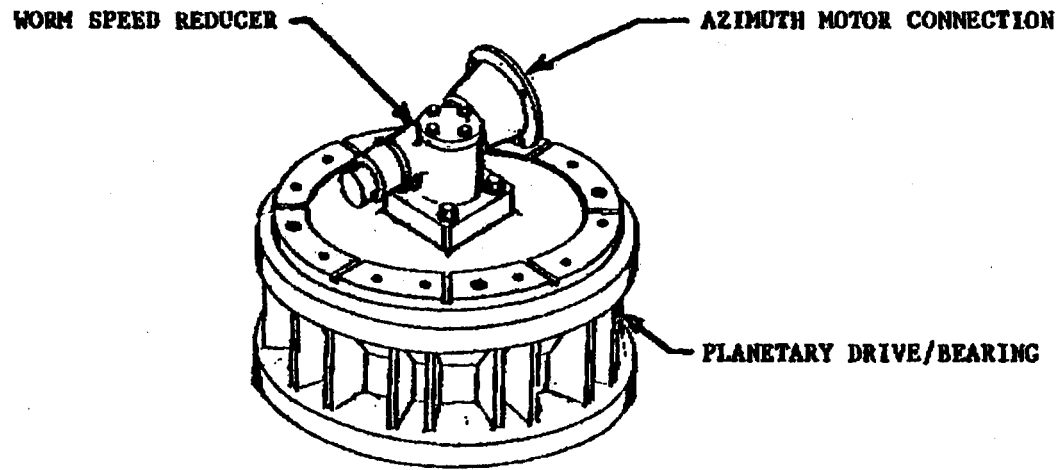


Figure 4.2-4. Azimuth Drive/Bearing Assembly

azimuth axis occurs with the reflector assembly vertical and at the maximum torque of 3128 Nm ( 2300 ft. lbs). The error decreases significantly as the reflector assembly is rotated to horizontal. The peak pointing error about the elevation axis occurs with the reflector assembly horizontal because backlash must be included under some wind conditions. Below approximately 85° elevation angle the elevation drive is always loaded in one direction due to unbalanced gravity torque, and consequently there is no backlash effect.

### Azimuth Stiffness Tests

The stiffness of the entire assembly about the azimuth axis was tested up to its maximum torque of 3128 Nm ( 2300 ft. lbs.) while in vertical orientation. The calculated peak error for this torque was  $\pm 1.80$  mrad, which included the effect of allowable backlash of  $\pm 0.61$  mrad plus  $\pm 1.19$  mrad wind-up due to drive compliance. The measured pointing error was  $\pm 1.43$  mrad which includes the effect of actual backlash of approximately  $\pm 0.5$  mrad plus the remaining  $\pm 0.93$  mrad wind-up due to drive compliance. Deflection vs torque curve is shown in Figure 4.2-5.- Compliance is .034 mrad/in. kip.

Azimuth stiffness tests were also conducted on both azimuth drive/bearing assemblies during the Winsmith tests. Unit #1 was tested at three positions and repeatability was very good. This unit was also individually tested at FACC with similar results. From the torque vs deflection curves, compliance was determined to be .013 mrad/in. kip and output backlash to be approximately  $\pm 0.6$  mrad. Unit #2 was tested twice in one position at Winsmith but it showed nearly twice the compliance and extremely low output backlash. Because of this discrepancy, FACC used unit #2 for the complete assembly tests plus another individual test. The FACC compliance results for unit #2 are similar to Unit #1, 0.013 mrad/in. kip, but output backlash is low at  $\pm 0.2$  mrad.

The input backlash was checked for both azimuth drive/bearing assemblies at Winsmith at three different positions by rotating the input shaft. Unit #1 measured  $\pm 0.31$  to  $\pm 0.52$  mrad, and Unit #2 was only  $\pm 0.04$  to  $\pm 0.05$  mrad.

Elevation Stiffness Tests ( Elevation angle 0°, reflector assembly vertical).

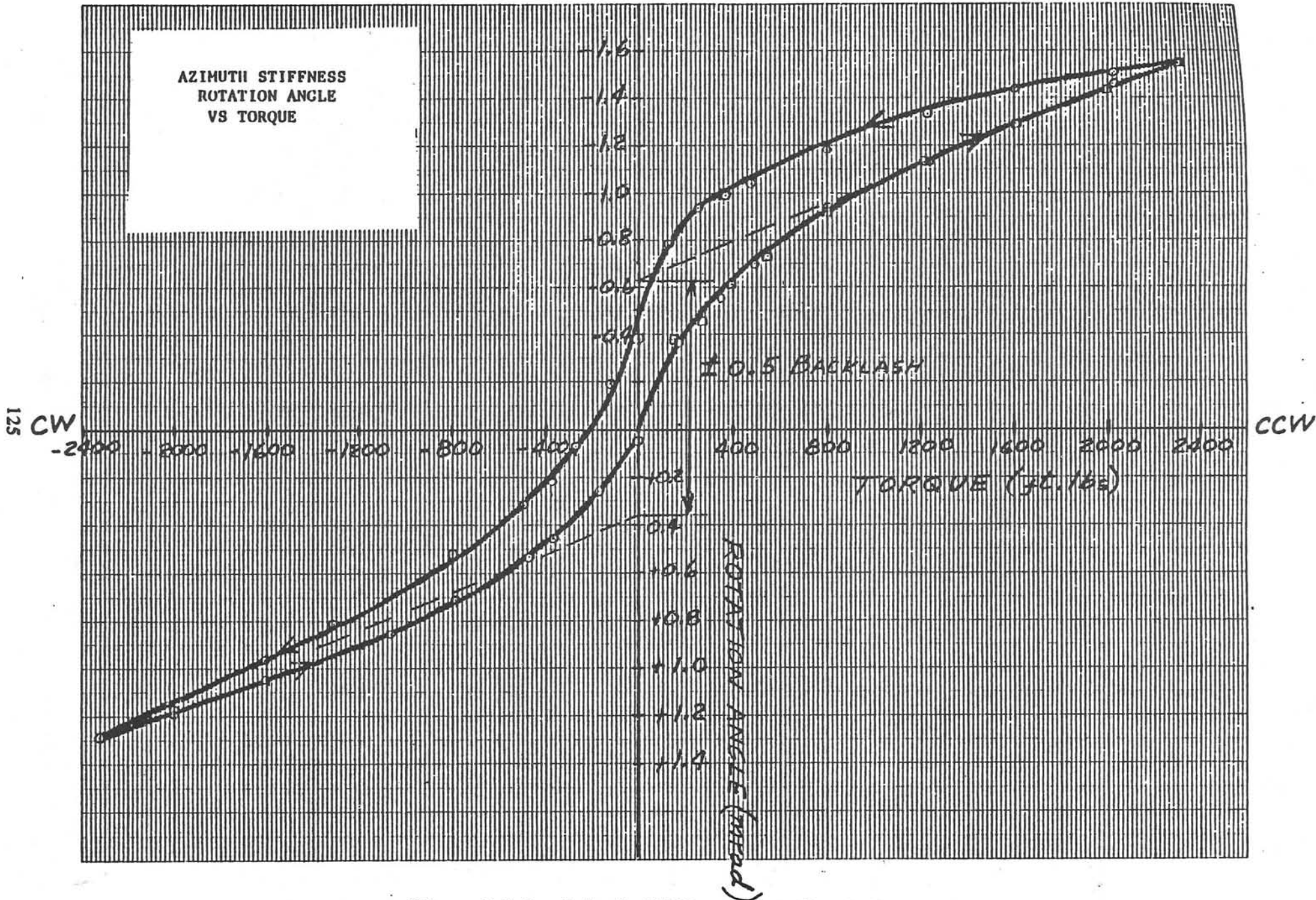


Figure 4.2-5. Azimuth Stiffness, Rotation Angle vs. Torque

The stiffness of the entire assembly about the elevation axis was tested up to its maximum operational torque of 6270  $\pm$  993 Nm (4610  $\pm$  730 ft. lbs.) in the vertical orientation. The calculated pointing error was  $\pm$  0.7 mrad. The measured pointing error is  $\pm$  0.87 mrad as shown on Figure 4.2-6. The compliance is .099 mrad/in. kip.

#### Elevation Stiffness Tests (Elevation angle 90°, reflector assembly horizontal)

The stiffness of the entire assembly about the elevation axis was tested up to its maximum operational torque of  $\pm$  2462 Nm ( $\pm$  1810 ft. lbs.) in the horizontal orientation. The calculated pointing error was  $\pm$  2.18 mrad, which included the effect of an allowable backlash of  $\pm$  0.6 mrad plus  $\pm$  1.58 mrad wind-up due to compliance. The measured pointing error is  $\pm$  1.07 mrad which includes the actual backlash of approximately  $\pm$  0.1 mrad plus  $\pm$  0.97 mrad wind-up due to compliance as shown on Figure 4.2-7. The compliance is .045 mrad/in. kip plus backlash.

Both azimuth drive/bearing assemblies were tested with an elevation moment to determine their contribution to the total elevation compliance. The compliance results were 0.005 mrad/in. kip. Linearity between deflection and load was good and hysteresis was low.

#### Backdriving

The maximum azimuth survival torque of 10,608 Nm ( 7800 ft. lbs.) was applied to the output shaft of the azimuth drive/bearing assembly without any rotation occurring on the input shaft confirming the non-backdriving capability. The tests were conducted on both units and in both directions (CW and CCW). Similarly, during elevation survival load tests, the maximum torque of 27,200 Nm ( 20,000 ft. lbs.) did not induce elevation backdriving.

#### Running Torque and Efficiency

The azimuth drive/bearing assemblies were tested to determine running torques and efficiencies by applying load to the output flange of the drive while operating with the 1750 rpm rated motor. Different test arrangements were used for the two units. Test results are summarized below:

ELEVATION STIFFNESS; & ELEVATION ANGLE,  $\theta^{\circ}$  (VERTICAL MIRROR)

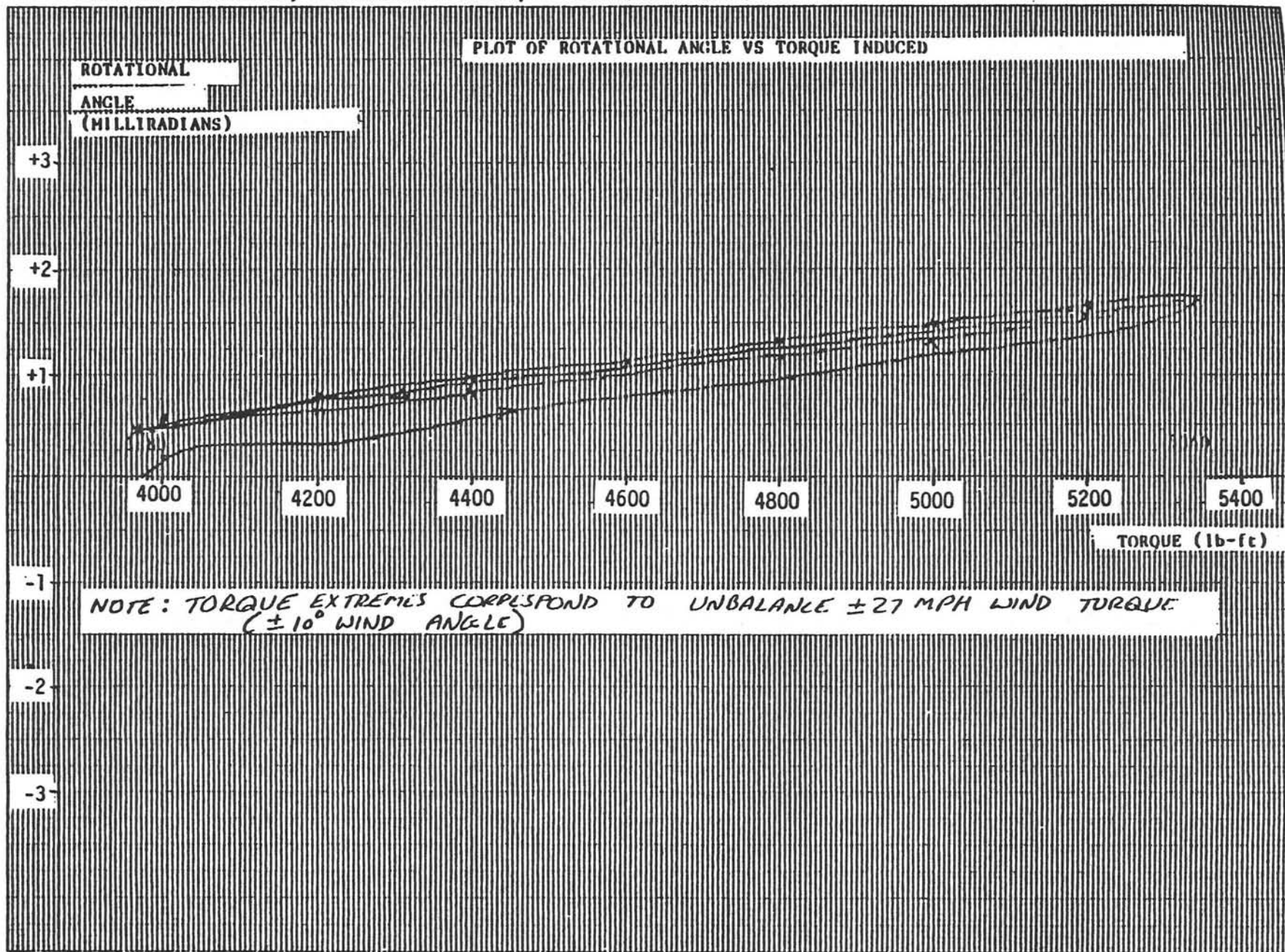


Figure 4.2-6. Elevation Stiffness, Vertical Reflector

ELEVATION STIFFNESS: ELEVATION ANGLE, 90° (HORIZONTAL MIRROR)

128

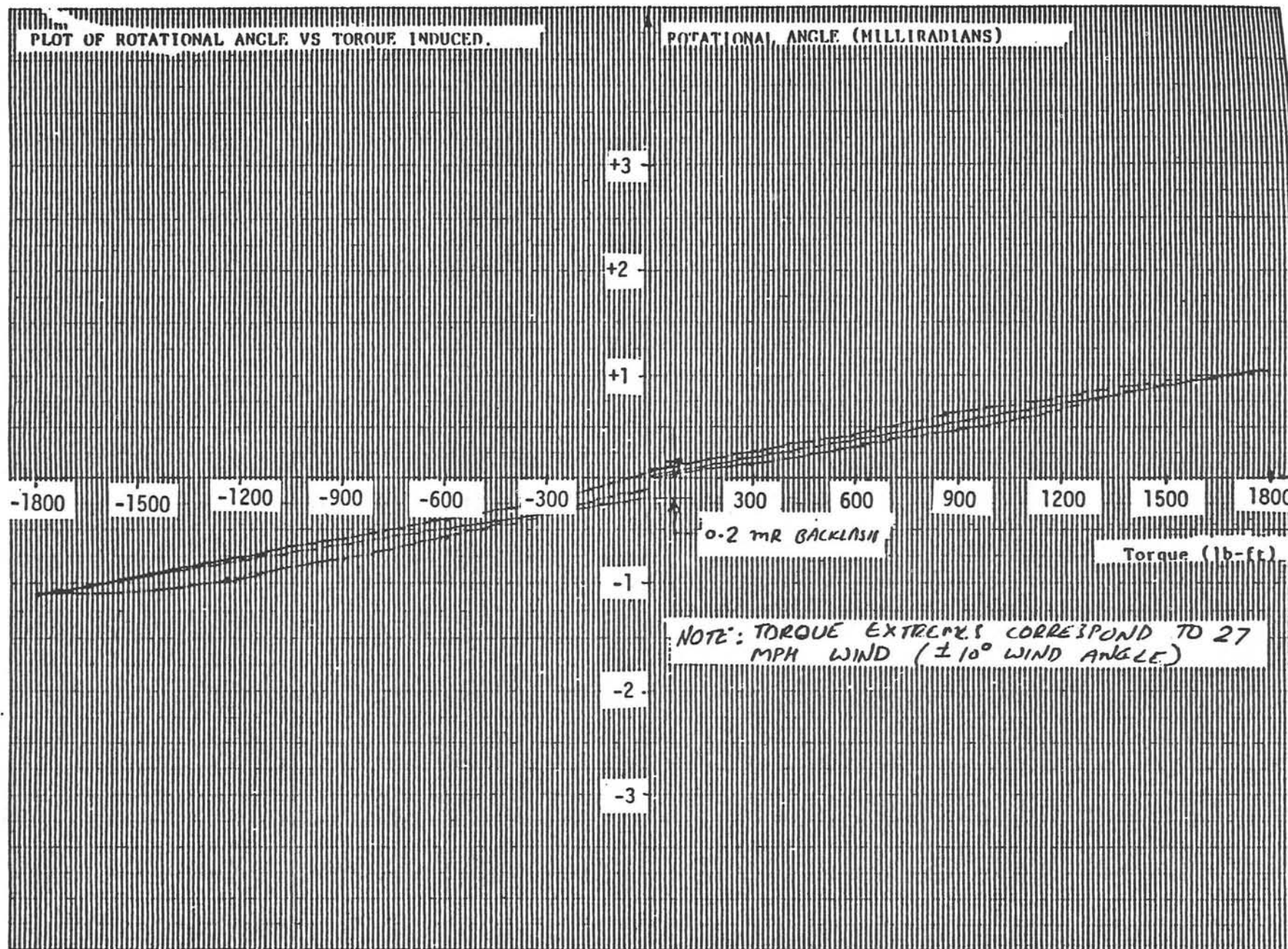


Figure 4.2-7. Elevation Stiffness, Horizontal Reflector

	<u>Unit #1</u>	<u>Unit #2</u>
<u>At No Load:</u>		
Input torque, Nm, (in. lbs)	.39 ± .05 (3.4 ± 0.4)	.39 (3.4)
Input horsepower (HP)	0.10 ± 0.1	0.10

At 5304 Nm (3900 ft. lbs)

Input torque, Nm, (in. lbs)	.78 (6.9)	.96 (8.5)
Input horsepower (HP)	0.20	0.24
Gear mesh loss (HP)	0.10	0.14
Efficiency (%)	12.8	10.5

Drive Motor Capability Under Operational Loads

Azimuth Drive

The above azimuth running torque and efficiency tests determined that the 1/6 HP motor would operate at 40% overload at 5304 Nm ( 3900 ft. lbs.) torque corresponding to 16 m (.35 mph) wind velocity. An extension of this test for unit #2 determined that the 1/6 HP motor would operate at 120% overload if an operating torque of 10,608 Nm ( 7800 ft. lbs.)( 22 m/s (50 mph)) was a requirement. Neither condition would harm motor performance since high wind torques during azimuth rotation are only maintained for short durations.

Elevation Drive

With the entire assembly oriented at four different elevation angles (0°, 30°, 60° and 90°), maximum elevation operational torques (up to 22 m/s (50 mph wind)) were applied by hanging weights at a predetermined moment arm. The 1/3 HP motor was operated successfully for about two minutes in each case, and no laboring or overheating was observable at the motor.

### Break-Loose Friction Torque

Break loose or friction drag torque was measured on both azimuth drive/bearing assemblies in a static condition with no load on the drive. Input torques varied between 0.23 and .34 Nm ( 2.0 and 3.0 in. lbs.) for the two units, three different positions and CW and CCW directions. One loaded condition for each assembly was also measured.

#### 4.2.2.2 Operational Verification Tests

### Travel Limits

There are no travel limits for azimuth drive. It can be rotated continuously about azimuth axis. Allowable travel is limited only by the electrical cables and placement of switches.

Elevation drive travel limits were measured as approximately  $-3^{\circ}$  to in excess of  $93^{\circ}$ .

### Emergency Operation of Elevation Drive

Emergency operation capability of elevation drive was verified by driving with a drill motor from the drive input shaft extension opposite the drive motor.

#### 4.2.2.3 Dimensional Verification Tests

### Azimuth and Elevation Axis Orthogonality

Allowable non-orthogonality between azimuth and elevation axes is  $\pm 0.25^{\circ}$ . The measured value for the first assembly was  $0.0007^{\circ}$  and for the second assembly it was  $0.0534^{\circ}$ .

Orthogonality of the azimuth axis to the drive mounting flange and pedestal interface flange was measured at Winsmith by placing the drive unit on a surface table with vertical azimuth axis. The pedestal interface flange was found to be parallel to drive mounting flange within .011 cm (0.0045 inch).



After this, the drive was rotated in azimuth by approximately 170° and again parallelism was found to be within 0.012 cm (0.0048 inch). These two measurements verify that the drive mounting flange and azimuth axis are very accurately, orthogonal to each other. Similarly, the pedestal interface flange is orthogonal to the azimuth axis to within 0.013 cm (0.005 inch) which corresponds to approximately 0.24 mrad).

### Major Dimensions

All dimensions specified in the Gimbal/Actuator Drive Assembly Test Procedures were found to be within the specified tolerances.

The major dimensions and gear ratio for the azimuth drive/bearing assemblies were also verified at Winsmith.

#### 4.2.3 Form/Fit/Functional Checkout

Prior to shipment of heliostat components and assemblies to the CRTF for installation, each heliostat was assembled completely (except for the pedestals) on a support fixture in a BEC laboratory. The purpose of this effort was to verify that all components were built per drawing, fit properly, had adequate clearances where required and functioned as designed. Following checkout, the heliostats were disassembled, packaged and shipped to the CRTF.

##### 4.2.3.1 Gimbal/Torque Tube

One set (gimbal drive and center torque tube) was assembled and structurally tested at FACC prior to shipment to BEC, as discussed in Paragraph 4.2.2. Both sets were reassembled and inspected at BEC. Figure 4.2-8 shows an assembled set. The primary purpose of this test was to verify that the elevation axis pins, the elevation drive pin and the elevation trunion pieces were assembled properly, with acceptable clearances.

The assembly operations went well with only two notable fixes required. While installing the two elevation axis pins and the elevation drive pin, the bushings in the gimbals were damaged. The damage consisted of the removal of

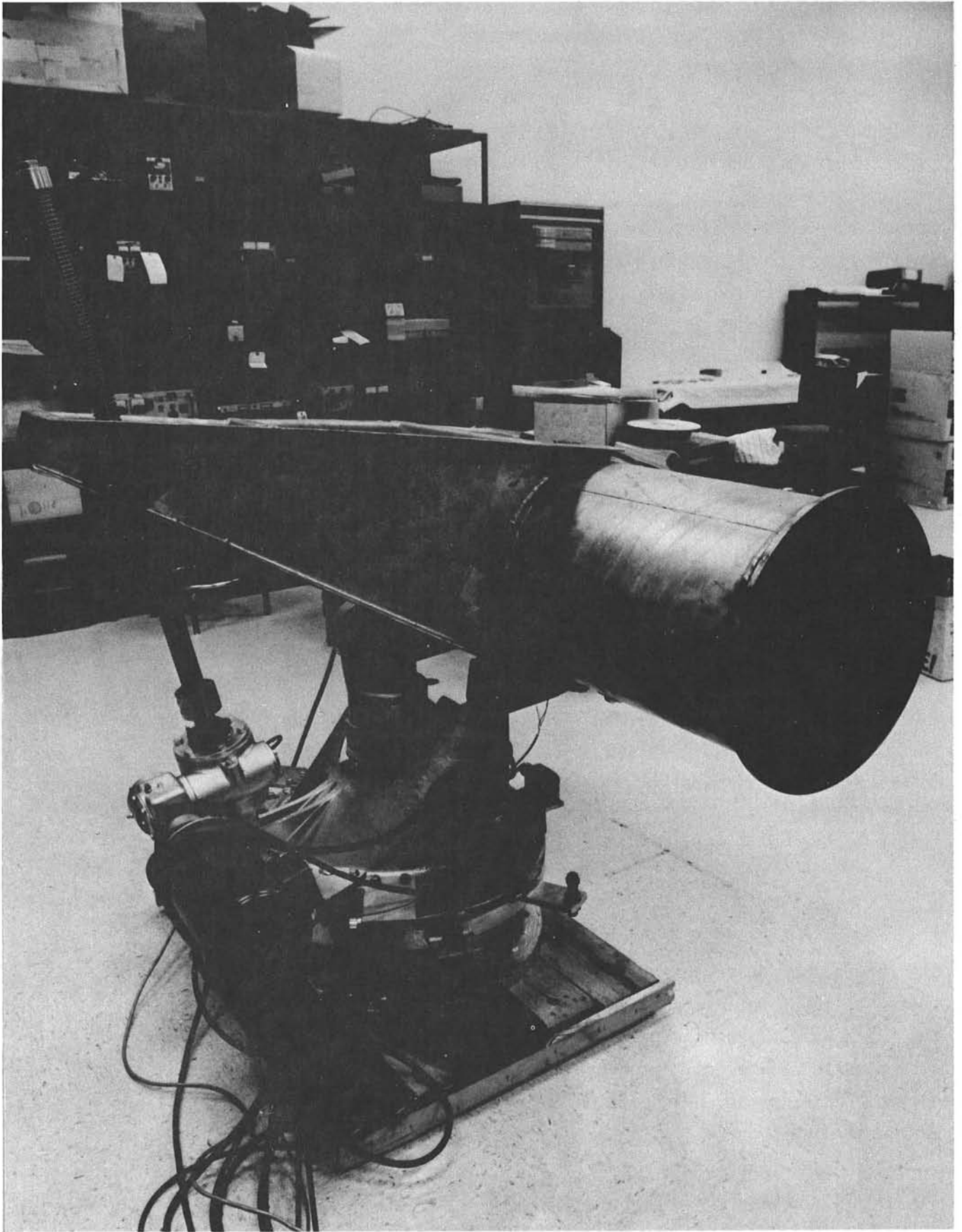


*Figure 4.2-8. Gimbal/Torque-Tube*

small pieces of the bearing material during pin insertion. This problem was eliminated by machining a smooth radius on the pin ends and the retaining ring groove, eliminating sharp edges on the pin. To further alleviate the problem, a long tapered pilot shaft was made and used to bring the parts into proper alignment prior to inserting the pins. The damaged bushings were replaced. An additional minor problem observed was that of excessive clearances between the ears of the torque tube ring adapter and the gimbal housing where they interface at the elevation axis. Excessive clearance was also observed between the ears of the gimbal housing and the elevation drive unit where it is pinned. The excess clearance in both cases was "end play" or axial clearance, rather than radial clearance. The clearances were reduced to acceptable levels by the use of stainless steel washers machined to displace the excess clearance. Revision in the design dimensional tolerancing will eliminate this problem from occurring on production units.

The drive motors were operated to exercise the azimuth and elevation axes to the limits of travel, with no physical interferences encountered.

Upon disassembly, the gimbal and torque tube were weighed:

Gimbal - 316 kg (695 lb)  
Center Torque tube section - 84 kg (185 lb)  
Oil - 9.1 kg (20 lb)

#### 4.2.3.2 Torque Tube/H-Frame (Support Frame)

The support frames, consisting of torque tubes, beams, and stiffeners were assembled on a gimbal to verify fit, develop assembly procedures in preparation for reflector mounting. No particular difficulties were encountered. A surveyors level was used to determine how nearly in-plane the top surfaces of the Z-beams were. This was done to assure that the range of adjustment of the reflector mounting brackets would be adequate to set the desired canting angles. The Z-beam top surfaces were found to lie in the same plane to within 0.95 cm ( $\pm 3/8$  inch). To maintain proper clocking of the flanges at the torque tube/H-frame interfaces, holes were drilled through the flanges and steel dowel pins driven in. These pins stayed with the H-frame

side of the interface after disassembly to serve as guides during reassembly. Figure 4.2-9 shows the assembled support frame. The H-frames weighed 227 kg (500 lbs).

#### 4.2.3.3 Reflector/Support Frame

All 12 reflectors were installed on each support frame. This was done to evaluate the fit of the support brackets to the reflector and the Z-beams, and methods of reflector handling. Figure 4.2-10 is a photograph of an installed mounting bracket. It was discovered during assembly testing that the mounting bracket configuration was not in agreement with the design drawing. The bend radii of the 2.54 cm x 1.27cm (1 x 1/2 inch) C-bracket were larger than called for. This resulted in interference between the Nylon pads and cap strips. To alleviate this problem, pads were reduced in width by trimming one edge.

#### 4.2.3.4 Reflector Canting

Development of a strategy for canting, tooling to set cant angles, and selection of instruments to measure cant angles was accomplished on the set up discussed in Paragraph 4.2.3.3.

The canting strategy selected for the 2 prototypes was to set the cant angles on individual reflector facets after field assembly. This involved adjusting mounting brackets until the desired angles were observed on an electronic level located on the surface of facets. This technique was selected for expedience on prototypes and is not intended for use on a volume production scenario. It would however, be a useful approach for setting angles on a replaced facet in maintenance operations.

The instruments evaluated for measuring cant angles were:

1. Hilger and Watts Precision Microptic Clinometer TB 80
2. Federal Electronic Level Model 232P-68

The electronic level was selected because of the lighter-weight head and its remotely located readout. The accuracy was approximately  $\pm 20$  arc seconds.

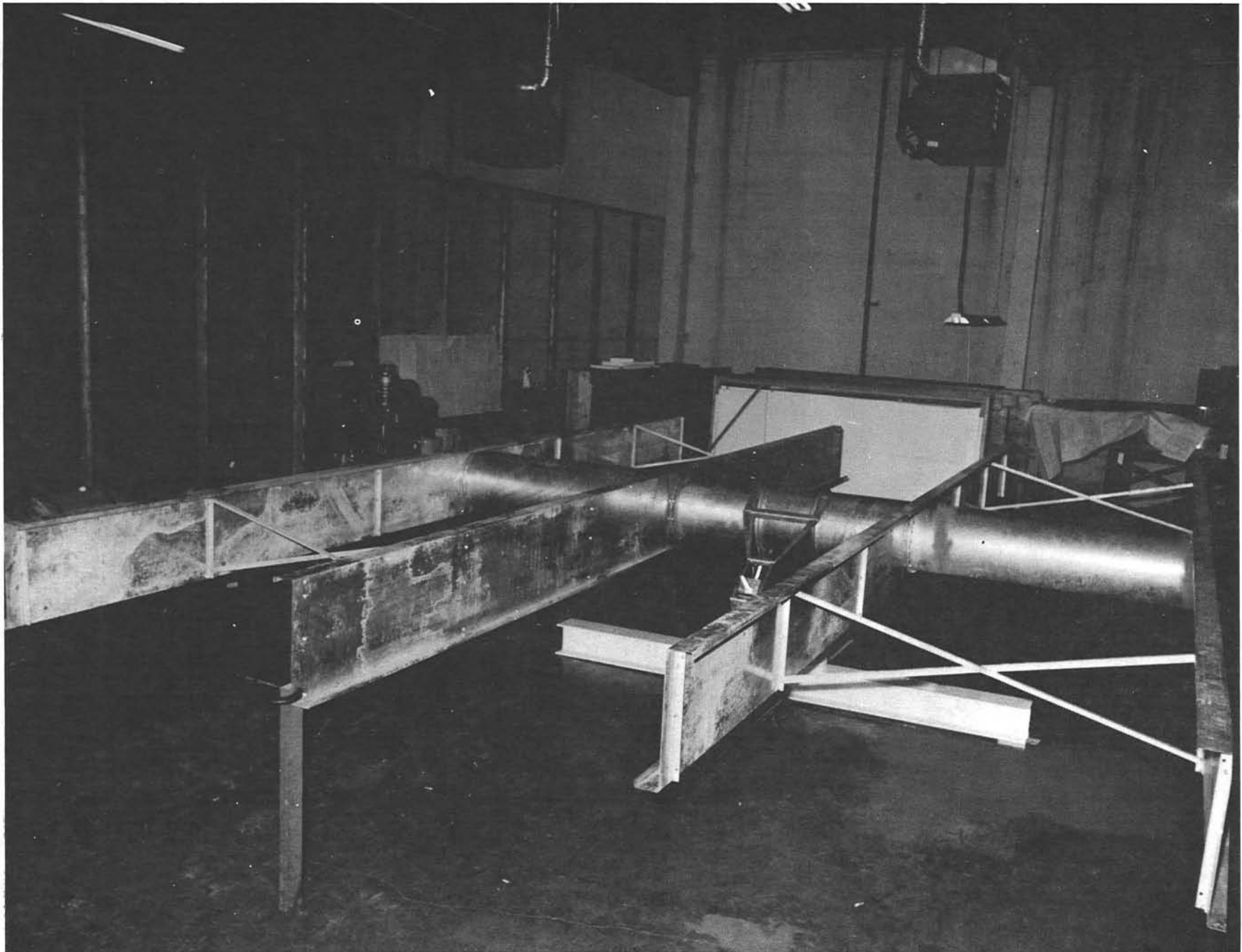
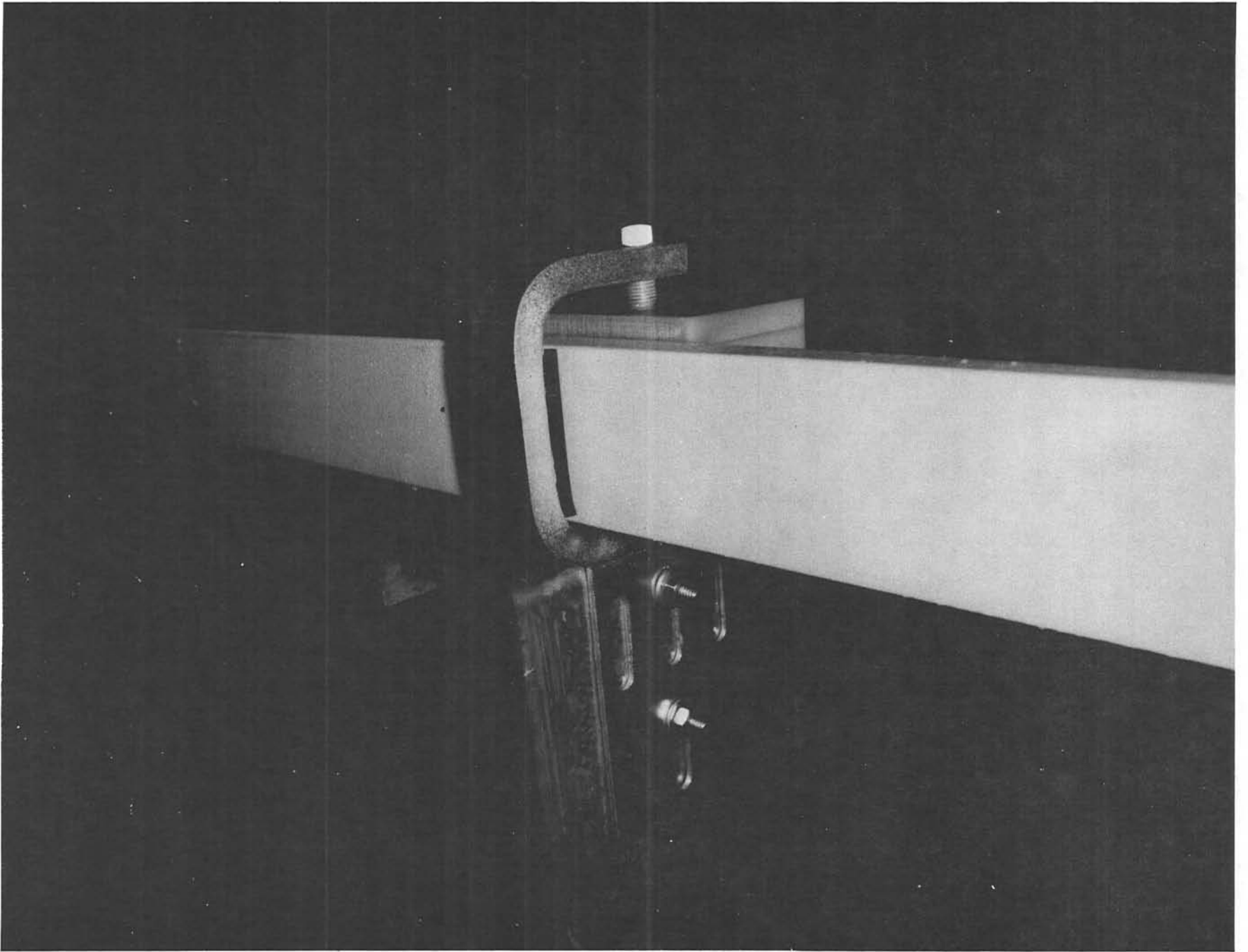


Figure 4.2-9. Support Frame



*Figure 4.2-10. Mounting Bracket Installation*

The canting procedure was initiated by positioning the support frame approximately horizontal, using a carpenter level. Vertical props, between the Z-beam ends and the floor were attached to assure that the position was not disturbed during facet adjustments. The electronic level was placed on a 12 inch parallel bar on the facet surface near its center, first along the long dimension, then at 90° to that direction, taking readings at those 2 positions. Adjustments were made with the canting tools to achieve the desired facet angles.

Figure 4.2-11 shows the assembled, canted array.

#### 4.2.3.5 Controls/Gimbal

Integration of the gimbal drive and the control system was performed in a BEC laboratory prior to shipment to CRTF. Figure 4.2-12 shows the set up in the laboratory.

The various pieces of the digital computer system were assembled and checked out for use in software development. The RT-11 single job monitor system was installed as delivered from DEC without the need for doing a system generation to get special options in the software operating system.

When the gimbal assembly arrived, preliminary versions of most software modules had been written and debugged for operation on the computer. The heliostat electronics were checked out by first disconnecting the power lines from the solid state relays (SSR's) and then verifying that the logic circuits and time delays all worked properly. Then power was connected to the SSR's, motor cables were connected to the gimbal assembly and checkout with the gimbal proceeded. Checkout with the gimbal started by operating the computer in the ODT mode so the output discrettes could be set manually by loading the desired values into the output registers, thus checking the communication lines and interface hardware. Then the software was checked by operating it in all modes and exercising it through various control tasks.

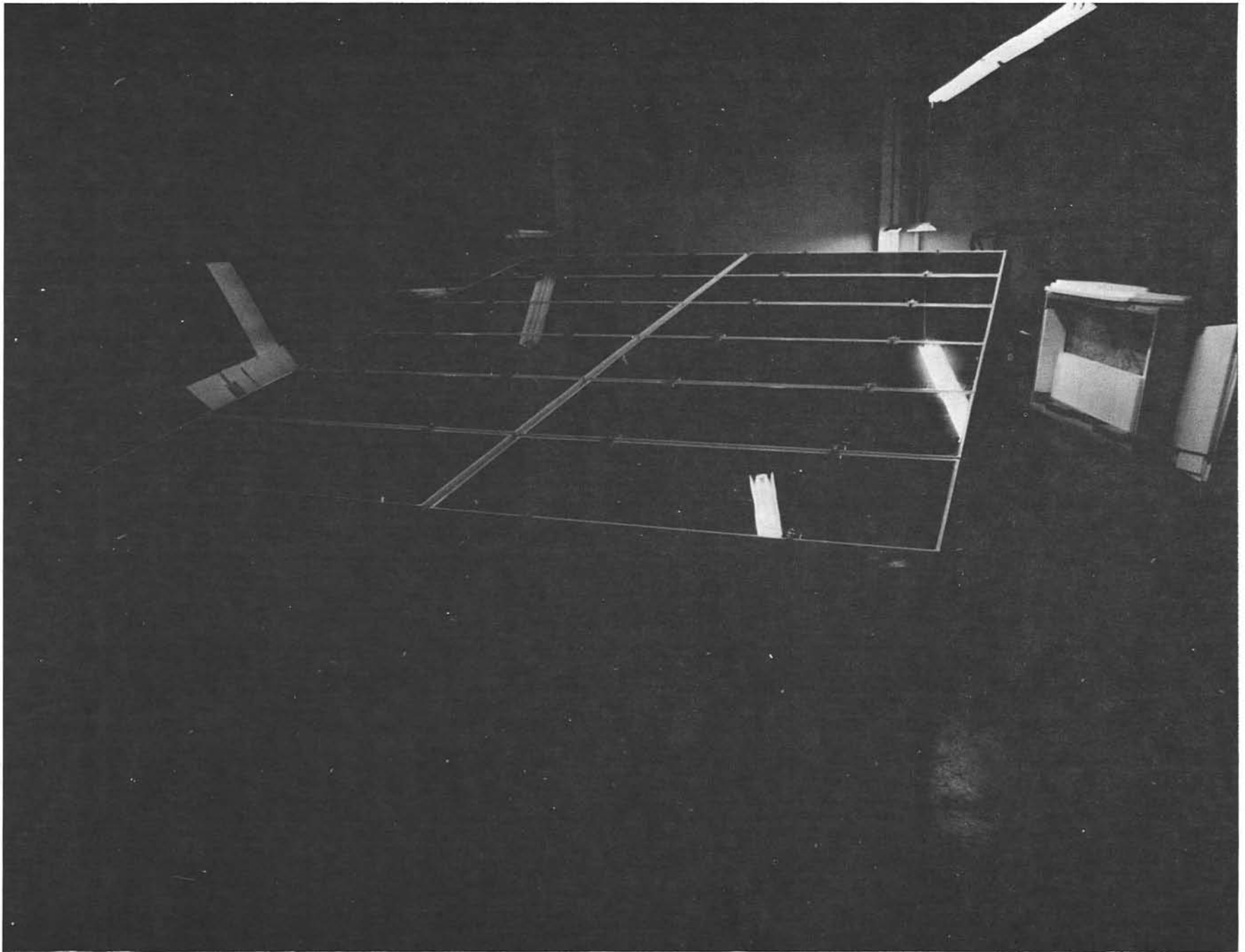


*Figure 4.2-11. Canted Reflector Array*





Figure 4.2-12. Controls/Gimbal Figure 4.3-1.

### 4.3 INSTALLATION AT CRTF

Following fit checks and functional testing, all components were shipped to the CRTF in Albuquerque for assembly, calibration and system test. No system level calibration or testing was performed in the Seattle area.

Two sites, designated B-1 and B-2, were assigned by Sandia. Slant ranges of 314 meters (1030 ft.) and 237 meters (777 ft.) were measured for B-1 and B-2, respectively.

#### 4.3.1 Pedestal

Pile driving operations for the BEC pedestals started on October 8, 1980. Peter Kewitt Construction Co., San Francisco, CA performed the driving using a crane and an open ended diesel hammer with  $5.30 \times 10^4$  Nm ( 39,000 ft. lb.) capacity. The setup for driving the pedestal at site B-2 is shown in Figure 4.3-1.

Driving started with a  $3.26 \times 10^4$  Nm (24,000 ft. lb.) driving energy on a 22.9cm (9 inch) thick laminated plywood pad on top of the pedestal. At approximately 1.68m ( 5 1/2 feet) into ground, progress stopped. The energy was increased to  $4.08 \times 10^4$  Nm ( 30,000 ft. lb.) and pad thickness to 45.7cm (18 inches). Driving was continued for 10 minutes at 50 strokes per minute, attaining 1.98m ( 6 1/2 feet) of depth. At this point, refusal was acknowledged. (The refusal rate had been predetermined to be 50 strokes per foot.)

The pedestal manufacturer, Centrecon, was consulted at this time. They recommended pre-drilling an undersized hole before driving. The pedestal was pulled and preparations were made for pre-drilling with an 45.7cm ( 18 inch) diameter drill. It was decided that the B-1 site installation be attempted next, prior to further work on B-2. The B-1 hole was drilled with the 45.7cm ( 18 inch) drill down approximately 4.88m ( 16 ft). Because of rocks and drill drift, the hole turned out to range from 57.2 to 76.2cm ( 22.5 to 30 inches) in diameter. The piling was prepared for driving. It slid down the



Figure 4.3-1. Pile-Driver and Pedestal - Site B2

first 2.13m ( 7 feet) into the hole under its own weight. The next 1.83m ( 6 feet) went easily with the pile driver operating at  $3.94 \times 10^4$  Nm ( 29,000 ft. lb.) on a 22.9cm ( 9 inch) pad. The last .61m (2 feet) required approximately 800 blows. (16 minutes at 50 blows/minute). It was noticed that a partial gap existed between the soil and the pedestal where it entered the ground. This problem was alleviated by water jetting loose soil into the pedestal/soil interface.

The predrilled hole for B-2 was first drilled with a 30.5cm ( 12 inch) auger and then followed with a 45.7cm ( 18 inch) auger. Since this hole was so much smaller in diameter it was drilled to a greater depth. The final hole turned out to be about 45.7-50.8cm ( 18-20 inches) in diameter near top and 7.9m ( 26 foot) deep. The pile driver was set up for 39,440 Nm ( 29,000 ft. lb.) with a 22.9cm (9 inch) pad. The pile was driven below grade with only the weight of the pedestal and hammer. The piling was then withdrawn several feet and soil was poured down the center hole of the piling to partially fill the predrilled hole. Driving commenced again and the pedestal was firmly set. The gap around the pedestal was filled in the same fashion as for heliostat B-1.

Sandia, Albuquerque structural engineering personnel performed a load deflection test on the B-2 pedestal. A 5340 N (1200 lb.) force was applied horizontally at the top of the pedestal while the angle of inclination of the top of the pedestal was monitored. The pedestal linearly deflected 0.3 milliradians at 5340 N ( 1200 lb.) load, and returned to zero deflection when the load was removed. Figure 4.3-2 is a photograph of this test in progress.

#### 4.3.2 Gimbal Drive

Inspection of the top surfaces of the 2 pedestals after driving revealed that the wood pads had adequately protected the surfaces from damage during driving. A gap-width check between the gimbal and pedestal flange showed the surfaces to be to within about 0.030 inches.

Stainless steel shims of selected thickness were inserted in the interface as required, during gimbal installation. The bolts were torqued to 354 Nm (260 ft. lb.) Figure 4.3-3 shows the gimbal installation at site B-1.

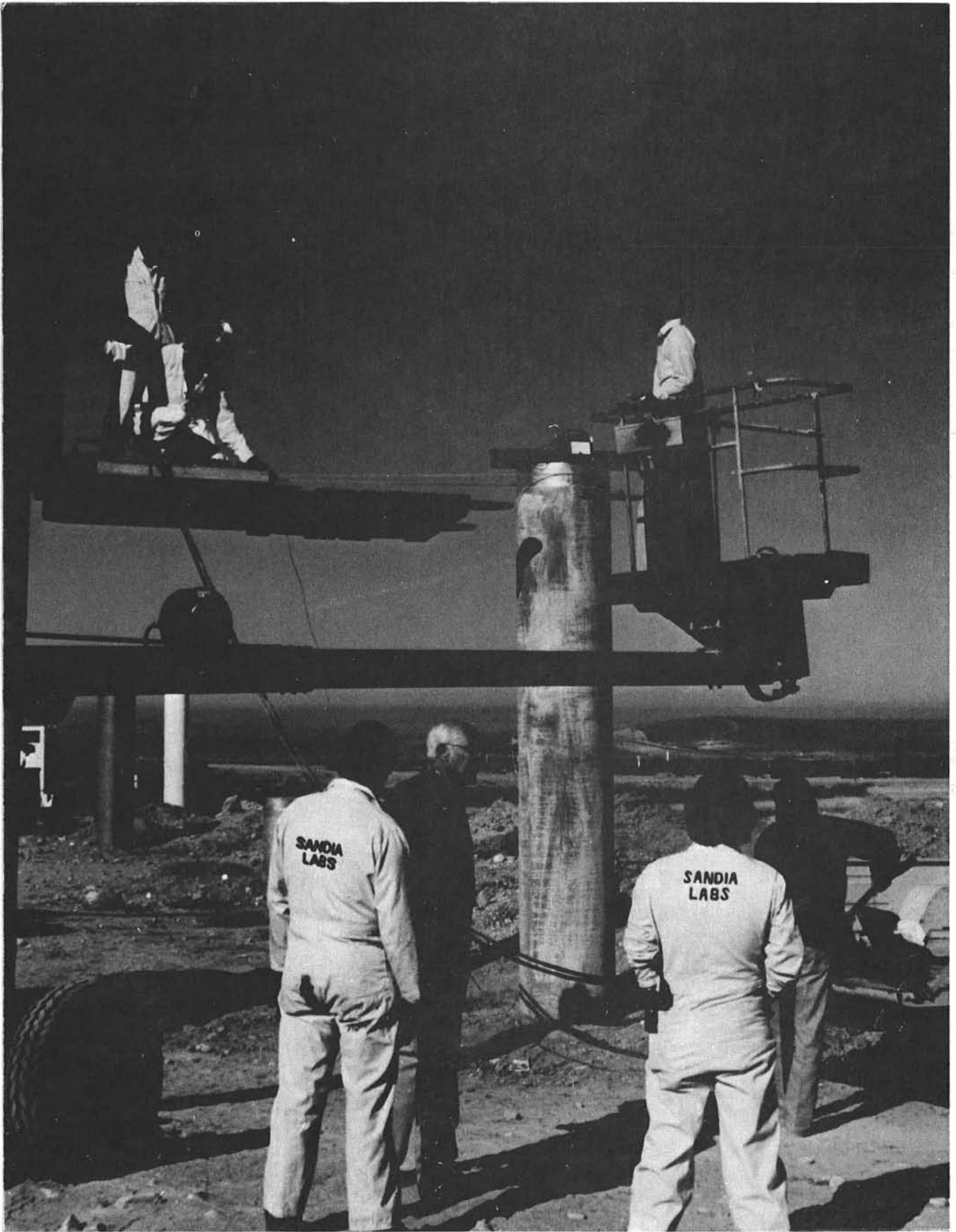


Figure 4.3-2. Pedestal Load/Deflection Test



Subsequent to the gimbal installation, and prior to the installation of the center torque-tube section, the pedestal verticality was measured with an electronic level, Section 4.3.7.

#### 4.3.3 Structural Frame

The center torque tube was lifted into position with web slings and a fork lift. A pilot shaft was used to align the pin holes of the torque tube with the bearings in the gimbal for installation of bearing pins, washers and retaining rings. Next, the elevation drive unit was installed using a Delrin "AF" polymeric nut on the jack screw. Figure 4.3-4 is a photograph of the center torque tube installation, and Figure 4.3-5 shows the installation of the elevation drive. On prototype heliostats, the center torque-tube section was installed in the field to allow access to the elevation axis bearings after gimbal installation, for azimuth axis tilt measurement (Section 4.3.7). In a production scenario, however, the gimbal and center torque-tube section would be pre-assembled before installation on the pedestal.

H-frames were lifted into approximate position and then finally located by rotating the center torque tube section until dowel pins in the H-frame bolt circle lined up with holes in the torque tube flange. Twenty-four, 0.79 cm (5/16-inch) bolts were installed and torqued to 23 Nm (17 ft. lbs.), completing the joint and effecting the proper alignment between the 2 H-frames. Figure 4.3-6 shows an H-frame being brought into position and Figure 4.3-7 is a photograph of a completed structural frame. (In a production installation, H-frames would have canted reflector facets installed before field installation).

#### 4.3.4 Reflector Facets

Reflector facets were field-installed on the structural frame in a horizontal position. Figure 4.3-8 shows mounting brackets being attached to a facet prior to lifting onto the frame. Mounting brackets and pads were installed loosely on the facet as shown, and then an overhead crane with web slings lifted the facet onto the frame. Figure 4.3-9 shows a facet being moved into position. To assure proper spacing between the underside of a facet and the

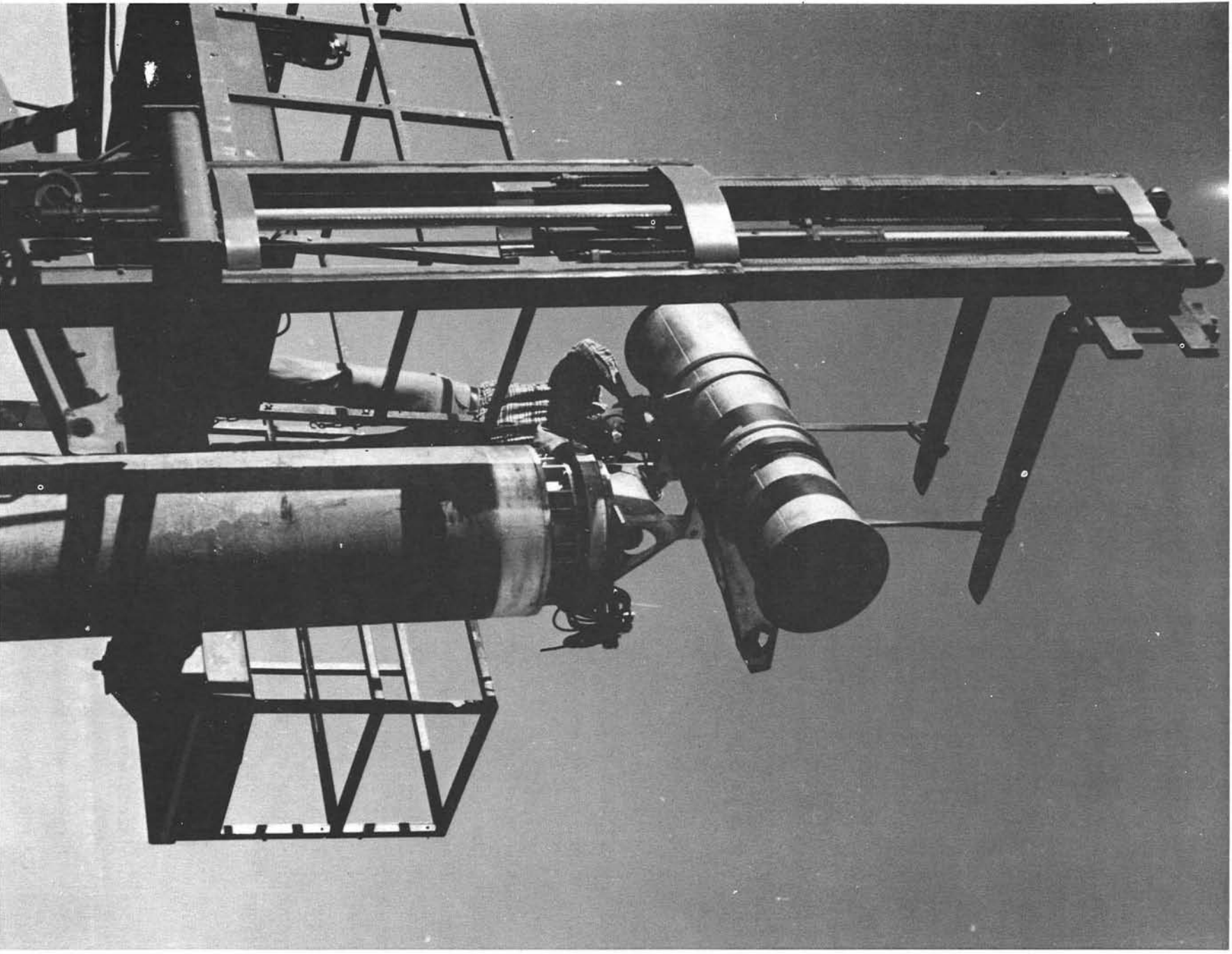


*Figure 4.3-4. Installation of Center Torque Tube*





*Figure 4.3-5. Installation of Elevation Drive*



*Figure 4.3-6. Installation of an H-Frame Assembly*

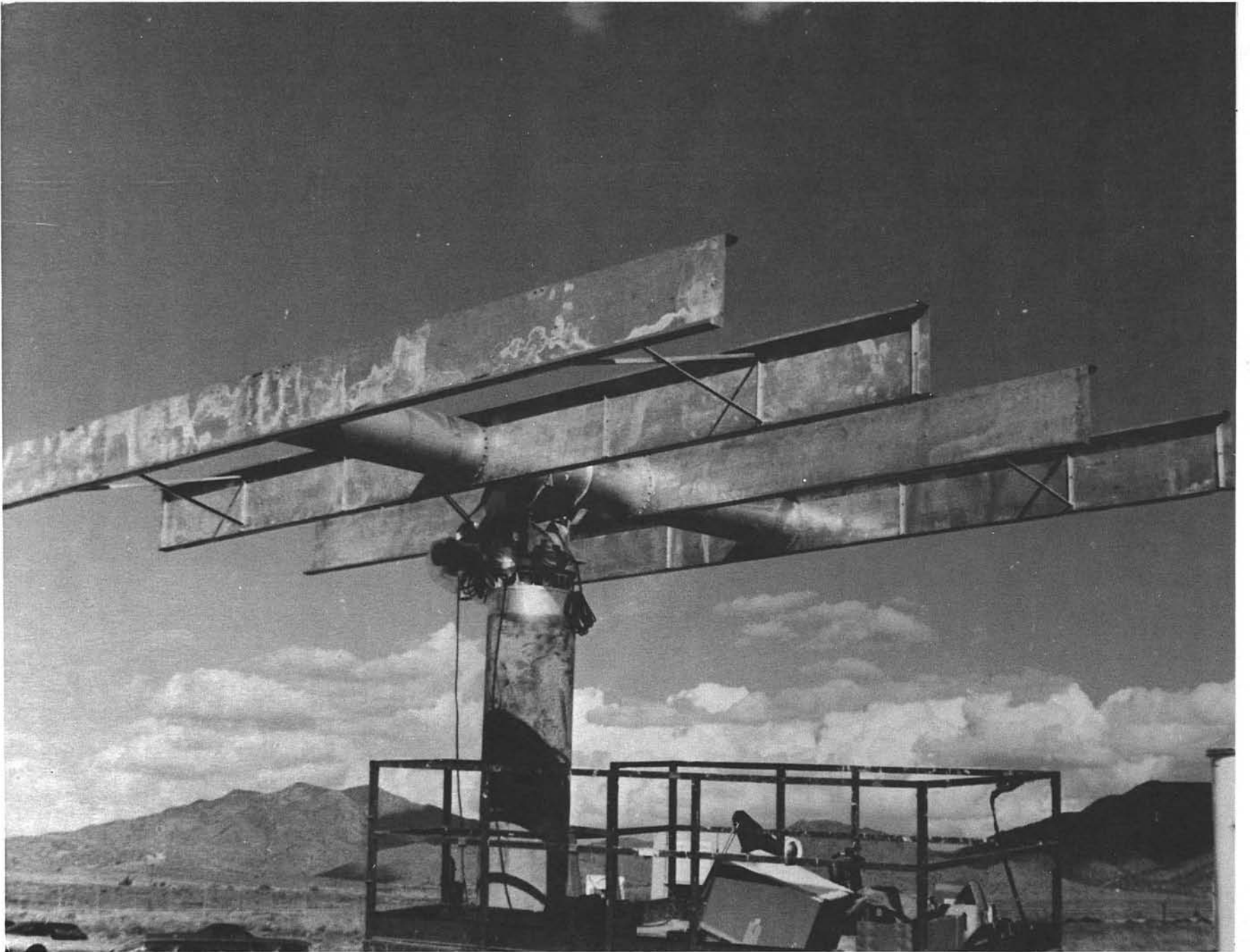


*Figure 4.3-7. Completed Structural Frame*



*Figure 4.3-8. Reflector Preparation*



*Figure* 4.3-9. Reflector Installation

top of a Z-beam, one inch thick wooden strips were placed temporarily on top of the Z-beam prior to placing the facet in position. The reflector was then manually moved into the desired position mounting brackets were adjusted and attachment bolts were used for attachment to Z-beams. The attachment bolts were temporarily tightened (permanently torqued following canting) and the wooden strips removed.

Prior to installing a subsequent reflector, the pad pressure was set for each mount. This was accomplished by loosening the jamb nut, and loosening or tightening the set screw until the pads could be rotated by hand with moderate force.

#### 4.3.5 Controls Installation at CRTF

Controls installation consisted of: computer system installation; heliostat electronics installation and cable hookups; and alignment and calibration.

The computer system installation involved assembling the computer equipment, and checking to see that it would bootup and run the RT-11 monitor program.

The heliostat electronics installation required assembly of mounting brackets to the electronics boxes, and then strapping the boxes to the pedestals via two straps which were tightened around the pedestal with turn brackets. The boxes were mounted on the north side of the pedestal for easy access to the prototype units.

After the boxes were mounted, control cables from the gimbal assembly were routed to the gimbal cable carrier, and tied together with cable ties. An expandable woven glass sheath was slipped over the cable bundle between the cable carrier and the electronics box. The purpose of the sheath is to protect the cables from sunlight and abrasion. The cables were then cut to proper length and lugs installed for attaching to the terminal strips in the electronics box. (In a production design the cables bundle would be completed before installation).

A cable support was added about mid-way between the electronics box and the top of the pedestal to lessen the tendency of the cable to swing in wind and to avoid the cable rubbing of the electronics box when the azimuth axis is run to large clockwise displacements.

The controls alignment procedure consisted of determining the locations of the elevation and azimuth reference sensors as described in Section 4.3.7.

The pedestal tilt and receiver target location data were processed by computer to transform the target coordinates into a tilted axis system. The analysis also gave the elements of the matrix used to transform the pointing vector into the tilted axis of the heliostat.

Results of preliminary full-day sun-tracking tests indicated the need for minor corrections in azimuth axis tilt data being used in algorithms. These corrections brought the daily RMS pointing error within the allowed error specification of 0.75 milliradians RMS per axis. To further improve aiming accuracy, the aiming calculations were modified to account for the effects of mirror offset from the elevation gimbal axis.

#### 4.3.6 Canting

Following installation of pedestals, Sandia provided BEC with exact heliostat-to-tower coordinates and the BCS target slant range. These values were used to compute cant angles for both heliostats as shown in Table 4.3-1. Table 4.3-2 provides the computed cant angles.

Table 4.3-1  
Heliostat Coordinates

Heliostat I.D.	Tower Coordinates (Meters)			Target Slant Range (Meters)
	X (east)	Y (north)	Z (vertical)	
B-1	39.47	319.73	4.73	314.18
B-2	20.32	243.68	4.33	237.13

Table 4.3-2  
Reflector Cant Angles

Heliostat I.D.	Cant Angles (arc sec)				Azimuth Angle
	Elevation Angles				
	Outside Facet	Intermediate Facet	Inside Facet		
B-1	1036	621.7	207.4	504.7	
B-2	1381	828.7	276.1	672.8	

Reflector canting was discussed in paragraph 4.2.3.4. The instruments, tools and procedures selected are discussed in greater detail there and will be only briefly mentioned here.



In preparation for canting, the azimuth drive was operated until the elevation axis was exactly horizontal, as determined from the verticality data (this is at right angle to plane of maximum tilt of pedestal). The elevation motor was then operated until the Z-beams were approximately level as measured by a carpenter's level. "T" braces were placed under each end of the Z-beams to prevent movement of the structural frame during canting operations. This position in elevation was considered the elevation axis calibration location since the mirror array normal vector was set exactly vertical in the canting operation.

Cant angles were set by placing wooden wedges between the underside of the reflector mounting brackets and the top of the Z-beams. The desired reflector facet orientation was then obtained by loosening the attachment bolts and moving the wedges in or out. Reflector angles were measured using the Federal Model 232P-68 electronic level on a 5 x 2.5 x 30.5cm ( 2 x 1 x 12 inch) ground parallel bar. The level and bar were positioned near the center of the facet, alternately oriented parallel to the long dimension and short dimension of the panel. Several iterations were required to achieve the desired cant angles along both axes. Following canting operations, the .79cm ( 5/16 inch) attachment bolts were torqued to 23.1 Nm ( 17 ft. lbs.). Figure 4.3-10 is a photograph showing the level and parallel bar being positioned on a facet . Subsequent image evaluation showed that the facet images superimposed well. While this technique is not practical for application in a large power plant installation, it would work well after replacing a damaged facet.

Subsequent to canting, the support braces were removed to allow operation of the gimbal drive. As the heliostat was brought down in elevation, motor steps were counted until the elevation reference mark was sensed. The number of motor counts was recorded and stored in the software, thereby calibrating the reference mark with respect to true vertical.

#### 4.3.7 Alignment

Geometry data needed by the computer to properly aim the sun's image at the beam characterization system (BCS) target was obtained in several steps. Table 4.3-3 lists the alignment requirements and how they were met. Subsequent paragraphs discuss details of the performance of these alignment tasks.

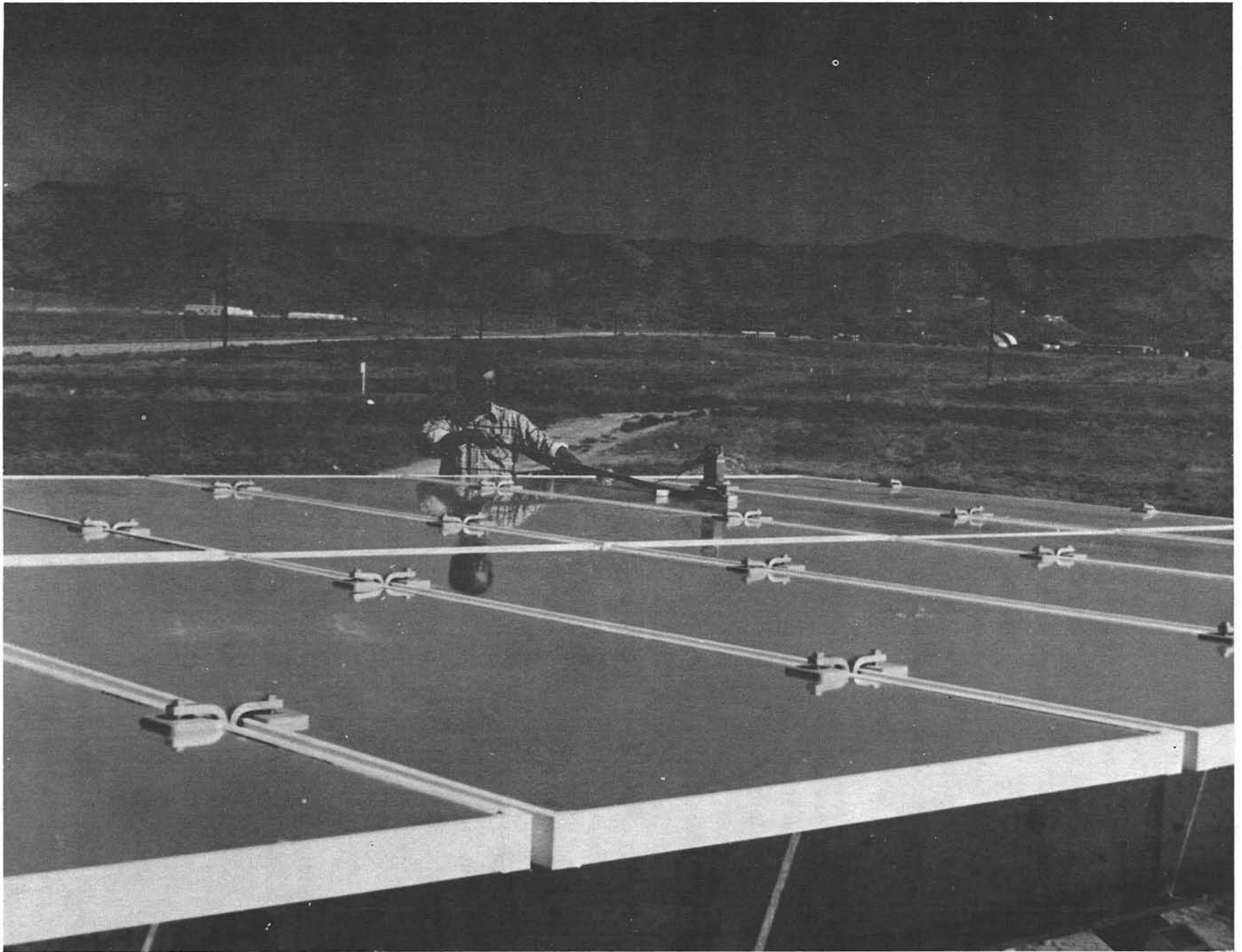


*Figure 4.3-10. Reflector Canting*

Table 4.3-3

Alignment Requirement and Procedures

<u>Requirement</u>	<u>Procedure</u>
Azimuth/Elevation Axis Non-Orthogonality	Instrumented gimbal elevation axis in field on pedestal - Electronic level
Azimuth Axis Verticality (Tilt)	Instrumented gimbal elevation axis in field on pedestal - Electronic level
Elevation Axis Reference	Count motors steps between zero ref. mark and position of vertical mirror normal
Azimuth Axis Reference	Attach laser along elevation axis; aim at target over monument; rotate in elevation to accurately determine bearing of elevation axis; rotate in azimuth to azimuth zero reference mark, counting motor steps
Mirror Normal - Elevation Axis Non-Orthogonality	Not measured, mirror canting done when elevation axis exactly horizontal
Elevation Axis Gravity Compensation	Rotated elevation from 0° to 90° reading motor steps and shaft encoder installed for a test only. Build look up table for correction.
Heliostat Longitude and Latitude	Survey Data
Heliostat Orientation With Respect to Target	Survey Data

#### 4.3.7.1 Azimuth/Elevation Non-Orthogonality

The non-orthogonality between the azimuth and elevation axes was measured at FACC and is discussed in detail in Paragraph 4.2.2.3. The non-orthogonality of the gimbal B-1 is 0.75 milliradians and for gimbal B-2 is 0.1 milliradians. (These values were confirmed during a field non-orthogonality measurement using the same setup as that used in the verticality calibration, paragraph 4.3.7.2).

#### 4.3.7.2 Azimuth Axis Verticality (Tilt)

Azimuth axis tilt includes tilt of both the pedestal and vertical axis of rotation of the gimbal with respect to the gimbal mounting flange. To measure the direction and magnitude of tilt, an electronic level was accurately referenced to the elevation axis and spun through 360° of azimuth rotation. This provided a measure of the deviation of the elevation axis from true horizontal as a function of azimuth bearing angle. Figure 4.3-11 is a schematic and Figure 4.3-12 a photograph of the verticality apparatus. Apparatus included a ground drill rod held in the elevation bearings, a ground plate supported over the drill rod with precision "Vee" blocks, a threaded rod supporting the other end of the ground plate, and an electronic level. The electronic level was read as the gimbal was incrementally rotated about the azimuth axis in 10° increments. A plot of tilt angle versus azimuth angle (sine wave) was made, from which the magnitude and direction of maximum azimuth tilt was determined. The results for B-1 and B-2 follow:

Heliostat I.D.	Tilt (arc seconds)	Direction (Degrees from North - CW)
B-1	1100	309.8°
B-2	1848	220.8°

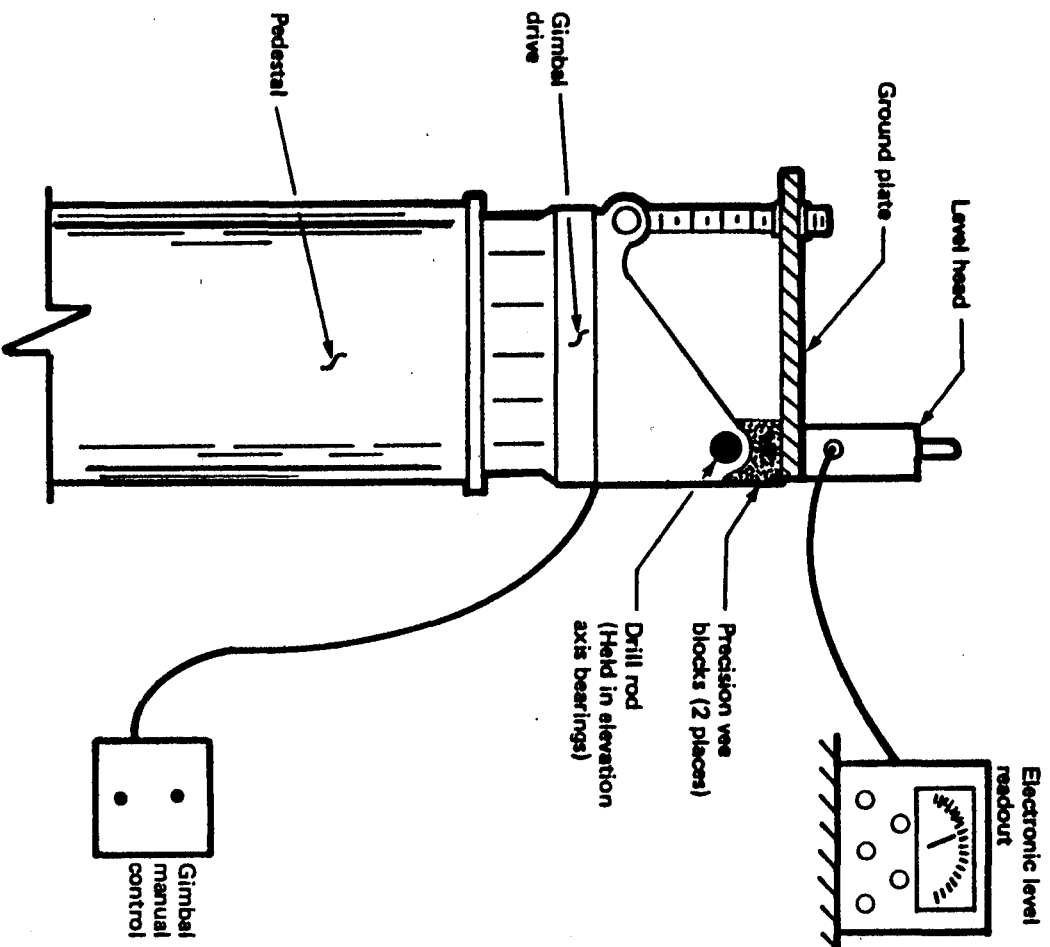


Figure 4.3-11. Verticality Measurement Set Up



*Figure 4.3-12. Verticality Measurement*

#### 4.3.7.3 Elevation Axis Reference

The purpose of this calibration was to correlate elevation motor drive count to either vertical or horizontal aiming of the mirror normal vector. A Hall-effect sensor is mounted on the elevation axis to provide initial calibration and periodic checks. The sensor is triggered by a small magnet which passes by it. Motor count is read when the sensor is triggered. After calibration, this motor count value corresponds to a specific elevation angle. Reading of the same value each time the reference mark is sensed confirms the initial calibration.

Calibration at the 90° elevation position (reflector normal vector vertical) was selected because of the horizontal attitude of the reflector and the ability to use a level for precise measurement. The azimuth was positioned such that the elevation axis was exactly horizontal as determined during the verticality measurement (Paragraph 4.3.7.2). An electronic level was placed on a reflector facet in the center of the reflector and at right angles to the elevation axis. The elevation drive motor was operated until the proper angle was read on the level, corresponding to the angle established during facet canting (Section 4.3.6). The level was moved to other reflectors and read for confirmation.

Actual calibration was accomplished by reading the motor count when the reflector vector was vertical, then again when the reference mark was sensed after rotating in elevation. An equation had been previously developed to correct for the non-linear relationship between the jack-screw arm mechanism of the motor revolutions.

#### 4.3.7.4 Azimuth Axis Reference

The purpose of this calibration was to correlate azimuth motor drive counts to true north bearing. A Hall-effect sensor, similar to the one on the elevation axis, is mounted to provide initial calibration and periodic checks.

The technique selected for the prototype heliostats involved the use of a laser and a known monument and is shown graphically in Figure 4.3-13.

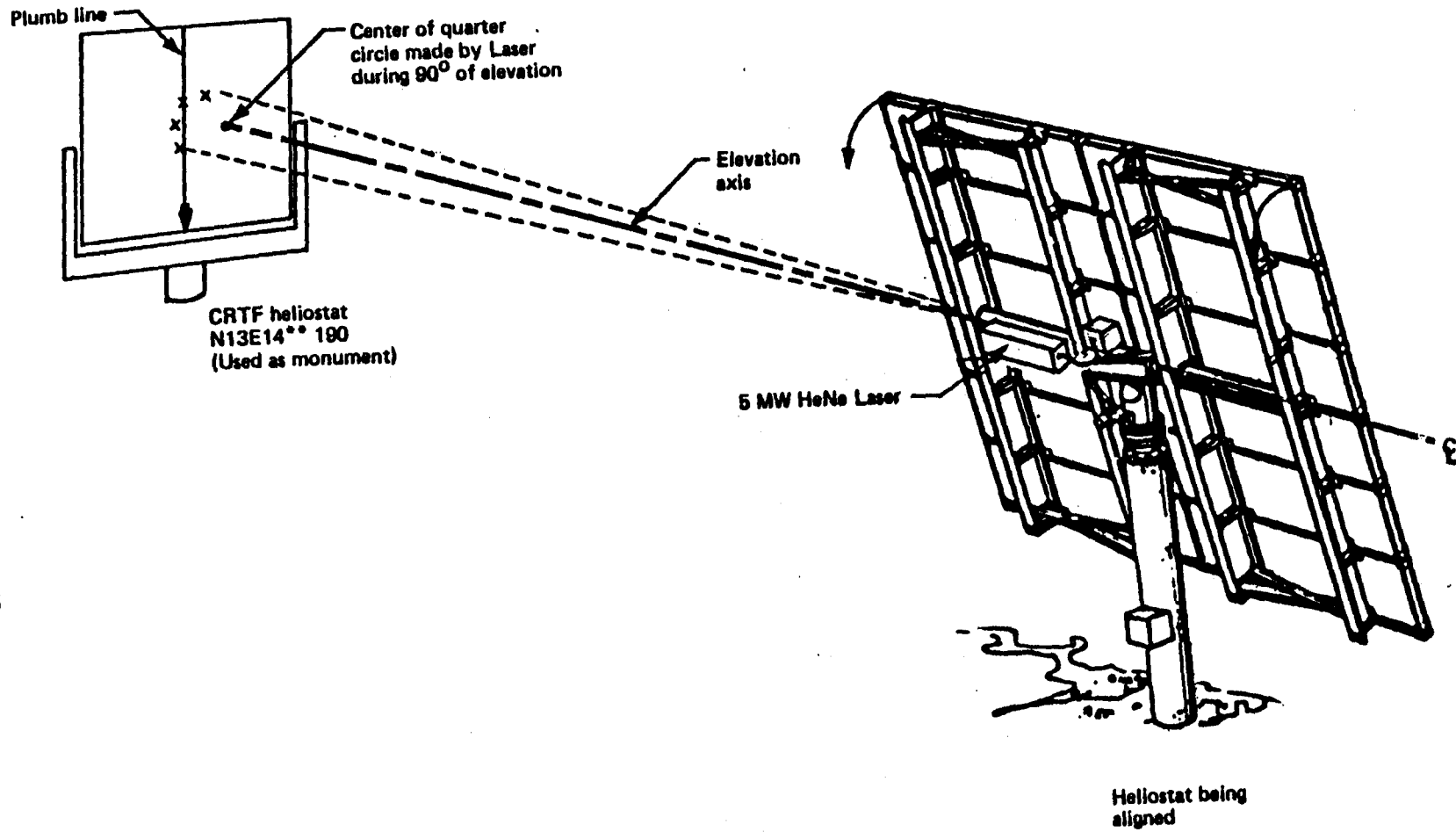


Figure 4.3-13. Azimuth Alignment Technique



The heliostat was fitted with a 5 milliwatt helium-neon laser, attached to an outboard torque tube with large hose clamps. It was aligned approximately parallel to the elevation axis. Next, a monument with target, in this case a CRTF heliostat, was selected and its exact coordinates obtained from CRTF files. The CRTF heliostat was rotated with its white painted back side facing toward the BEC heliostat to be calibrated. A plumb-bob was hung over the survey mark of the CRTF heliostat. The BEC heliostat was then rotated in azimuth until the laser beam was observed on the back side of the target heliostat (CRTF heliostat). A large piece of cardboard was taped to the target heliostat to serve as a target surface. The laser spot was marked with a pencil. Next, the BEC heliostat was rotated in elevation, incrementally, and as the laser spot advanced in an arc on the target, it was marked with the pencil. This was continued throughout the 90° of elevation travel, producing a quarter circle on the surface. The center of the quarter circle was determined graphically and plotted. This point represented the actual aim point of the BEC heliostat elevation axis. The distance of this aim point from the plumb line was measured and recorded.

Since the BEC heliostat and CRTF heliostat coordinates were both known from accurate surveys, the bearing of the elevation axis could be accurately computed. The azimuth motor count was read and recorded. Then the azimuth drive was advanced until the reference mark was sensed. Again the motor count was read and recorded. With the knowledge of the number of motor counts per degree, the azimuth bearing of the elevation axis (and reflector normal, which is 90° away from the el. axis) was calculated for the reference mark position and then for true North. This completed the calibration of the azimuth axis.

#### 4.3.7.5 Reflector Normal/Elevation Axis Non-Orthogonality

No method was developed for verifying the orthogonality of the reflector normal vector with respect to the elevation axis. It was assumed that a high degree of orthogonality existed because of the method in which the reflectors were canted. The elevation axis was accurately leveled ( $\pm 20$  arc sec) before canting started, and the facet canting was performed with respect to horizontal ( $\pm 50$  arc sec). This placed the average plane of the facets parallel to the elevation axis; and hence the normal vector from the average plane, orthogonal to the elevation axis, within 55 arc sec.

#### 4.3.7.6 Elevation Axis Gravity Compensation

The design of the gimbal drive is such that a varying moment is applied by the reflector assembly as a function of elevation angle. This results in the possibility of slight elastic deformations in gimbal components between the elevation motor shaft, where the elevation angle is controlled, and the elevation axis about which the reflector and frame rotate. To evaluate this effect and provide a correction table( if the effect was found to be significant), a shaft encoder was installed on the elevation axis. A BEI, 15 bit, absolute position encoder was used. Encoder output and motor counts were monitored while rotating 90° in elevation. From this data, constants were computed to modify the equations relating motor counts to actual elevation angle. Tests at the CRTF showed that a small amount of deformation did occur. Software adjustments were made to compensate for this effect.

Encoders will not be necessary on production heliostats. It may, however, be cost effective to install encoders on a few heliostats to determine the average deformation correction needed for input to the software.

5.0 REFERENCES

- 1-1 King, D.L. and Meyers, J.E., Environmental Reflectance Degradation of CRTF Heliostats, Proceedings of Society of Photo-Optical Instrument Engineers, "Optics in Adverse Environments," Los Angeles, Ca.; Feb. 4, 1980.
- 2-1 Lind, M.A. and Rusin, J.M., Heliostat Glass Survey and Analysis, Battelle Pacific Northwest Laboratory, Richland, Washington; September, 1978.
- 2-2 Lind, M.A. and Buckwalter, C.Q., Barstow Heliostat Mirror Glass Characteristics; Battelle Pacific Northwest Laboratory, Richland, Washington; September, 1980.
- 2-3 Davidson, W.S., et. al., Evaluation, Selection, Conceptual Design and Assessment of a Closed Brayton Cycle Advanced Central Receiver Solar-Electric Power Plant with Coupled Sensible Heat Storage; Boeing Engineering and Construction Co., Seattle, Washington; November, 1978.
- 2-4 Letter from James G. Zwissler, Jet Propulsion Laboratories, California Institute of Technology, Pasadena, California; February 19, 1980; letter summarized results of testing of low and high-density Foamsil 75 at Pittsburgh Corning's Sedalia, Missouri, plant, 28-31, January, 1980.
- 3-1 Specification A10772, Collector Subsystem Requirements, Revision D, dated 10/10/72; Sandia Laboratories, Livermore, CA.; memo.

- 3-2 DELSOL, a computer code program for determining heliostat field sizes and layouts, and other requirements for solar-electric power plants; revision dated 12/4/79; Sandia Laboratories, Livermore, CA.
- 3-3 HELIOS, a computer program for determining heliostat image shapes; Revision dated 10/8/79, Sandia Laboratories, Livermore, CA.
- 4-1 Facet Fabrication Records; BEC and Pittsburgh Corning quality assurance records prepared at Pittsburgh Corning plant at Port Allegany, PA., during time period of June 6 through June 26, 1980, contained in BEC files in Seattle, WA.

UNLIMITED RELEASE  
INITIAL DISTRIBUTION

UC-62d (350)

U.S. Department of Energy  
600 E Street NW  
Washington, D. C. 20585  
Attn: W. W. Auer  
G. W. Braun  
K. Cherian  
M. U. Gutstein  
L. Melamed  
J. E. Rannels

U.S. Department of Energy  
San Francisco Operations Office  
1333 Broadway  
Oakland, CA 94612  
Attn: S. D. Elliott  
S. Fisk  
R. W. Hughey  
W. Nettleton

U.S. Department of Energy  
Solar Ten Megawatt Project Office  
P. O. Box 1449  
Canoga Park, CA 91304  
Attn: M. Slaminski

U.S. Department of Energy  
Solar Ten Megawatt Project Office  
5301 Bolsa Ave. MS14-1  
Huntington Beach, CA 92649  
Attn: R. N. Schweinberg

USAF Logistics Command  
P. O. Box 33140  
Wright-Patterson AFB  
Ohio 45433  
Attn: G. Kastanos

UCLA  
900 Veteran Avenue  
Los Angeles, CA 90024  
Attn: F. Turner

Georgia Institute of Technology  
Engineering Experiment St.  
Atlanta, GA 30332  
Attn: S. H. Bomar, Jr.

University of Houston  
Houston  
Solar Energy Laboratory  
4800 Calhoun  
Houston, TX 77004  
Attn: A. F. Hildebrandt  
L. L. Vant-Hull

U.S. Department of Interior  
Water & Power Res. Service  
P.O. Box 427  
Boulder City, NV 89005  
Attn: J. Sundberg

Acurex  
485 Clyde Avenue  
Mountain View, CA 94042  
Attn: J. Hull

Aerospace Corporation  
Solar Thermal Projects  
Energy Systems Group, D-5  
Room 1110  
P.O. Box 92957  
El Segundo, CA 90009  
Attn: P. deRienzo  
P. Mathur

Airesearch Manufacturing Co.  
2525 West 190th Street  
Torrance, CA 90509  
Attn: M. G. Coombs  
For: P. F. Connelly

AMFAC  
700 Bishop Street  
Honolulu, HI 96801  
Attn: G. St. John

ARCO  
911 Wilshire Blvd  
Los Angeles, CA 90017  
Attn: J. H. Caldwell, Jr.

Arizona Public Service  
P. O. Box 21666  
Phoenix, AZ 85036  
Attn: D. L. Barnes  
For: E. Weber

Arizona Solar Energy Commission  
1700 W. Washington - 502  
Phoenix, AZ 85007  
Attn: R. Sears

Babcock & Wilcox  
91 Stirling Avenue  
Barberton, OH 44203  
Attn: G. Grant  
For: J. Pletcher  
M. Seale

Babcock & Wilcox  
P. O. Box 1260  
Lynchburg, VA 24505  
Attn: W. Smith

Babcock & Wilcox  
20 S. VanBuren Avenue  
Barberton, OH 44203  
Attn: M. Wiener

Badger Energy, Inc.  
One Broadway  
Cambridge, MA 02142  
Attn: F. D. Gardner

Battelle Pacific Northwest Labs  
P. O. Box 999  
Richland, WA 99352  
Attn: M. A. Lind

Bechtel National, Inc.  
P. O. Box 3965  
San Francisco, CA 94119  
Attn: E. Lam  
For: J. B. Darnell  
R. L. Lessley

Black & Veatch  
P. O. Box 8405  
Kansas City, MO 64114  
Attn: C. Grosskreutz  
For: J. E. Harder  
S. Levy

Boeing Engineering & Construction  
P. O. Box 3707  
Seattle, WA 98124  
Attn: R. L. Campbell  
R. Gillette  
J. R. Gintz

Booz, Allen & Hamilton, Inc.  
8801 E. Pleasant Valley Road  
Cleveland, OH 44131  
Attn: W. Hahn

Brookhaven National Laboratory  
Upton, NY 11973  
Attn: G. Cottingham

Burns and Roe, Inc.  
550 Kinderkamack Rd.  
Oradell, NJ 07649  
Attn: J. Willson

Burns and Roe, Inc.  
185 Crossways Park Drive  
Woodbury, NY 11797  
Attn: R. Vondrasek

Busche Energy Systems  
7288 Murdy Circle  
Huntington Beach, CA 92647  
Attn: K. Busche

California Public Utilities Commission  
350 McAllister St., Room 5024  
San Francisco, CA 94102  
Attn: B. Barkovich  
For: C. Waddell

Chevron Research  
P. O. Box 1627  
Richmond, CA 94804  
Attn: L. Fraas

Chevron Oil Research  
P. O. Box 446  
La Habra, CA 90631  
Attn: W. Peake  
For: J. Ploeg  
W. Stiles

Colt Industries  
Trent Tube Division  
East Troy, WI 53170  
Attn: J. Thackray

Corning Glass Works  
Advanced Products Dept.  
M/S 25  
Corning, NY 14830  
Attn: W. M. Baldwin  
A. Shoemaker

Custom Metals Enterprises, Inc.  
3288 Main Street  
Chula Vista, CA 92011  
Attn: T. J. Bauer

Data Science Corp.  
1189 Oddstad Drive  
Redwood City, CA 94063  
Attn: M. Liang



Electric Power Research Institute  
P. O. Box 10412  
Palo Alto, CA 93403  
Attn: J. Bigger

El Paso Electric Company  
P. O. Box 982  
El Paso, TX 79946  
Attn: J. E. Brown

Energy, Inc.  
P. O. Box 736  
Idaho Falls, ID 83401  
Attn: G. Meredith

Exxon Enterprises-Solar Thermal Systems  
P. O. Box 592  
Florham Park, NJ 07932  
Attn: P. Joy  
For: D. Nelson  
G. Yenetchi

Ford Aerospace  
3939 Fabian Way, T33  
Palo Alto, CA 94303  
Attn: I. E. Lewis  
For: H. Sund

Foster-Miller Associates  
135 Second Avenue  
Waltham, MA 02154  
Attn: E. Poulin

Foster Wheeler Dev. Corp.  
12 Peach Tree Hill Road  
Livingston, NJ 07039  
Attn: A. C. Gangadharan  
For: R. Zoschak

GAI Consultants, Inc.  
570 Beatty Rd.  
Monroeville, PA 15146  
Attn: H. Davidson

General Atomic Company  
P. O. Box 81608  
San Diego, CA 92138  
Attn: H. A. Chiger

General Electric Company  
Advanced Energy Programs  
P. O. Box 8661  
Philadelphia, PA 19101  
Attn: A. A. Koenig

General Electric Company  
1 River Road  
Schenectady, NY 12345  
tric Company  
1 River Road  
Schenectady, NY 12345  
Attn: J. A. Elsner  
For: R. N. Griffin  
R. Horton

GM Transportation System Center  
GM Technical Center  
Warren, MI 48090  
Attn: J. Britt

GM Corp. Harrison Rad. Division  
A and E Building  
Lockport, NY 14094  
Attn: A. Stocker

Houston Lighting and Power  
P. O. Box 1700  
Houston, TX 77001  
Attn: J. Ridgway

Institute of Gas Technology  
Suite 218  
1825 K Street, NW  
Washington, D. C. 25006  
Attn: D. R. Glenn

Jet Propulsion Laboratory  
Building 520-201  
4800 Oak Grove Drive  
Pasadena, CA 91103  
Attn: M. Adams  
H. Bank  
W. Carley  
E. Cuddihy  
J. Sheldon  
J. Swan  
V. Truscello

Kaiser Engineers, Inc.  
300 Lakeside Drive  
Oakland, CA 94612  
Attn: I. Kornye

Lawrence Berkeley National Laboratory  
University of California  
Berkeley, CA 94720  
Attn: A. J. Hunt

Los Alamos National Laboratory  
P. O. Box 1663  
Los Alamos, NM 87545  
Attn: S. W. Moore

Los Angeles Water and Power  
111 North Hope Street  
Los Angeles, CA 90051  
Attn: B. M. Tuller  
R. Radmacher

Martin Marietta Corporation  
P. O. Box 179  
Denver, CO 80201  
Attn: P. R. Brown  
A. E. Hawkins  
T. Heaton  
L. Oldham  
H. C. Wroton

McDonnell Douglas Astronautics Co.  
5301 Bolsa Avenue  
Huntington Beach, CA 92647  
Attn: P. Drummond  
R. L. Gervais  
D. A. Steinmeyer  
L. Weinstein

Meridian Corporation  
5515 Cherokee Avenue  
Alexandria, VA 22312  
Attn: B. S. Macazeer

Nielsen Engineering. & Research  
510 Clyde Avenue  
Mt. View, CA 94043  
Attn: R. Schwind

Northrup, Inc.  
302 Nichols Drive  
Hutchins, TX 75141  
Attn: J. A. Pietsch

ARCO Power Systems  
Suite 301  
7061 S. University Boulevard  
Littleton, CO 80122  
Attn: J. Anderson  
F. Blake

Olin Corporation  
275 Winchester Avenue  
New Haven, CT 06511  
Attn: S. L. Goldstein

OSC Department of Commerce  
341 West 2d Street  
San Bernardino, CA 92401  
Attn: M. G. Heaviside

Pacific Gas and Electric Co.  
77 Beale Street  
San Francisco, CA 94105  
Attn: P. D. Hindley  
For: J. F. Doyle  
A. Lam

Pacific Gas and Electric Co.  
3400 Crow Canyon Road  
San Ramon, CA 9426  
Attn: H. Seielstad  
For: J. Raggio

Phillips Chemical Co.  
13-D2 Phillips Building  
Bartlesville, OK 74004  
Attn: M. Bowman

Pittsburgh Corning  
800 Presque Isle Drive  
Pittsburgh, PA 15239  
Attn: W. F. Lynsavage

Pittsburgh Corning  
723 N. Main Street  
Port Allegany, PA 16743  
Attn: W. J. Binder  
For: R. Greene

PPG Industries, Inc.  
One Gateway Center  
Pittsburgh, PA 15222  
Attn: C. R. Frownfelter

Public Service Co. of New Mexico  
P. O. Box 2267  
Albuquerque, NM 87103  
Attn: A. Akhil

Research and Development  
Public Service Co. of Oklahoma  
P. O. Box 201  
Tulsa, OK 74102  
Attn: F. Meyer

Rockwell International  
Energy Systems Group  
8900 De Soto Avenue  
Canoga Park, CA 91304  
Attn: T. Springer

S. C. Plotkin & Associates  
6451 West 83rd Street  
Los Angeles, CA 90045  
Attn: W. Raser

Safeguard Power Transmission Co.  
Hub City Division  
P. O. Box 1089  
Aberdeen, SD 57401  
Attn: R. E. Feldges

Sargent and Lundy  
55 East Monroe  
Chicago, IL 60603  
Attn: N. Weber

Schumacher & Associates  
2550 Fair Oaks Blvd., Suite 120  
Sacramento, CA 95825  
Attn: J. C. Schumacher

Sierra Pacific Power Co.  
P. O. Box 10100  
Reno, NV 89510  
Attn: W. K. Branch

Solar Energy Research Institute  
1617 Cole Boulevard  
Golden, CO 80401  
Attn: L. Duhham, TID  
G. Gross  
B. Gupta  
D. W. Kearney  
L. M. Murphy  
R. Ortiz, SEIDB  
J. Thornton

Solar Thermal Test Facility  
User Association  
Suite 1205  
First National Bank East  
Albuquerque, NM 87112  
Attn: F. Smith

Solar Turbines International  
P. O. Box 80966  
San Diego, CA 92138  
Attn: P. Roberts

Southern California Edison  
2244 Walnut Grove Road  
Rosemead, CA 91770  
Attn: J. Reeves  
For: C. Winarski

Southwestern Public Service Co.  
P. O. Box 1261  
Amarillo, TX 78170  
Attn: A. Higgins

Standard Oil of California  
555 Market Street  
San Francisco, CA 94105  
Attn: S. Kleespies

Stanford Research Institute  
333 Ravenswood Avenue  
Menlo Park, CA 94025  
Attn: A. Slemmons

Stearns-Roger  
P. O. Box 5888  
Denver, CO 80217  
Attn: W. Lang  
For: J. Hopson

Stone & Webster Engineering Corp.  
245 Summer Street  
P. O. Box 2325  
Boston, MA 02107  
Attn: R. Kuhr

Townsend and Bottum  
9550 Flair Drive  
El Monte, CA 91731  
Attn: R. Schwing

US Gypsum  
101 S. Wacker Drive  
Chicago, IL 60606  
Attn: Ray McCleary

US Water & Power Resources Service  
Bureau of Reclamation  
Code 1500 E  
Denver Federal Center  
P. O. Box 25007  
Denver, CO 80225  
Attn: S. J. Hightower

Van Leer Plastics  
15581 Computer Lane  
Huntington Beach, CA 92649  
Attn: Larry Nelson

Veda, Inc.  
400 N. Mobile, Building D  
Camarillo, CA 90310  
Attn: L. E. Ehrhardt  
For: W. Moore

Westinghouse Corporation  
Box 10864  
Pittsburgh, PA 15236  
Attn: J. J. Buggy  
For: R. W. Devlin  
W. Parker

Winsmith  
Division of UMC Industries  
Springville, NY 14141  
Attn: W. H. Heller

K. R. Miller, 3153  
G. E. Brandvold, 4710; Attn: J. F. Banas, 4716  
J. A. Leonard, 4717  
B. W. Marshall, 4713; Attn: D. L. King  
A. B. Maish, 4724  
R. G. Kepler, 5810; Attn: L. A. Harrah, 5811  
J. G. Curro, 5813  
F. P. Gerstle, 5814  
J. N. Sweet, 5824; Attn: R. B. Pettit and E. P. Roth  
T. B. Cook, 8000; Attn: A. N. Blackwell, 8200  
B. F. Murphey, 8300  
C. S. Hoyle, 8122; Attn: V. D. Dunder  
R. J. Gallagher, 8124; Attn: B. A. Meyer  
D. M. Schuster, 8310; Attn: R. E. Stoltz, 8312, for M. D. Skibo  
A. J. West, 8314  
W. R. Even, 8315

R. L. Rinne, 8320  
C. T. Yokomizo, 8326; Attn: L. D. Brandt  
P. L. Mattern, 8342  
L. Gutierrez, 8400; Attn: R. A. Baroody, 8410  
D. E. Gregson, 8440  
C. M. Tapp, 8460

C. S. Selvage, 8420  
V. Burolla, 8424; Attn: C. B. Frost  
R. C. Wayne, 8450  
T. D. Brumleve, 8451  
W. R. Delameter, 8451  
P. J. Eicker, 8451 (5)  
R. M. Houser, 8451  
C. L. Mavis, 8451  
W. L. Morehouse, 8451  
H. F. Norris, Jr., 8451  
W. S. Rorke, Jr., 8451  
D. N. Tanner, 8451  
S. S. White, 8451  
A. C. Skinrod, 8452  
W. G. Wilson, 8453  
Publications Division, 8265/Technical Library Processes Division, 3141  
Technical Library Processes Division, 3141 (2)  
M. A. Pound, 8214, for Central Technical Files (3)